Study on the Fabrication, Optimization of Processing Parameters and Characterization of Collagen Based Vascularized Scaffolds for Biomedical Application

Khulna University Library
Thesis Acc. No: 4011
Authorised Sign:
Date: 18.12.2019

A Thesis

Submitted to

Biotechnology and Genetic Engineering Discipline, Life Science School,
Khulna University

For the partial fulfillment of the requirements for the degree of one and half years Masters of Science in Biotechnology and Genetic Engineering

Submitted By

RASHED HASAN NAYEEM
Examination Roll No: MS-170717
Session: 2016-2017

BIOTECHNOLOGY AND GENETIC ENGINEERING DISCIPLINE
LIFE SCIENCE SCHOOL, KHULNA UNIVERSITY
KHULNA - 9208, BANGLADESH

Study on the Fabrication, Optimization of Processing Parameters and Characterization of Collagen Based Vascularized Scaffolds for Biomedical Application

A Thesis By

Rashed Hasan Nayeem

Examination Roll No: MS 170717

Session: 2016-2017

Approved as to the style and content by

KHULNA UNIVERSITY Central Library KHULNA.

.....

External Supervisor
S. M. Asaduzzaman, PhD
Chief Scientific Officer and Director
Institute of Tissue Banking and Biomaterial Research
Atomic Energy Research Establishment
Savar, Dhaka.

.....

Internal Supervisor
Dr. Md. Shamim Akhter
Professor
Biotechnology and Genetic Engineering Discipline, Life Science School
Khulna University
Khulna.

.....

Professor Dr. Ayesha Ashraf
Chairman
Examination Committee
Biotechnology and Genetic Engineering Discipline
Khulna University
Khulna-9208
Bangladesh.

DECLARATION

I hereby declare that this thesis is based on my original work except quotations and citations which have been duly acknowledged. The material here has not ever been submitted in a whole or in a part for a degree from Khulna University or any other institutions. This research work will not be published anywhere without the concern of supervisor.

Rashed Hasan Nayeem

Examination Roll No: MS-170717

Date: 16.09.18

DEDICATED

TO

MY ADORED PARENTS
AND
BELOVED SIBLINGS, NADIA & NASIF

ACKNOWLEDGEMENT

At first, I want to express my humble gratitude to Almighty Allah for successfully completing my thesis work. This thesis was conducted by Institute of Tissue Banking and Biomaterial Research (ITBBR) in Atomic Energy Research Establishment (AERE), Savar, Dhaka. Therefore, I am thankful to the authority of ITBBR for providing all the facilities.

Form the very beginning; I have the greatest pleasure to express my heartfelt indebtedness, deepest sense of gratitude to my respectable supervisor, Dr. S. M. Asaduzzaman, Chief Scientific Officer and Director of ITBBR, for his generous permission to research in the institute. Moreover, his immeasurable encouragement, guidance and support and his invaluable advice, cooperation and constructive criticism throughout my thesis work, I owe him a debt of gratitude for motivating me to my absolute limits of intellectual development and never allowing me to settle for anything less than my utmost best.

I also express thanks to my internal supervisor, Dr. Md. Shamim Akhter, Professor, Biotechnology and Genetic Engineering Discipline, Khulna University, for allowing me to complete my thesis under his wise supervision.

I am also grateful to Md. Masud Rana, Research Fellow, ITBBR for co-ordination and co-operation throughout my research work.

Finally, I would like to convey my heartiest gratitude to my beloved family members.

Rashed Hasan Nayeem

Biotechnology and Genetic Engineering Discipline, Khulna University.

ABSTRACT

Tissue engineering aims to produce biological substitutes which may overcome the limitations of conventional clinical treatments for damaged tissues or organs. Bone tissue engineering is aimed at repairing diseased or fractured bone, which cannot be replaced naturally. Skeletal tissue is a highly organized structure comprising mainly type I collagen, nanometer sized carbonate-substituted hydroxyapatite crystals, water and various other non-collagenous proteins. In this study, naturally derived collagen from rabbit skin and chemically synthesized hydroxyapatite, and chitosan were used for fabrication of highly porous hydroxyapatite-collagen-chitosan scaffolds through thermally induced phase separation technique and cross-linked with both chemical (GTA&EDAC/NHS) and physical (DHT treatment & radiation) cross-linkers. Morphological properties of the scaffolds were characterized by determination of its porosity, density, swelling ratio, biodegradability, compressive strength and chemical interaction within the composite etc. The porosity and density of the scaffolds were measured by liquid displacement method; the chemical interaction was analyzed by Fourier transform infrared spectroscopy (FTIR) analysis. The resulted data showed that the selected optimized scaffold possessed three dimensional interconnected homogenous porous structures with a porosity of >91% and the density were 0.13 to 0.18 g/cm^3. The rate of swelling ratio of the scaffolds were 80 to 120%. The *in-vitro* biodegradability rate (after 28 days) of the fabricated scaffolds were varied from 38 to 42%. The mechanical strength of the scaffolds were ranged between 0.03 to 0.88 Nmm^{-2}. FTIR data confirmed that there had an intermolecular interactions among the polymers and mineral content within the composites and with different types of cross-linkers. Biological properties of scaffolds are characterized by determination of its biocompatibility and cytotoxicity. Scaffolds have shown very inferior blood clotting propensity (clot weight 2.1 to 10.5 mg), slight rate of hemolysis (0.22 to 0.62%) which is acceptable for medical devices. The cytotoxicity test indicated that the fabricated scaffolds have no cytotoxic property (100% live count of nauplii at low scaffold inducted concentration) against brine shrimp cells. Above results suggest that, these promising hydroxyapatite-collagen-chitosan scaffolds are useful candidates for bone tissue engineering applications.

KHULNA UNIVERSITY Central Library KHULNA.

TABLE OF CONTENTS

TITLE PAGE i

APPROVAL PAGE ii

DECLARATION PAGE iii

DEDICATION iv

ACKNOWLEDGEMENT v

ABSTRACT vi

TABLE OF CONTENTS vii

LIST OF FIGURES ix

LIST OF TABLES xi

Serial No.	Title	Page No.
1.	**INTRODUCTION**	**1-4**
1.1	Background	1
1.2	Objectives	4
2.	**LITERATURE REVIEW**	**5-45**
2.1.	Bone	5
2.1.1.	Characteristics of bone	5
2.2.	Grafting	6
2.2.1.	Bone grafts	7
2.2.2.	Autograft	7
2.2.3.	Soft tissue grafts	8
2.2.3.1.	Free gingival graft	9
2.2.3.2.	Connective tissue graft	9
2.2.3.3.	Pedicle graft	9
2.2.4.	Allograft	9
2.2.4.1.	Dentin grafting	9
2.3.	Tissue engineering	10
2.3.1.	Bone tissue engineering	12
2.3.2.	Scaffolds	14
2.3.2.1.	Evolution of scaffold	14
2.3.2.2.	Requirements of scaffold	19
2.3.2.3.	Biomaterial of scaffold	21
2.3.2.3.1.	Natural polymers	22
2.3.2.3.2.	Synthetic polymers	24
2.3.2.3.3.	Bio ceramics	25
2.3.2.4.	Scaffold fabrication method	27
2.3.2.4.1.	Traditional manufacturing techniques	27
2.3.2.4.2.	Advanced manufacturing techniques	29
2.3.2.5.	Scaffolds for *in vitro* cell culture	33

2.3.2.6.	Scaffolds for *in vivo* tissue-induced regeneration	36
2.3.2.7.	Platforms for the controlled delivery of bioactive agents	38
2.3.2.8.	Microscaffolds for *in situ* cell delivery and tissue fabrication	39
2.3.2.9.	Three-dimensional tumour models	41
2.3.2.10.	Bone tissue engineering in bangladesh perspective	42
3.	**MATERIALS AND METHODS**	**46-59**
3.1.	Working Place	46
3.2.	Extraction of collagen	48
3.3.	Preparation of hydroxyapatite powder	49
3.4.	Fabrication of Hydroxyapatite-Collagen-Chitosan scaffolds	50
3.5.	Addition of Cross-Linkers	51
3.5.1.	Addition of Chemical Cross-Linkers	51
3.5.2.	Addition of Physical Cross-Linkers	52
3.6.	Scaffold characterization	52
3.6.1.	Porosity and Density Determination	52
3.6.2.	Swelling Kinetics test	54
3.6.3.	Biodegradation Test	55
3.7.	Vascularization of Scaffold	56
3.8.	*In Vitro* Cytotoxicity Test	56
3.9.	Blood Compatibility	57
3.9.1.	Clot Formation Testing	57
3.9.2.	Degree of Hemolysis Test	58
3.10.	Fourier Transform Infrared Spectroscopy (FTIR) Analysis	58
3.11.	Mechanical Properties of Scaffold	59
4.	**RESULTS**	**60-96**
4.1.	Selection of Hydroxyapatite-Collagen-Chitosan Based Scaffold Composition	60
4.2.	Optimization of Scaffold through Cross-linking	62
4.2.1.	Optimization of NS_{19} Scaffold through Cross-linking	63
4.2.2.	Optimization of NS_{48} Scaffold through Cross-linking	74
4.3.	Fourier Transform Infrared Spectroscopy (FTIR) Analysis	85
4.4.	Vascularization of Scaffold	90
4.5.	Comparison between NS_{19} and NS_{48} scaffold	91
4.6.	Mechanical Properties of Scaffold	92
4.7.	Cytotoxicity Testing of Scaffolds using Brine Shrimp Lethal Assay	92
4.8.	Clot Formation Test	94
4.9.	Degree of Hemolysis Test	95
5.	**DISCUSSION**	**97-106**
6.	**CONCLUSION**	**107**
7.	REFERENCE	108-124
8.	Appendix - I	126
9.	Appendix-II	128

LIST OF FIGURES

Serial No.	Title	Page No.
Figure 2.1	Bone Architecture	5
Figure 2.2	Bone grafting	7
Figure 2.3	Illustration of an autograft harvested from iliac crest	8
Figure 2.4	Principle of Tissue Engineering Principle	10
Figure 2.5	Schema of the Three Pillars of Tissue Engineering	11
Figure 2.6	Schematic of Various Potential Drug Delivery Approaches	13
Figure 2.7	Scheme of the evolution of biomedical foams from tissue substitution to repair	15
Figure 2.8	Biomaterials for Scaffold Fabrication	22
Figure 2.9	Forming Chitosan by Partial Decaetylation of Chitin	23
Figure 2.10	Hierarchical Organization of Collagen Fibres	24
Figure 2.11	Crystalline structure of hydroxyapatite	25
Figure 2.12	Microscaffold approaches for *in vitro* and *in vivo* tissue regeneration	40
Figure 3.1	Flow Chart of Experimental Design	46
Figure 3.2	Schematic Diagram of Experimental Design	47
Figure 3.3	Extraction of collagen	48
Figure 3.4	Preparation of hydroxyapatite powder	50
Figure 3.5	Porosity and Density Determination	52
Figure 3.6	Swelling Kinetics test	54
Figure 3.7	Biodegradation Test	55
Figure 3.8	*In Vitro* Cytotoxicity Test of Scaffold on Brine Shrimp	56
Figure 3.9	Blood Clot Formation Test of scaffold composites	58
Figure 3.10	Fourier Transform Infrared Spectroscopy	59
Figure 3.11	Universal testing machine	59
Figure 4.2	(A) Effect of cross-linking on the porosity (%)±SD of NS_{19} scaffold	64
	(B) Effect of cross-linking on the density (%)±SD of NS_{19} scaffold	65
	(C1) Effect of cross-linking on the swelling rate (%)±SD of NS_{19} scaffold	66
	(C2) Effect of cross-linking on the swelling rate (%)±SD of NS_{19} scaffold	67
	(C3) Effect of cross-linking on the swelling rate (%)±SD of NS_{19} scaffold	69
	(D) Day vs. Biodegradability (%)±SD Curve	71
Figure 4.3	(A) Effect of cross-linking on the porosity (%)±SD of NS_{48} scaffold	75
	(B) Effect of cross-linking on the density (%)±SD of NS_{48} scaffold	76
	(C1) Effect of cross-linking on the swelling rate (%)±SD of NS_{48} scaffold	77
	(C2) Effect of cross-linking on the swelling rate (%)±SD of NS_{48} scaffold	78
	(C3) Effect of cross-linking on the swelling rate (%)±SD of NS_{48} scaffold	79
	(D) Day vs. Biodegradability (%)±SD Curve	82

KHULNA UNIVERSITY Central Library KHULNA.

Figure 4.4	FTIR analysis of NS_{19} scaffold with its chemical cross-linker	85
Figure 4.5	FTIR analysis of NS_{19} scaffold with its physical cross-linker	87
Figure 4.6	FTIR analysis of NS_{48} scaffold with its chemical cross-linker	88
Figure 4.7	FTIR analysis of NS_{48} scaffold with its physical cross-linker	89
Figure 4.8	Vascularization of Scaffold	90
Figure 4.9	Mechanical Properties of Scaffold	92
Figure 4.10	Blood Clot Weight Determination on Scaffold Surface	94
Figure 4.11	Visual observation of hemolysis on scaffold surface	96

LIST OF TABLES

Serial No.	Title	Page No.
Table 2.1	Advantages and Disadvantages of Different Biomaterials	26
Table 2.2	Overview of fabrication methods that applied for tissue engineering scaffolds	32
Table 2.3	National Institute of Truamatology & Orthopaedic Rehabilitation (NITOR) annual report, 2011- 2017	43
Table 4.1	Study of Hydroxyapatite-Collagen-Chitosan (HCC) scaffold	61
Table 4.2	(A) Effect of cross-linking on the porosity (%) of NS_{19} scaffold	63
	(B) Effect of cross-linking on the density (%) of NS_{19} scaffold	64
	(C1) Effect of cross-linking on the swelling rate (%) of NS_{19} scaffold	66
	(C2) Effect of cross-linking on the swelling rate (%) of NS_{19} scaffold	67
	(C3) Effect of cross-linking on the swelling rate (%) of NS_{19} scaffold	68
	(D1) Effect of cross-linking on the Biodegradability (%) of NS_{19} scaffold	69
	(D2) Effect of cross-linking on the Biodegradability (%) of NS_{19} scaffold	70
	(D3) Effect of cross-linking on the Biodegradability (%) of NS_{19} scaffold	70
	(D4) Effect of cross-linking on the Biodegradability (%) of NS_{19} scaffold	71
Table 4.3	(A) Effect of cross-linking on the porosity (%) of NS_{48} scaffold	74
	(B) Effect of cross-linking on the density (%) of NS_{19} scaffold	75
	(C1) Effect of cross-linking on the swelling rate (%) of NS_{48} scaffold	77
	(C2) Effect of cross-linking on the swelling rate (%) of NS_{48} scaffold	78
	(C3) Effect of cross-linking on the swelling rate (%) of NS_{48} scaffold	79
	(D1) Effect of cross-linking on the Biodegradability (%) of NS_{48} scaffold	80
	(D2) Effect of cross-linking on the Biodegradability (%) of NS_{48} scaffold	80
	(D3) Effect of cross-linking on the Biodegradability (%) of NS_{48} scaffold	81
	(D4) Effect of cross-linking on the Biodegradability (%) of NS_{48} scaffold	81
Table 4.4	Number and Percentage of Mortality of Nauplii after the Cytotoxicity Test	93
Table 4.5	Percentage (%) of Hemolysis Test	95

CHAPTER ONE

INTRODUCTION

1.1 Background

Bone is a highly complex material with different levels of hierarchy in structure that is composed of organic–inorganic composite and other minor components. It has an exceptional capacity to heal and remodel itself for repair of small fractures using different cells like osteoblasts, osteocytes and osteoclasts. The resorption, expansion and maintenance of this remarkable tissue result from the interrelated interaction of these cells. The large-scale bone defects however, cannot be healed completely by the body itself (Salgado *et al.,* 2004). Hence, large scale bone injuries and defects present a significant clinical problem. The worldwide incidence of bone degenerative diseases, road accidents and fracture mediated disorders has increased sharply and is predicted to be more by proximate future, especially in populations suffering from increased obesity and physical inactivity. In addition, the case of serious fractures and defects in elderly patients, complications such as mal-union or non-union occur frequently which inhibit the bone from healing naturally. It ultimately results in hundreds of millions of surgical measures annually all over the world (Yan *et al.,* 2016). Moreover, bone tissue repair accounts for approximately 500,000 surgical procedures per year in the United States alone.

The accessible best treatment strategy for those abnormalities is an invasive surgery to support and stabilize the bone, usually with metallic pins, screws, plates, or rods, but these surgical procedures has prolonged healing time and can require multiple surgeries. So, the other effective bone treating options came up as grafting methods are currently being used including, autogenic bone grafts (autografts), allogenic bone grafts (allografts), xenografts and synthetic bone substitutes. Still considered the gold standard, autografts are used in approximately 50% of all orthopedic bone grafting procedures. Allograft, are used in approximately 40% of bone grafting surgeries. However, Bone grafts are recorded as second only to blood transfusions of transplanted materials worldwide at a global cost valued at over $30 billion every year in the healthcare systems. On top, harvesting grafts (auto-, allo-, xeno-) have a number of drawbacks along with defective implementation depending on blood supply and need to avoid visceral

injuries of the patient (Mekala, 2012) as well as a significant structural failure rate of ~15 –25% due to poor tissue integration. These dramatic limitations inherent in the current clinical approaches have motivated the development of bone tissue engineering as a new research field in current tissue transplantation methodologies (Yunfeng, *et al.,* 2009) for viable synthetic bone substitute alternatives. Since all the current techniques of bone treatments have significant drawbacks, bone tissue engineering holds promise in providing an improved clinically therapeutic approach.

In this perspective, bone tissue engineering has brought a rapidly growing new interdisciplinary field with the application of principles and methods joining biomedical engineering, cellular and molecular biology, biomaterial science, mechanical engineering toward the fundamental understanding of bone structure-function relationships and the development of biological substitutes to restore, maintain or improve tissue function using biomaterials, cells and growth factors (Chan *et al.,* 2008). By combining scaffold, cells and growth factors, tissue engineering seeks to create an alternative biological solution to repair bone injuries. Tissue engineering is superior to other strategies in many ways. The use of an engineered implant would reduce the need for multiple surgeries associated with the pulling out of metallic implants and graft harvesting. Lessening need of surgeries favors a more rapid healing time with diminutive risk and cost effectiveness. The tissue engineering implant can also be integrated into the existing tissue, resulting in a flawless evolution between them. This assesses against stress and resorption of the vigorous bone surrounding. These advantages can be primarily attributed to the development of biomimetic scaffolds and that is what this research will focus on.

An ideal scaffold must maintain certain criteria to assure bone tissue regeneration and restoration of its structure and function. Therefore, the scaffolds for bone tissue engineering should have several properties such as biocompatibility, biodegradability, mechanical similarities with the target tissue and high porosity for cell adhesion, proliferation, and tissue development. The ideal scaffold mimics the structural and biological functions of a naturally occurring extracellular matrix in terms of physical structure and chemical composition (Zhang and Ma., 2000). The selection of the most appreciate material to fabricate a scaffold to be used in bone tissue engineering application is a critically significant step towards the construction of a tissue-engineered product, since its properties will govern the properties of the scaffold. To meet these

requirements, in recent years many researchers have been carried out to explore potential biomaterials and their composites to fabricate a suitable scaffold that will be used as bone tissue regenerative medicine. Biomaterials mimicking the structure and composition of bone tissues have been fascinated noteworthy attention over the past few decades. They focus on providing a 3D environment for cell proliferation and differentiation. To achieve the best properties for scaffolds, the optimum combination of different components is important (O'Brien, 2011). Up to now, numerous biomaterials have been used to develop scaffolds for bone tissue engineering and bone repair, including metals, natural and synthetic polymers, bioceramics and composite materials. Metals are strong but not biodegradable, on the other handbioceramics and polymers are appropriate for bone tissue engineering as native bone comprises of a naturally occurring polymer and biological apatite.

In this research work, to fabricate biomimicking scaffolds we used hydroxyapatite (HA, Ca10(PO4)6(OH)2) which provides rigidity to bones as it is the main inorganic component of natural bone, type I collagen and chitosan use as polymar. Collagen is suitable for tissue regeneration because of its proper pore structure, permeability, hydrophilicity, and in vivo stability (Trandafir *et al.*, 2007). Collagen is easily degradable and resorbable by the body and permits good attachment to cells. Chitosan has been considerably used as a scaffold in orthopedic and other biomedical applications due to its high biocompatibility, biodegradability, porous structure, suitability for cell ingrowth, and intrinsic antibacterial nature (Vandevord *et al.*, 2002, Martino *et al.*, 2008, Muzzarelli 2009). Chitosan based composite biomaterials of low interconnected porosity for cell attachment and optimum mechanical strength need to be improved. Among the different fabrication techniques, phase separation technique has been shown to be one of the simplest and most promising techniques for developing porous scaffolds. On this basis, three dimensional and constructively stable, highly porous and functional HA-collagen scaffolds were fabricated and studied in this research.

1.2 Objectives

The specific goal of the present study is to fabricate a hydroxyapatite based optimized scaffold through the thermally induced phase separation technique and optimized their concentration, cross-linked with physical and chemical way in order to improve their properties to meet the high demand of bone tissue. Different tests were conducted to characterize the fabricated scaffolds and to assess the feasibility of the composites for bone tissue engineering. The aim of the present study was to fabricate hydroxyapatite-collagen-chitosan based scaffold by exploring the effective method using chemically derived HA and type I collagen extracted from rabbit skin. The specific objectives of this study are as follows:

a) Fabrication, optimization of processing parameter of the hydroxyapatite-collagen-chitosan based vascularized scaffold
b) Physicochemical characterization of the fabricated scaffold by assessing the pore morphology, porosity, density, swelling ability, bio-degradability and cytotoxicity
c) Determination of suitable radiation dose for the physical crosslinking of the scaffold
d) Evaluation of the biocompatibility of the fabricated scaffold for further implementation *in vivo*.

KHULNA UNIVERSITY Central Library KHULNA.

CHAPTER TWO
LITERATURE REVIEW

2.1. Bone

A bone is a rigid organ that constitutes part of the vertebrate skeleton. Bones support and protect the various organs of the body, produce red and white blood cells, store minerals, provide structure and support for the body, and enable mobility. Bones come in a variety of shapes and sizes and have a complex internal and external structure. They are lightweight yet strong and hard, and serve multiple functions.

In the human body at birth, there are over 270 bones (Steele and Bramblett 1988) but many of these fuse together during development, leaving a total of 206 separate bones in the adult (Ali 2017) . The largest bone in the body is the femur and the smallest is the stapes in the middle ear.

2.1.1. Characteristics of bone

Bone is a key constituent of human body. To design an ideal biomimetic artificial scaffold using biomaterials, a full understanding of the structural compositions, biomechanical and biochemical properties of natural bone is obligatory. Bone is a composite material consisted of mineral, matrix, cells and water. It is the most rigid feature of all the connective tissues, largely related with the calcium phosphate (hydroxyapatite) deposited within the bone matrix (collagen) (Ruffieux *et al.*, 2010).

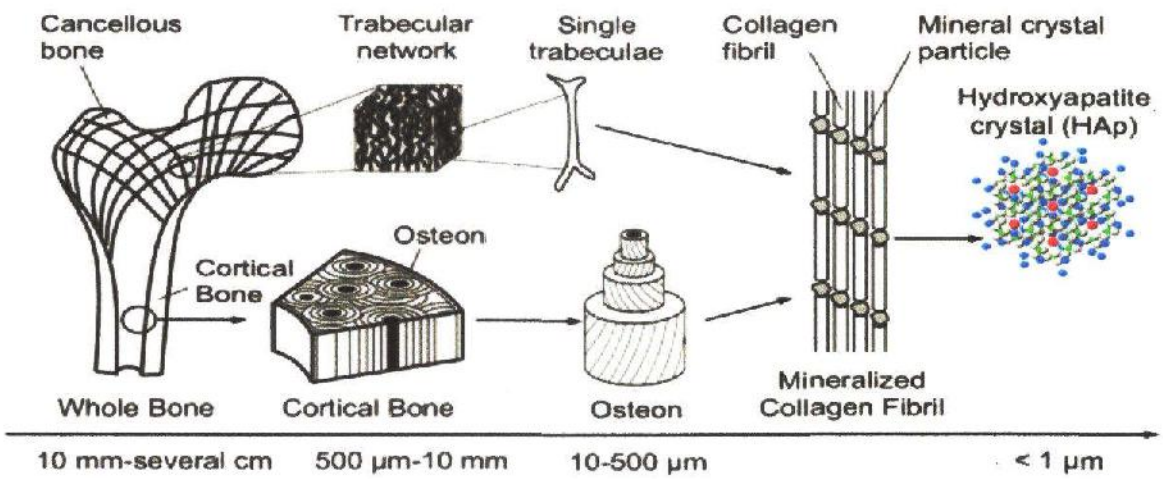


Figure 2.1: Bone Architecture (Webster 2007)

Wahl and Czernuszka, (2006) emphasized the need to produce scaffold as artificial substitute biomaterials for bone replacement by introducing Hydroxyapatite into polymer matrices like collagen or gelatin that will be a leading nanocomposite for bone regeneration.

The basic unit of bone is a hollow coated rod called Haversian system, encompassed with collagen and calcium phosphate materials (Figure 2.1). Cortical bone or compact bone is naturally optimized to control mechanical stability (Sultana and Wang 2008), whereas, inwardly the Haversian systems split off to form a lattice of cancellous bone. Matured bone contains 65% hydroxyapatite (HA) as mineral content; 25–30% collagen as natural polymer and remainder is the milieu (Swain and Sarkar 2014).

The cortical bone and the cancellous bone have 10-20% and 50–90 % porosity respectively. Cortical bone is made up of an interconnected meshwork of rods or plates and average pore size ~125 μm, in which HA nanocrystals provide rigidity being incorporated within collagen matrix (Parkinson and Fazzalari 2013).

Macroscopically the cortical bone has higher compressive stiffness (12-20 GPa vs 0.2-0.8 GPa) and strength (100-230 MPa vs 2-12 MPa) than the cancellous bone (Frohlich and Potvin 2008). The specific organization of tissue microstructure for instance, the Young's modulus along the cortical bone axis is 17 GPa, much larger than the cancellous transverse direction (9.6 GPa) results in strong mechanical strength (Vahabzadeh *et al.*, 2013).

Bone tissue plays vital role in the organization of human body. It provides mechanical support, mineral reservoir; protection for vital organs, milieu for immune system, calcium supply to bloodstream. To fulfill these functions, bone is continuously broken down and rebuilt by certain bone cells (Crampton, 2017).

2.2. Grafting

Grafting a surgical procedure to move tissue from one site to another on the body, or from another creature, without bringing its own blood supply with it. Instead, a new blood supply grows in after it is placed. There are many kinds of grafting are available.

2.2.1. Bone grafts

Bone grafting is a surgical procedure that replaces missing bone in order to repair bone fractures that are extremely complex, pose a significant health risk to the patient, or fail to heal properly (Figure 2.2). Some kind of small or acute fractures can be cured but the risk is greater for large fractures like compound fractures.



Figure 2.2: Bone grafting, wikimedicine

Bone generally has the ability to regenerate completely but requires a very small fracture space or some sort of scaffold to do so. Bone grafts may be autologous (bone harvested from the patient's own body, often from the iliac crest), allograft (cadaveric bone usually obtained from a bone bank), or synthetic (often made of hydroxyapatite or other naturally occurring and biocompatible substances) with similar mechanical properties to bone. Most bone grafts are expected to be reabsorbed and replaced as the natural bone heals over a few months' time.

2.2.2. Autograft

Autografting is a process (Figure 2.3) that involves utilizing bone obtained from the same individual receiving the graft. Bone can be harvested from non-essential bones, such as from the iliac crest, or more commonly in oral and maxillofacial surgery, from the mandibular symphysis (chin area) or anterior mandibular ramus (the coronoid process); this is particularly true for block grafts, in which a small block of bone is placed whole in the area being grafted. When a block graft will be performed, autogenous bone is the most preferred because there is less risk of the graft rejection because the graft originated from the patient's own body (Jeffrey

and Wang 2006). As indicated in the chart above, such a graft would be osteoinductive and osteogenic, as well as osteoconductive.

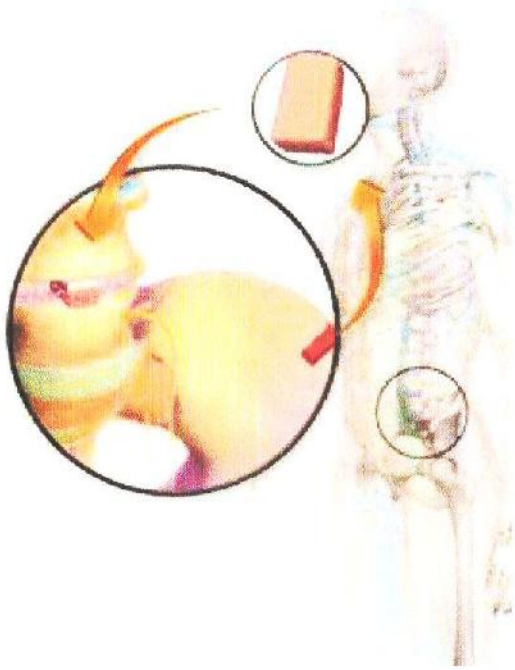


Figure 2.3: Illustration of an autograft harvested from iliac crest. (Jayaswal *et al.*, 2017)

A negative aspect of autologous grafts is that an additional surgical site is required, in effect adding another potential location for post-operative pain and complications (Jayaswal *et al.*, 2017).

2.2.3. Soft tissue grafts

Soft tissue grafting is often necessary to combat gum recession. Periodontal disease, trauma, aging, over brushing, and poor tooth positioning are the leading causes of gum recession which can lead to tooth-root exposure in severe cases (Klokkevold, 2019).

When the roots of the teeth become exposed, eating hot and cold foods can be uncomfortable, decay is more prevalent and the aesthetic appearance of the smile is altered. The main goal of

soft tissue grafting is to either cover the exposed root or to thicken the existing gum tissue in order to halt further tissue loss (Sanz-Martin *et al.,* 2019) The three different types of common soft tissue grafts (Wolfinbarger *et al.,* 2019) include:

2.2.3.1. Free gingival graft

A strip of tissue is removed from the roof of the mouth and stitched to the grafting site in order to promote natural growth. This type of graft is most commonly used for thickening existing tissue.

2.2.3.2 Connective tissue graft

For larger areas or root exposure, subepithelial tissue is needed to remedy the problem. This subepithelial connective tissue is removed from a small flap in the mouth and sutured to the grafting site. This is the most common treatment for root exposure.

2.2.3.3. Pedicle graft

This type of graft involves the "sharing" of soft tissue between the affected site and adjacent gum. A flap of tissue is partially cut away and moved sideways to cover the root. The results of this type of graft are excellent because the tissue that is moved to the adjacent area includes blood vessels that are left in place.

2.2.4. Allograft

An allograft is tissue that is transplanted from one person to another. The prefix alo comes from a Greek word meaning "other." (If tissue is moved from one place to another in your own body, it is called an autograft.) More than 1 million allografts are transplanted each year all over the word (FAD annual report, 2018). Allografts are used in a number of procedures to save lives, repair limbs, relieve pain, or improve a patient's quality of life.

2.2.4.1. Dentin grafting

Dentin bone is made from human extracted teeth (Akazawa *et al.,* 2011). Dentin comprises more than 85% of tooth structure; the enamel consists of HA mineral and comprises 10% of tooth structure. Dentin is similar to bone in its chemical composition, by volume 70-75% is HA

mineral and 20% organic matrix, mostly fibrous type I collagen (Berardini *et al.*, 2019). Dentin, like bone, may release growth and differentiating factors while being resorbed by osteoclasts. In order to make the dentin graft usable and bacteria-free some companies have developed clinical procedures which include grinding, sorting and cleaning of the teeth for immediate or future use.

2.3. Tissue engineering

Tissue Engineering (TE) is a new interdisciplinary subject, established in the 1980s. Its fundamental purpose is to construct artificial substitutes with biological function in vitro, based on the application of basic principles and techniques of engineering and life science (Barber *et al.*, 2015) , for the repair and regeneration of damaged tissues and organs, or to replace part, or all, features of the failing tissues or organs. It represents the connection between the rapid developments in cell and molecular biology, materials science, chemical, and mechanical engineering. The ability to manipulate and reconstruct the tissue function has tremendous clinical implications and could play a major role in cell and gene therapies during the next few years in addition to expand the tissue supply for transplantation therapies (Park *et al.*, 2000).

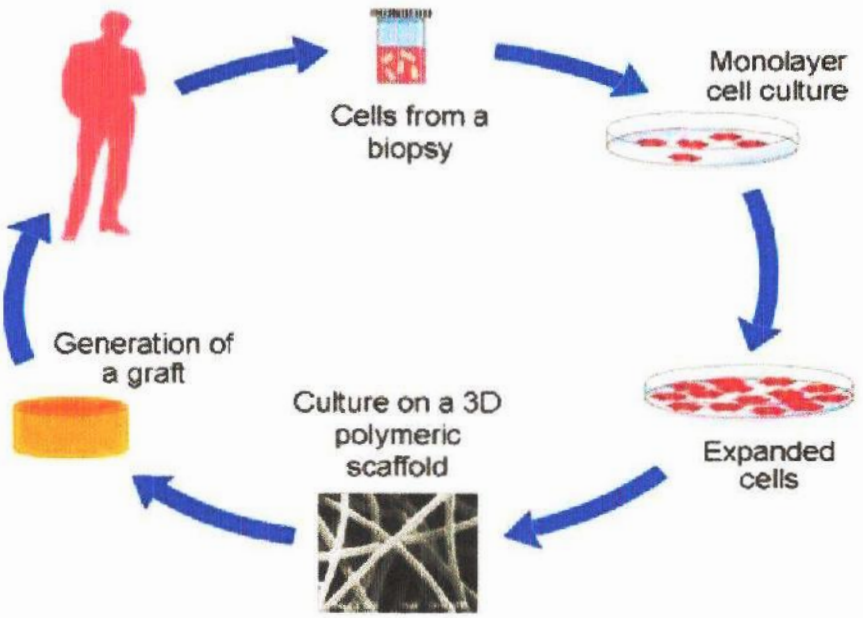


Figure 2.4: Principle of Tissue Engineering Principle, (Ansuja *et al.*, 2016).

The term tissue engineering was initially defined by the attendees of the first NSF sponsored meeting in 1988 as "application of the principles (Figure 2.4) and methods of engineering and life sciences toward fundamental understanding of structure function relationship in normal and pathological mammalian tissues and the development of biological substitutes for the repair or regeneration of tissue or organ function." In 1993, Langer and Vacanti summarized the early developments in this field and defined tissue engineering as "an interdisciplinary field that applies the principles of engineering and life sciences toward the development of biological substitutes that restore, maintain or improve tissue or organ function" (Chapekar 2000).

The goal of tissue engineering is to overcome the limitations of conventional treatments based on organ transplantation and biomaterial implantation (Sachlos and Czernuszka 2003). Through this technology, tissue loss or organ failure may be treated either by implantation of an engineered biological substitute or alternatively with ex vivo perfusion systems.

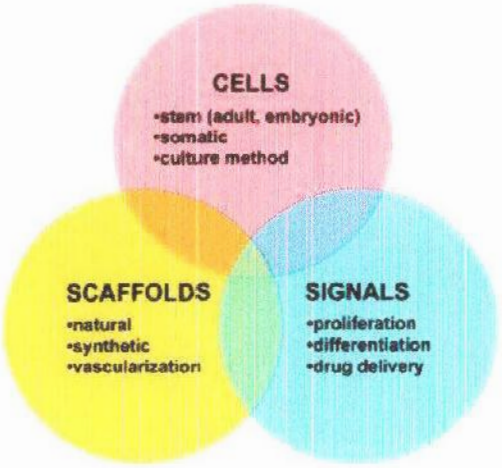


Figure 2.5: Schema of the Three Pillars of Tissue Engineering (Shinsuke *et al.*, 2009)

Tissue engineering has therefore attracted great attention in science, engineering, medicine and in the society. The tissue engineering products may be fully functional at the time of treatment (e.g., liver assisting devices, encapsulated islets), or may have potential to integrate and form the expected functional tissue upon implantation (e.g., chondrocytes encapsulated in a matrix carrier) (Chapekar 2000). The reconstruction of a new tissue by tissue engineering should need some components (figure 2.5). These include: (1) cells; (2) biomaterials as scaffolds substrates; and (3)

growth factors that promote and/or prevent cell migration, adhesion, proliferation, and differentiation (figure 2.5) by upregulating or down-regulating the synthesis of proteins and growth factors (Khang *et al.*, 2007).

2.3.1. Bone tissue engineering

Compared to traditional procedures, bone tissue engineering techniques based on autogenous cell/tissue transplantation would eliminate problems of donor compatibility, supply limitation, pathogen transfer and immune response. Consequently, it has become a rapidly expanding research area since it immerges from the concept of tissue engineering. Bone Engineering usually uses an artificial extracellular matrix (or scaffold), osteoblasts or cells which can become osteoblasts (i.e. bone marrow mesenchymal stem cells) and regulating factors which promote cell adhesion, differentiation, proliferation and bone formation (Liu and Ma 2004). Currently, the scientific challenges of bone tissue engineering are developing suitable 3D scaffolds which act as a template for cell adhesion and proliferation in favored 3D orientations. The scaffolds provide the necessary support for the cells to proliferate, and the ultimate shapes of new bones are defined by the scaffold architectures. Over the past decade, one of the main goals of bone tissue engineering has been to develop biodegradable materials as bone substitutes for filling large bone defects. In addition, such scaffolds must allow the proper diffusion of oxygen and nutrients for the seeded cells on the scaffold as well as proper diffusion of waste out of the materials. The final goal is to return full biological and mechanical functionality to a damaged bone tissue (Chun and Webster 2009).

Bone tissue engineering using biomaterials and cells ranging from primary adult osteoblasts (bone cells) to bone marrow mesenchymal stem cells has found a number of successes in animal models. However, the majority of studies take place in rodents and only a handful have orthoptic applications (i.e. in a bone defect) in larger animals (Cancedda *et al.*, 2007; Meijer *et al.*, 2007). Despite a few clinical successes, translation to human use has suffered from the poor predictive capacity for clinical outcome of the ectopic model in rodents (Marcacciet *et al.*, 2007, Quarto *et al.*, 2001, Cancedda *et al.*, 2003, Schimming *et al.*, 2004, Morishita *et al.*, 2006). This is understandable because in the case of rodents the defect size much smaller and bone modeling rates are much higher than human. But when it comes to human, there is a lack of vascular

However, there are some limitations in the application of such potent biologicals and indeed other growth factors involved in osteogenesis, such as bone morphogenetic proteins (e.g. BMP2 and BMP7, which are now in clinical use) (Ito *et al.*, 2005, Govender *et al.*, 2002, Seeherman *et al.*, 2005). Exogenous administration of BMPs is costly and runs the risk of causing heterotopic ossification (i.e. formation of bone outside the skeleton). Various growth factor delivery strategies may help overcome currently suboptimal release kinetics and the need for unphysiologically high concentrations of growth factors and their problematic short half-life. Gene therapy approaches offer the possibility of local sustained gene expression from genetically modified cells, but the delivery vectors still need optimization (Verma *et al.*, 1997, Hidaka *et al.*, 2003). It is worth noting that both of these approaches fail to recapitulate the complex temporal sequence and combination of growth factors involved in safe and stable bone formation *in vivo* (Figure 2.6).

2.3.2. Scaffolds

Scaffold is a well-designed three dimensional structure that guide tissue formation both *in vitro* and *in vivo*. The scaffold is crucial for the successful engineering of bone tissues as it provides a suitable environment for osteogenic cells to migrate, proliferate, differentiate, and promote new bone formation, and it also provides mechanical competence during the bone regeneration (Vunjak *et al.*, 2005). Degradable porous materials integrated with biological cell or molecules to regenerate tissue are an advanced approach to the tissue engineering that utilizes synthetic implants and tissue graft (Hollister *et al.*, 2006). Consequently, the selection of scaffold is important that enable the cells to behave in the desired manner so that the regeneration of tissue and organs has desired shape and size.

2.3.2.1. Evolution of scaffold

The history of biomedical foams started rather shortly after the discovery of the first implantable biomaterials. Biomaterials initially developed for use inside the human body were selected and designed in order to match the biophysical properties of the replaced tissue, and to induce a minimal toxic response by the host (Hench and Polak, 2002). Suitable implants were fabricated mainly from materials used and developed for different applications, such as metals, ceramics

and thermosetting polymers, which ensured an adequate inertness when in contact with the body's aggressive environment (Figure 2.7).

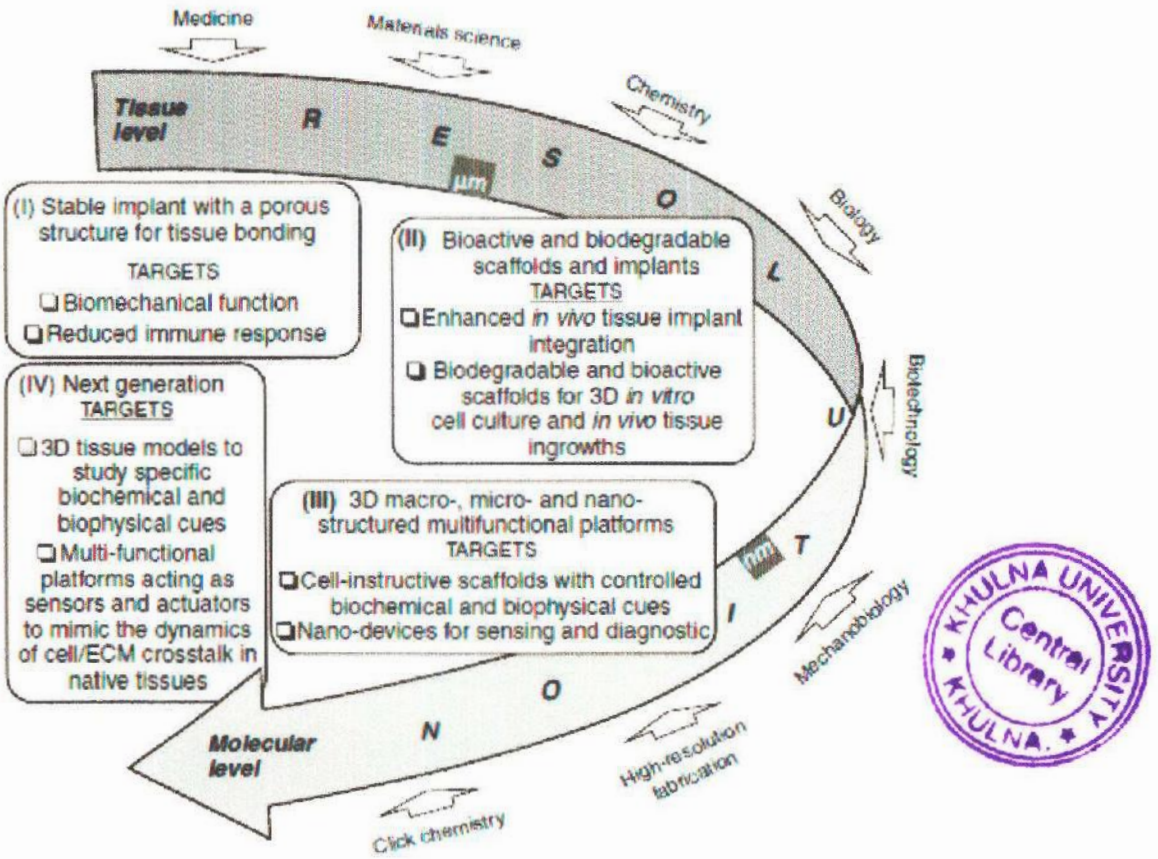


Figure 2.7: Scheme of the evolution of biomedical foams from tissue substitution to repair/regeneration (Netti *et al.*, 2018)

Recreating a porous structure on the surface of bone and vascular prosthetic devices was proposed to improve the bonding between prosthesis and surrounding tissues, and to overcome clinical problems related to implant mobility and stabilization (Poth *et al.*, 1955; Nilles and Coletti, 1973). For instance, Nilles and Coletti (1973) demonstrated that bone prostheses characterized by open porous surfaces can induce tissue in growth at the interface and, therefore, improve their biomechanical performance as compared to non-porous ones. The efficacy of this approach is demonstrated by the fact that modern implants still follow this design principle and features.

KHULNA UNIVERSITY Central Library KHULNA.

Although inert foams allowed the fabrication of prostheses able to replace the mechanical functionality of tissues such as bone, the absence of biologically active surfaces render these materials unable to control the biological response at the interface between implant and surrounding tissue (Hench, 1998; Hench and Polak, 2002). As a direct consequence, an avascular, collagenous fibrous capsule that is typically 50–200 μ m forms all around the implant, leading to several complications and, ultimately, to implant failure.

Improvement of biomedical foams occurred mainly between 1980 and 2000, when novel bioactive materials were developed with the aim of enhancing integration with the surrounding tissue. This was achieved by using, among others, bioactive ceramics and biodegradable polymers obtained from both synthetic and natural resources. The philosophy of these novel materials is that the body should no longer adjust to the materials, but that the materials should interact with the biological components, developing features that improve their response. An example of these materials are bioactive ceramics, such as bioglasses, that promote the in vitro and in vivo deposition and formation of a biological hydroxyapatite layer at the material surface, thus providing a biochemical bonding with the surrounding tissues (Hench, 1998). Bioglasses were used, for example, to coat the porous surface of metallic prostheses, which found clinical use in a variety of orthopaedic and dental applications (Cao and Hench, 1996).

Another advance was the development of biomaterials that exhibited clinically relevant chemical breakdown and degradation. These materials, mainly composed of biodegradable polymers and composites with ceramic particles, were engineered to provide a final solution to the foreign-body reaction, as they have the potential of being ultimately replaced by regenerating tissues (Hench and Polak, 2002).

The development of bioactive and biodegradable biomaterials in the 1980s coincided with the birth of tissue engineering science and the first significant paradigm shift of biomedical foams, from substitution to repair/regeneration (Figure 2.9). During two decades, from 1980 to 2000, great efforts were devoted to designing 3D porous biodegradable substrates, named scaffolds, able to stimulate transplanted cells to regenerate biological tissues with defined sizes and shapes (Langer and Vacanti, 1993). In particular, the scaffold is intended as a three-dimensional temporary support for cells growth and proliferation, while its degradation and mechanical properties are tailored until the formation of a self-supporting newly generated matrix.

Collagen sponge was among the first scaffolds used in tissue engineering for the regeneration of skin-equivalent tissue of full thickness for the treatment of ulcers and acute wounds (Bell *et al.*, 1981). Furthermore, porous scaffolds made of a wide range of synthetic and natural polymers, bioactive glasses and their composites were prepared, and their regeneration potential was assessed by using different cell lines and in vivo models. In particular, great effort was devoted to finding the optimal combination of scaffold composition, degradation rate, pore structure and mechanical properties for the repair/regeneration of tissues such as bone, cartilage, blood vessels, nerve and derma.

Most importantly, cultivating cells on porous scaffolds evidenced several technological problems related to in vitro cell seeding and survival within the 3D porosity. Indeed, inadequate fluid transport and cell viability inside cell/scaffold constructs may result in a necrotic core and the formation of inhomogeneous tissues. Technological approaches based on the use of bioreactors for dynamic cell seeding and cultivation represented a step forward to a more controllable and reliable in vitro tissue regeneration (Martin *et al.*, 2004). Indeed, these bioreactors can improve cell distribution and colonization within the scaffold and, to date, are essential component of in vitro tissue engineering scaffold-based strategies.

The optimization of scaffold fabrication and culture conditions allowed new tissue synthesis both *in vitro* and *in vivo*. However, researchers observed that the biophysical and biochemical properties of these tissues were significantly different from those observed in native conditions. This was ascribed to the fact that cells in native tissues are exposed to a highly dynamic and complex array of biophysical and biochemical signals, originating from the extracellular matrix (ECM). The ECM is the main regulatory and structural component of the tissues, and is composed of fibrous proteins, proteoglycans and glycoproteins (Chan and Mooney, 2008). The ECM signals are transmitted to the outside of a cell by various cell surface receptors and integrated by intracellular signaling pathways, finally regulating gene expression and cell phenotype (Lutolf and Hubbell, 2005). Then, the ultimate decision of a cell to migrate, proliferate, differentiate or perform other specific functions is regulated by this cell/ECM crosstalk. Furthermore, the bidirectional nature of this crosstalk, whereby a cell continuously modifies the properties of the ECM, stimulated further research towards developing scaffolds able to be remodeled by the cells. In particular, over the last decade the concept of cell guidance

in tissue regeneration was discussed and revised, and new knowledge of the complex features of cell–material interaction has been disclosed and elucidated (Causa *et al* ., 2007).

Advancement in chemistry, materials science and nanotechnology allowed studying cell–material interactions by designing and fabricating platforms presenting predefined spatial and temporal patterns of many different biochemical and biophysical signals (Lo *et al*., 2000, Hersel *et al*., 2003, Mart í nez *et al*., 2009, Guarnieri *et al*., 2010, Sharma and Snedeker, 2010, Ventre *et al*., 2012). Cell culture onto the surface of 2D platforms of controlled properties was performed to assess cell response to a wide range of material properties, including topography (Mart í nez *et al*., 2009), stiffness (Lo *et al*., 2000), molecular cues such as cell adhesion peptides (Hersel *et al*., 2003; Guarnieri *et al*., 2010), as well as combination of biophysical and biochemical properties (Sharma and Snedeker, 2010).

It is, however, important to point out that in native tissues cell fate is governed by a plethora of 3D biophysical and biochemical signals in continuous spatial and temporal evolution. Furthermore, the translation of biochemical and biophysical information from 2D platforms to 3D porous scaffolds is rather difficult. Mimicking the functionality of the ECM by using synthetic analogues able to replicate all of the complex biochemical and biophysical functions of ECM is far from being achieved, and represents a great challenge for the tissue engineering community. Recent technological progress has allowed the design and fabrication of three-dimensional scaffolds with high resolution of biophysical and biochemical signal presentation, therefore suitable to test novel molecularly tailored biomaterials for tissue engineering. Such examples are (Figure 2.9): (i) drug releasing scaffolds able to stimulate cell differentiation and tissue vascularization (Shea *et al*., 1999; Huang *et al*., 2002; Ungaro *et al*., 2006; Jeon *et al*., 2007; Tayalia and Mooney, 2009); (ii) photodegradable poly ethylene glycolate (PEG)-based hydrogels that can be manipulated to induce molecular-scale degradation and consequent stem cell spreading, migration or ECM elaboration at any time of culture (Kloxin *et al*., 2009); (iii) 3D porous scaffolds with both precisely engineered architecture and tailored surface topography to study the role of surface topography on stem cells differentiation (Mata *et al* ., 2009); (iv) scaffolds with precise pore structure prepared using two-photon polymerization to study cell migration (Tayalia *et al*., 2008) and; (v) gene- activated scaffolds to study cell recruitment and transfection (Orsi *et al*., 2010).

In the past decade, the impressive increase of high resolution technologies and processes able to control biomaterial chemistry and physical properties down to micrometric and nanometric scales has opened new routes for the application of biomedical foams. Porous devices miniaturized from the macroscal (higher than 1 mm) to the microscale (0.1–100 μ m) have received great attention as microscaffolds for cell transplantation and drug release (Urciuolo *et al.*, 2010; Chen *et al.*, 2011; Choi *et al.*, 2012). Furthermore, nanoscale (down to 1–100 nm) foams ultimately promise integrated implantable systems that can monitor health status and provide prophylactic or therapeutic treatment in situ (LaVan *et al.*, 2003).

It is clear that the synthesis of new materials and the development of advanced manufacturing processes are key requirements for the successful implementation of tissue engineering approaches and, ultimately, for the introduction of biomedical foams into the clinic.

2.3.2.2. Requirements of scaffold

Within tissue engineering, scaffold design is one of the major research areas. A scaffold acts as a temporary support for the isolated cells to grow and develop into new tissue before transplantation back to the host. The functionality of the scaffold depends to a large degree on the design of the construct. Although the specific purpose of the scaffold determinesits final requirements, several general characteristics are needed to consider designing a scaffold for tissue engineering.

The scaffold should have

Biocompatibility- One of the primary requirements of any bone scaffolds is biocompatibilitywhich implies no toxicity, no teratogenicity, no inflammatory reaction, no hemolysis, and no coagulation reaction, etc., meaning that a material can be safely used in the human body. Implanted in the body, the material should not be repelled or cause chronic infection. Moreover, the material should not be cytotoxic to newly formed tissue/surrounding host tissue or display systemic cytotoxicity (Diogo *et al.*, 2014, Chandorkar *et al.*, 2015). An ideal bone scaffold must be osteoconductive where the scaffold allows the bone cells to adhere, proliferate, and form extracellular matrix on its surface and pores. Furthermore, an ideal scaffold

needs to form blood vessels in or around the implant within few weeks of implantation to actively support nutrient, oxygen, and waste transport (Olszta *et al.*, 2007).

Biodegradability- The objective of tissue engineering is to allow the body's own cells, over time, to eventually replace the implanted scaffold or tissue engineered construct. Scaffolds and constructs, are not intended as permanent implants. The scaffold must therefore be biodegradable so as to allow cells to produce their own extracellular matrix. The by-products of this degradation should also be nontoxic and able to exit the body without interference with other organs. In order to allow degradation to occur in tandem with tissue formation, an inflammatory response combined with controlled infusion of cells such as macrophages is required (Whitney *et al.*, 2014).

Osteoinductivity and Osteoconductivity- In addition to good biocompatibility, the synthetic bone scaffold should simultaneously have good osteoinductivity and osteoconductivity. Osteoinductive bone scaffold materials, in combination with growth factors, promote the proliferation of bone marrow mesenchymal stem cells (MMSCs), as well as their differentiation into osteoblasts after implantation. The three-dimensional structure and porous matrix of the bone scaffold with good osteoconductivity, enable the growth of the bone tissue along its surface or internal pores. The newly formed osteoblasts in bone scaffolds with good osteogenesis have the potential for further mineralization and formation of new external bone matrix. Therefore, many scholars have improved the osteoinductivity of bone scaffolds, by changing their physical and chemical properties or by incorporating bone supplements into the scaffolds (Subramanian *et al.*, 2015).

Moreover, the porosity and pore structure of bone scaffolds can be adjusted to enhance the Osteoconductivity (Giannitelli *et al.*, 2015, Veronesi *et al.*, 2015).

Porosity, Pore Diameter and Pore Structure-Ideal bone scaffolds should have interconnected pore networks to promote oxygen, nutrient and waste exchange. This structure plays a decisive role in the osteogenesis of seed cells. Scaffolds with high porosity and large specific surface area promote seed cell adhesion and growth, extracellular matrix deposition, nutrient and oxygen entry, metabolite discharge, and the in growth of blood vessels and nerves (You, 2011).

The ideal pore diameter of scaffold materials should be similar to the size of the normal bone unit (the average size of the human bone unit is about 223 μm). Generally, a scaffold pore diameter ranging between 200 and 400 μm is considered adequate (Akeda *et al.*, 2006).

Furthermore, recent studies have indicated that multi-scale porous scaffolds involving both micro and macro porosities can perform better than only macro porous scaffolds.

Unfortunately, porosity reduces mechanical properties such as compressive strength, and increases the complexity for reproducible scaffold manufacturing. Ideally, the porosity of the three-dimensional structure should be more than 90%, to successfully promote cells adhesion and growth, bone in growth into the material, the transport of nutrients and discharge of metabolites (Datta *et al.*, 2006, Zhang *et al.*, 2007).

Suitable Surface Characteristics- In addition to optimal physicochemical properties, research suggest that introduction of surface topography into the scaffold improves tissue engineering leading to increased tissue function (Falconnet *et al.*, 2006).

2.3.2.3. Biomaterial of scaffold

Biomaterials are originated from a wide range of natural as well as synthetic sources. This section only describes the selection of widely used materials and focuses more on the materials used in this thesis. Many biomaterials have been used as scaffold for cell culture and they can be divided into four main categories: natural polymers, synthetic polymers, bio ceramics and composites (Figure 2.8) (Garg *et al.*, 2012, Zanetti *et al.*, 2013).

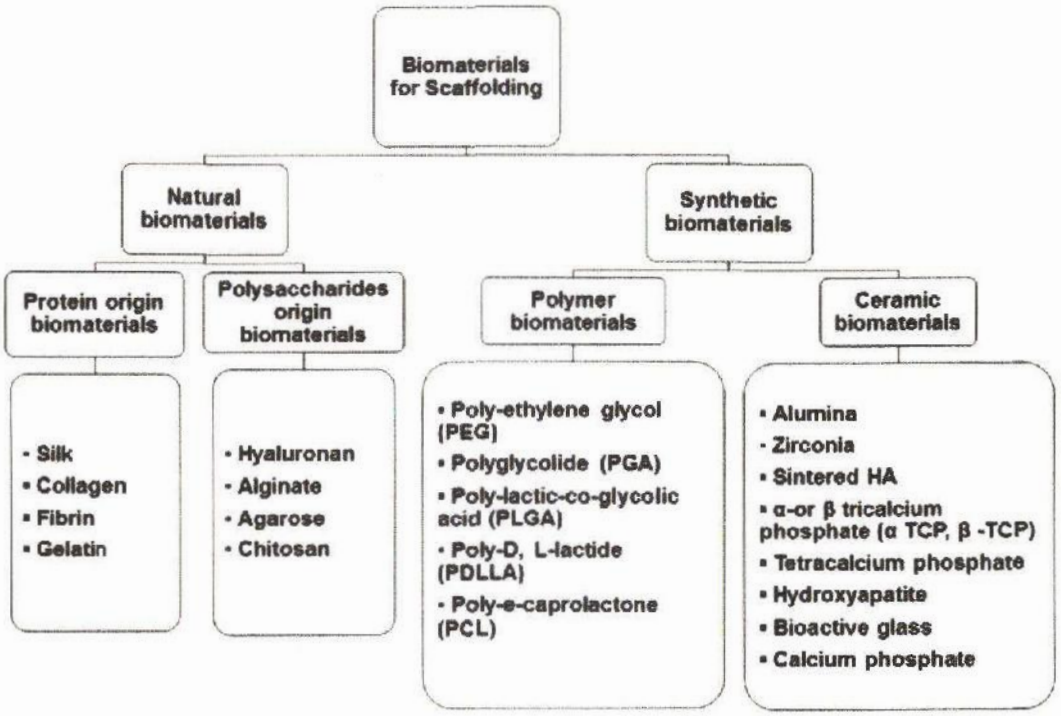


Figure 2.8: Biomaterials for Scaffold Fabrication (Alaribe *et al.*,2016)

2.3.2.3.1. Natural polymers

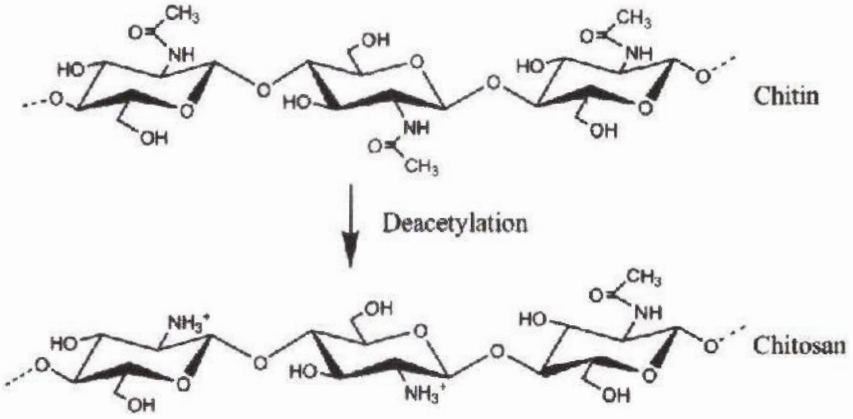
Presently, biomimetic natural biopolymer scaffolds have acquired significance as tissue scaffolds for tissue regeneration because of their superior biological response compared to synthetic scaffolds (Watanabe *et al.*, 2007). These naturally occurring biomaterials can be obtained from their natural sources and processed to make porous scaffolds. The natural biomaterials have several advantages ranging from their availability from replenishable agricultural food resources, biodegradability, to biocompatibility. The natural biomaterials are also known for their ecological safety and possibility of producing numerous enzymatically modified derivatives for different purposes or applications (Watanabe *et al.*, 2007). However, they have limited physical and mechanical stability and therefore they may not be suitable for some load-bearing applications.

Chitosan: Chitosan is a linear polysaccharide derived from partial deacetylation of chitin. Chitin consists of 2- acetamido-2-deoxy-β-D-glucose through a linkage (Figure 2.9) commonly found in the shells of marine crustaceans, insects and the cell walls of fungi (Watanabe *et al.*, 2007). Chitosan has been well investigated for tissue engineering applications. It has been used

extensively as material for regenerating bone, skin and nerve tissues and for use in combination with stem cells.

Studies have shown that in bone tissue engineering, adipose-derived mesenchymal stem cells seeded inside chitosan scaffolds aggregated to form scaffolds (Ma *et al.*, 2006). Effects of using chitosan scaffolds seeded with mesenchymal stem cells and transforming growth factor-β as treatment for lesions on patella of sheep has also been evaluated (Ma *et al.*, 2006). These studies depict that chitosan scaffolds can support both in vivo and in vitro differentiation of stem cells in tissue engineering and regenerative medicine.

Chitosan is usually considered as a statistic copolymer made of N-acetyl-D-glucosamine (GlcNAc) and Dglucosamine (GlcN) repeat units. Chitosan is easier to process and is used to prepare hydrogels, films, fibres or sponges from neutralization of its aqueous acidic solution (Watanabe *et al.*, 2007)..



KHULNA UNIVERSITY Central Library KHULNA

Figure 2.9 Forming Chitosan by Partial Decaetylation of Chitin (Nilsen *et al.*, 2015).

Collagen: Collagen provides strength and structural stability to tissues in the body, such as the skin, blood vessels, tendon, cartilage and bone. It is also the most common protein in the body. Collagen is one of the two major components of the bone, making up 89% of the organic matrix and 32% of the volumetric composition of bone (Figure 2.10). In this sense, it possesses significant potential for culturing cells to produce bone (Ahmed *et al.*, 2008).

2.3.2.3.3. Bio ceramics

A ceramic material used in a biomedical application can be defined a bioceramic material. Bioceramics is the science governing the production of solid ceramic bodies, porous or dense, by the melting of raw inorganic material (Garg *et al.*, 2012) the main application field of bioceramic materials is orthopedics, because of the great affinity of the chemical composition of some ceramic materials with the mineral constituent of bones. The bioceramic materials can be grouped into three classes according to their behavior in the physiological environment: (a) bioresorbable, i.e. calcium and tri-calcium phosphates (TCP), (b) bioactive or surfaceactive, i.e. hydroxyapatite, (c) non-resorbable or inert, i.e. alumina and zirconia. The main disadvantages of these materials are their low mechanical resistance and high brittleness; their main advantages are their high biocompatibility and good osteconductivity.

Hydroxyapatite

Human bone consists (Figure 2.11) of 65–70% hydroxyapatite and 30–35% organic compounds. Hydroxy-apatite (HA, $Ca_{10}(PO4)_6(OH)_2$), is widely used due to its chemical and structural similarity to the mineral portion of bone and the ability of creating a stable bond with the host tissue, consequently, promote a familiar environment of ions for cell migration (Baino *et al.*, 2015). HA ceramics are highly biocompatible in bone tissue regeneration, demonstrate exquisitely good integrative properties and high osteogenic potential (Prakasam *et al.*, 2015). Osteoclast cells appear around the material and subsequently new bone is regenerated with the surrounding osteoblasts. However, the brittleness and fatigue failure of HA in the human body limits the clinical applications only for flexible tissue repair and substitute (Gao *et al.*, 2014).

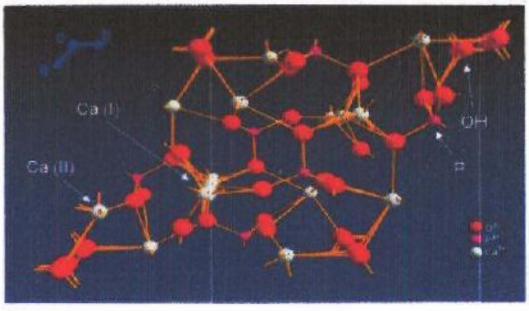


Figure. 2.11: Crystalline structure of hydroxyapatite (Rivera, 2011).

It can be improved by combining HA with synthetic and natural polymers to make the scaffold biocompatible and induce desirable biodegradability in tissue regeneration purpose. This bioceramic has been synthesized by many methods such as ultrasonic irradiation, emulsion liquid membrane, microwave-mediated metathesis, RF thermal plasma, chemical precipitation, micro emulsion and hydrolysis (Barakat *et al.*, 2009). Recently, according to researchers, it has been suggested that, heat treatment could be a demandable alternative strategy to obtain protein-free bovine bone which has inter-connective porous structure and allows faster bone in-growth (Ooi *et al.*, 2007). However, these synthesis processes might be either complicated or biologically unsafe processes, so, recently natural hydroxyapatite bioceramic has been extracted by normal calcinations of some bio-wastes (e.g. fish bones, bovine bones and teeth and bones of pig) (Barakat *et al.*, 2009). Hydroxyapatite consists of Ca^{+2} ions as binding group and carboxyl group of gelatin forms a strong bond between them along with the amino group of polyvinyl alcohol.

Table 2.1: Advantages and Disadvantages of Different Biomaterials (Bhattacharjee, Urrios *et al.*, 2016)

Biomaterials	Advantages	Disadvantages
Metals	1. High mechanical strength 2. High level of osteointegration 3. Allow personalized manufacturing by laser sintering 4. The surface of titanium can be osteoconductive	1. Titanium is not degradable 2. Magnesium degrades but forms hydrogen gas
Natural polymers	1. Biologically active 2. Promote excellent cellular adhesion 3. Biodegradable 4. Minimal adverse immunological response	1. Difficulty in fabricating scaffold homogenously and reproducibly 2. Poor mechanical properties
Synthetic polymers	1. Fabricated with tailored architecture 2. Controlled degradation	1. Risk of rejection due to reduced bioactivity 2. The degradation by-products could cause cellular damage and tissue necrosis
Ceramics	1. Widely used for bone regeneration and display good bone integration 2. High mechanical stiffness Excellent biocompatible 3. Enhance osteoblast differentiation and proliferation	1. Hard brittle surface 2. Very low elasticity 3. Lack remodeling ability 4. Slow rate of degradation

2.3.2.4. Scaffold fabrication method

In native biological tissues, the 3D organization of cells and ECM provides tissues with biophysical and biochemical properties suitable to exploit appropriate function within the body. As in the native tissue, the ideal scaffold for tissue engineering should be able to allow for the correct 3D localization and development of cells and ECM by means of appropriate cues – chemical, biochemical and biophysical. In particular, scaffolds for tissue engineering must be characterized by a porous network of open pores with appropriate size, distribution, shape, surface texture and topography. Concomitantly, the chemical composition of the scaffold material, its surface chemistry and mechanical function, as well as its ability to sequestrate and deliver bioactive factors (e.g. growth factors, ions) to the cells also are key requirements for tissue engineering applications.

Engineering porous scaffolds with tailored properties strongly depend on the manufacturing technique. In this section, a description of traditional and advanced scaffold manufacturing processes is reported, discussing their advantages and current limitations.

2.3.2.4.1. Traditional manufacturing techniques

Conventional techniques for porous scaffold fabrication include textile technologies, porogen leaching, thermodynamic-based processing of polymeric solutions such as gas foaming, phase separation and freeze drying, as well as microsphere sintering.

Textile technologies were among the first approaches for fabricating porous scaffolds for cell culture and in vivo implantation. Indeed, fibres may provide a large surface area/volume that is beneficial for protein adsorption and cell adhesion. Fibre meshes consisting of woven or knitted synthetic fibres made of polyglycolic acid, polylactic acid or their co-polymers have been investigated for cell transplantation and regeneration of various tissues such as nerve, skin, ligament and cartilage (Chen *et al.*, 2002). Increased structural stability of textile scaffolds can be achieved by fibre bonding techniques based on the melting and linking of the polymeric fibres at the cross points (Mikos *et al.*, 1993).

The method of reverse templating was first described by Mikos *et al.,* (1994) to fabricate highly porous (up to 93%) biodegradable polylactic acid foams. The process involves the preparation of polymeric solutions containing appropriate salt (sodium chloride, sodium tartrate or sodium citrate) particles, followed by the setting of the polymer and the dissolution of the salt. This technique has been successively applied to different classes of biomaterials, such as synthetic and natural polymers (Gomes *et al.*, 2002; Guarino *et al.*, 2008), ceramics (Chevalier *et al.*, 2007) and metals (Staiger *et al.*, 2006) to fabricate scaffolds and porous implant for biomedical applications. Further improvements over pore architecture control and mechanical function for load-bearing applications have been reported by the use of continuous porogens (Salerno *et al.*, 2009b).

Gas foaming, phase separation and freeze drying techniques create porous scaffolds by inducing thermodynamic instabilities in multi-phase polymeric systems. In the gas foaming process, a blowing agent is dissolved inside the biomaterials at high pressure, typically in the range of 10–30 MPa, followed by a controlled pressure drop to ambient pressure. This depressurization starts the nucleation and growth of pores inside the material (Salerno *et al.*, 2009a). The absence of toxic chemicals and the optimization of processing temperatures can offer the great advantage of preserving polymer structure and fabricating bioactive and biomimetic scaffolds (Mathieu *et al.*, 2006).

Phase separation and freeze drying are thermodynamic-based processes typically used for fabricating porous polymeric scaffolds by using organic solvents. In these techniques, the synthetic or natural polymer is dissolved in the solvent and the solution brought into a thermodynamically unstable state by decreasing the temperature or adding a non-solvent. This step leads to the formation of a multi-phase system characterized by polymer-rich and polymer-lean phases. The subsequent removal of the solvent from the system induces the crystallization of the polymer-rich phase and the formation of the porous network in the polymer-lean phase. Depending on the polymer–solvent choice and phase separation conditions, highly porous scaffolds, up to 99%, with random or oriented pores can be produced (Guarino *et al.*, 2008).

Microsphere-based tissue engineering scaffold designs have attracted significant attention in recent years, as the microspheres as building blocks offer several benefits, including ease of

fabrication, control over morphology and physicochemical characteristics, and versatility in controlling the release kinetics of encapsulated factors (Shi *et al.*, 2010; Salerno *et al.*, 2012). The properties of the scaffold, in turn, can be tailored by the selection of the raw material as well as by altering the microsphere design and fabrication method.

2.3.2.4.2. Advanced manufacturing techniques

Solid freeform fabrication

One of the common shortcomings of the fabrication technologies discussed above is the difficulty of fabricating scaffolds with predefined reliable and reproducible internal morphology and external shape. To overcome these limitations, in the last decade computer-aided design and manufacturing (CAD-CAM) approaches, namely solid freeform fabrication (SFF), have been implemented to manufacture tissue engineering porous scaffolds with complex architecture and full pore interconnectivity starting from a computer-generated CAD model of the scaffold. The scaffold is then built by using layered manufacturing strategies. Commercially available CAM systems may be categorized into three major groups based on the way materials are deposited (Hollister, 2005):

(i) Laser-based machines that either photopolymerize liquid monomer or sinter powdered materials

(ii) The printing of a chemical binder onto powdered material or directly printing wax, and;

(iii) Nozzle-based systems, such as Bioplotter, that is able to print biological cells as well as a range of biomaterials.

These hierarchical computational techniques have allowed design of three-dimensional anatomic scaffolds from polymers, hydrogels, ceramic and even metal biomaterials and characterized by a porous architecture that balances function and mass transport (Hollister, 2005; Li *et al* ., 2005; Simon *et al.*, 2007). Because of their highly ordered microstructures and full pore interconnectivity, SFF scaffolds often endowed mechanical properties and biological performance better than those achievable by using traditional approaches (Hollister, 2005).

Stereolithography was developed by 3D Systems in 1986, being the first commercially available SFF technique. The manufacturing of porous scaffolds by stereolithography is based on the layer-by-layer spatially controlled solidification of a liquid resin by photo-polymerization using a computer controlled laser beam or a digital light projector (Melchels *et al.*, 2010). A post-curing polymerization is often necessary after draining and washing off the excess of resin, in order to complete the conversion of un-reacted material. To date, stereolithography has been applied to fabricate porous scaffolds made of poly(propylene fumarate) for bone tissue engineering (Cooke *et al.*, 2003), polytrimethylene carbonate for drug delivery application (Jansen *et al.*, 2010), as well as poly(ethylene oxide) and poly(ethyleneglycol) hydrogels-cell constructs for soft tissue engineering (Dhariwala *et al.*, 2004). Recently, microstereolithographic approaches have been also proposed in order to improve the resolution of stereolithographic scaffolds down to few micrometres (Bertsch *et al.*, 2003).

Two-photon polymerization, which belongs to the class of stereolithographic techniques, uses multi-photon excitation of photoinitiator molecules to induce polymerization of a resin. Due to the non-linear nature of two-photon absorption, the resolution of the polymerization volume canbe beyond the diffraction limit, resulting in photopolymerized materials with resolution down to 100 nm (Lee *et al.*, 2008). Although the majority of two-photon polymerization works focused on cell culture on 2D substrates with three-dimensional nano-/micro-structures, some pioneering works also used two-photon polymerization for fabricating 3D porous scaffolds for cell culture and migration (Tayalia *et al.*, 2008). Wylie and Shoichet (2008) also proposed the use of two-photon technique to imprint amines micropatterns inside agarose hydrogel, which can serve as reactive sites for further water-based chemistry and may also create cell adhesion patterns inside agarose scaffolds.

Robotic additive biofabrication, named bioprinting, has emerged as a flexible tool in tissue engineering with potential to build organs or viable tissues (Mironov *et al.*, 2009; Norotte *et al.*, 2009). Bioprinting uses a computer controlled 3D printing device to accurately deposit cells and biomaterials into precise geometries – the goal being the creation of anatomically correct structures. A computer-assisted design can be used to guide the placement of specific types of cells and polymers into precise geometries that mimic natural tissue/organ structure. Although, to date, a complete organ has not been printed yet, bioprinting approaches have been reported for

the manufacturing, among others, of vascular structures (Norotte *et al.*, 2009). The broad spectrum of potential applications and rapidly growing toolboxes of biofabrication approaches can make this technique one of the leading platforms of next scaffold and tissue manufacturing.

High resolution integrated approaches

The increasing demand for nano- and micro-metric controlled 3D scaffolding materials for tissue engineering has led to the development of integrated approaches that combine high resolution 2D structure manufacturing with layer-by-layer assembly. These approaches differ from those of SFF because the 'multi-layer scaffolds' are built in a semi- automated two-step process. This approach has been used for constructing, among others, complex three-dimensional microfluidic scaffolds for tissue vascularization (Vacanti *et al.*, 2010) as well as biomimetic and bioactive scaffolds with precise micro-architecture and surface micro- and nano- textures for controlled cell in growth and differentiation (Mata *et al.*, 2009). In particular, Mata and co-workers have recently proposed a novel 3D production technique that combines microfabrication and soft lithography to construct high resolution porous scaffolds. This technique consists of dual-sided moulding and stacking of polydimethylsiloxane (PDMS) layers characterized by predefined and precise micro-architectures and surface micro-textures and obtained by PDMS replication of photopatterned SU8 layers. The results of their work corroborates those widely reported in 2D that appropriately patterned scaffold surfaces can promote and guide cell adhesion, migration and osteogenic differentiation in three dimensions (Mata *et al.*, 2009). Although integrated approaches can be useful for manufacturing scaffolds with micro- and nano-metric pore surface resolution, there is still the need for improved approaches for a precision layer positioning, as well as a consistent layer bonding and automated assembly.

Table 2.2 Overview of fabrication methods that applied for tissue engineering scaffolds (Mohammadi *et al.*, 2014, Baino *et al.*, 2015, Sabree *et al.*, 2015, Bose *et al.*, 2013).

Type	Process feature	Process method	Used polymer	Advantages	Disadvantages
Electro-spinning	Solvent based	Usually polymer is dissolved into proper solvent and using high-voltage electrostatic field the fiber is formed	Synthetic or natural polymers	No heat, ultrafine fibers (micro- or nanoscale), a wide range of pore size distribution, high porosity and a high surface area	Low mechanical strength because of micro- or nanoscale fibers, possibility of solvent residues
Particulate-Leaching	Solvent based	Polymer solution cast with water soluble particulates and afterwards salt is leached from the system using water	Synthetic or natural polymers	Easy to process, no heat, pore size can be controlled by the size of the salt crystals and the porosity by the salt/polymer ratio	Inter-pore openings may not be controlled, possible solvent residues
Freeze-drying	Transient temperature, solvent based	Solvent in polymer solution is removed by sublimation under very low pressure	Synthetic or natural polymers	High porosity, neither high temperature nor a separate leaching step used in processing, architecture of the scaffold can be controlled by phase separation conditions	Possible solvent residues
H_2O_2 foaming	Sintering, varying the amount of H_2O_2 and thermal treatment	mixing ceramic powder with H_2O_2	Synthetic or natural	Simple	Low porosity control laminar pore structure with poor 3-D interconnection
Sol–gel foaming	initiator and a catalyst provides in situ polymerization	chemical-based wet synthesis involves the conversion of a solution containing ceramic precursors into network of covalently bonded silica via inorganic polymerization	Synthetic or natural	Hierarchical structure can be obtained	Need for a high degree of control of the foam
SLS (Selective laser sintering)	Forming 3D structure, lamination technology	During the SLS process, small particles (powder) of polymer, glass or ceramic are fused together by heat from a high power laser using external force.	Synthetic or natural	Complex internal features can be obtained	Only applicable using ceramic/photopolymer blends, photo-labile high processing temperatures and difficulty removing materials trapped in small inner
Melt Molding Technique	Scaffolds are prepared based on melting polymers/ceramics in the presence of porogens	Porogen helps to melt composition and cooled and freeze dried	Synthetic or natural	control of porosity and pore size possible	High temperature required for non-amorphous polymers and residual porogens

Organic phase burning-out/space holder	Combustion	Organic compounds are burned and mineral formation occurs	Synthetic or natural	High mechanical strength	Difficult to obtain a homogeneous distribution of pores, poor inter-connectivity
CO2 gas techniques	Gas-aided, transient temperature	Solid piece of polymer (usually thermoplastic) is foamed with high pressure CO2 gas	Synthetic or natural polymers	No toxic solvents used	Nonporous surface, mixed open and closed pores
Rapid prototyping Techniques	Transient temperature, solvent based	Computer-aided design fabricated into scaffold usually with layer-by-layer grown constructions	Synthetic or natural polymers	Porosity, pore size, interconnectivity, and geometric stability precisely controlled	Specific material properties needed, limited by the resolution of the used machine
Thermally induced phase separation (TIPS)	separation of solid-liquid, solvent based	solvent-rich phase is removed by sublimation using vacuum leaving behind the polymer as foam	Synthetic or natural polymers	simple and cost effective	precise control over pore size of developed scaffolds
Solid-liquid phase separation	freeze-gelation based, sublimation or solvent exchange	nucleation and growth mechanism, interconnected pores, removal of solvent, freezing polymer solution, followed by solvent removal by either freeze drying	Synthetic or natural polymers	Simple, no toxicity produced	Separation is unstable, porosity lower, solvent limited

2.3.2.5. Scaffolds for *in vitro* cell culture

Engineering of tissues for therapeutic applications by means of culturing transplanted cells within 3D porous scaffolds is one of the most investigated approaches of the tissue engineering research. Indeed, the creation of biological tissues in vitro is desirable for their potential use as replacements for full animal models in basic biological studies and pharmacological and toxicological screens, and as replacement tissues for clinical applications.

In vivo, cell behavior is the result of a cascade of events that relies on the interaction between cells and the 3D microenvironment, comprising the ECM, surrounding cells and molecular cues. In order to recapitulate the in vivo milieu, a key issue is to understand how cells respond to such micro environmental stimuli by determining cell–scaffold crosstalk dynamics. This aspect is essential towards developing cell-instructive materials able to guide successful tissue regeneration.

To date, the effect of scaffolds features, namely composition, degradation, pore structure and mechanical properties on in vitro tissue formation has been assessed extensively for different cell–scaffold combinations. For instance, it has been reported that scaffold-induced regeneration in vitro can be optimized by selecting the constituent material and, in turn, surface chemistry, degradation rate and mechanical properties (Lee *et al.*, 2001; Hu *et al.*, 2003; Sung *et al.*, 2004). Furthermore, the pore structure, namely porosity, pore size, shape and interconnectivity, act in synergy with the other parameters by controlling cell spatial distribution, infiltration and the transport of fluids, such as nutrients and oxygen, across the entire cell–scaffold constructs (Guarino *et al.*, 2008, Salerno *et al.*, 2010b).

Major obstacles to the in vitro generation of functional tissues and their widespread clinical use are related to a limited understanding of the regulatory role of specific physicochemical culture parameters on tissue development (Martin *et al.*, 2004). Furthermore, it has long been known that the supply of oxygen and soluble nutrients becomes critically limiting for the in vitro culture of 3D tissues of thickness higher than 200 μ m (Salerno *et al.*, 2010b). Bioreactors, are devices which able to provide a tight control and monitoring of biological and biochemical processes, have been developed aimed at overcoming limitations of static cultures by providing a dynamically stimulating environment for improved cell behaviour and new tissue development. In particular, bioreactors have demonstrated great potential for

1. Improving cell seeding uniformity, proliferation and ECM biosynthesis within the entire scaffold pore structure characterized by different physical and chemical properties, and
2. Stimulating mechanically transplanted cells to induce correct cell differentiation and tissue development (Martin *et al.*, 2004; Mauney *et al.*, 2004).

Surface modification of porous scaffolds to control protein adsorption and cell interaction is also an important aspect for in vitro strategies. Chemical modifications of synthetic polymers with entire ECM molecules or relevant peptide or glycan fragments, such as arginine–glycine–aspartic acid (RGD), have been used to mediate specific mechanisms of cell adhesion and to control tissue morphogenesis (Chan and Mooney, 2008). This has been almost exhaustively achieved in the case of 2D platforms, allowing the building of a broad library of cell-responsive material properties. For example, it has been demonstrated that the type of peptides used, their

density and spatial distribution at the micro- and nano-scale, significantly affect cell responses (Ratner and Bryant, 2004, Hildebrand *et al.*, 2006). The possibility to extend these procedures to immobilize functional motifs on 3D porous scaffold surfaces has been mainly investigated by means of post-treatments on settled scaffolds. These approaches, involving the dipping of the scaffolds inside reactive solutions of appropriate compositions for a definite time, was successfully used for fabricating RGD-functionalized poly epsilon-caprolactone (PCL) scaffolds prepared via SFF technique for improved fibroblast attachment (Gloria *et al.*, 2012), as well as chitosan/poly(lactic acid–glycolic acid) sintered microsphere scaffolds for bone tissue engineering (Jiang *et al.*, 2009). It is, however, important to point out that, to date, the precise translation of the information achieved in 2D to the cell culture in 3D is still far to be achieved, as it requires high-throughput approaches of combinations and screening of 3D microenvironmental variables.

Considerable knowledge on in vitro new tissue formation has been also obtained by cell culture within hydrogel scaffolds. Indeed, hydrogels are mainly composed of water (99%) inside a highly dense nanofibrous polymeric network, thereby providing a biomimetic environment for cell culture. Furthermore, these materials can be synthesized and processed under physiological conditions and with functionalities adjustable to obtain cell and tissue specificity (Drury and Mooney, 2003; Lutolf and Hubbell, 2005).

Lutholf and Hubbell (2005) fabricated polyethylene glycol-based synthetic hydrogels containing proteolytic domains inside the chemical structure to study cell migration by means of proteolytic degradation of the 3D fibrous structure. This way, the biomaterial becomes the recipient of information differentiation of encapsulated stem cells (Kloxin *et al.*, 2009), as well as gene-activated 3D matrices for cell recruitment (Orsi *et al.*, 2010). Produced by cells and can be remodelled depending on the amount of proteases produced during cell migration. Many hydrogels can be also polymerized in the presence of cells, thereby ensuring a uniform cellular distribution throughout the three-dimensional network (Khetani and Bhatia, 2006). Hydrogels have also been used to test the effect of spatially and temporally controlled three-dimensional gradients of biomolecules on cell fate to finally control tissue development and regeneration. Such examples are photodegradable poly (ethylene glycol)-based hydrogels with local control of stiffness and cell-adhesive peptide ligands to influence chondrogenic differentiation of

encapsulated stem cells (Kloxin *et al.*, 2009), as well as gene-activated 3D matrices for cell recruitment (Orsi *et al.*, 2010).

2.3.2.6. Scaffolds for *in vivo* tissue-induced regeneration

Achieving in vivo tissue-induced regeneration for injured tissues and/or organs by means of porous scaffolds represents the most important goal of tissue engineering. In general, optimal scaffolds for the in vivo tissue repair/regeneration must serve four primary purposes:

(i) They must define a space that will shape the regenerating tissue
(ii) They must provide temporary structural function in the implantation site while tissue regenerates
(iii) They must stimulate the progressive formation of a functional new tissue within the pore structure
(iv) They must degrade progressively, matching the rate of new tissue growth, without releasing toxic by-products

Since scaffold-based approaches were first proposed in tissue engineering, a massive research effort has been carried out about the effect of scaffold composition, microstructure and degradation on in vivo tissue-induced regeneration. Materials from synthetic or natural resources, as well as multiphase composites, have been implanted in well-established in vivo models for the repair/regeneration of tissues such as bone, cartilage and skin (Staiger *et al.*, 2006; Mano *et al.*, 2007; Nair and Laurencin, 2007).

The presence of the pore structure and the maintenance of sufficient structural integrity are critical aspects for in vivo implantation. Indeed, porosity is necessary for initial cell attachment and migration, and for mass transfer of nutrients and metabolites, and provides sufficient space for development and later remodelling of the organized tissue (Karangeorgiu and Kaplan, 2005). Concomitantly, the structural integrity may permit cell and tissue remodelling until achieving stable biomechanical conditions and vascularization at the host site. As the degree of remodelling depends on the tissue itself and its host anatomy and physiology, scaffold degradation and concomitant evolution of structural properties must be accurately controlled for the envisioned application.

In general, scaffold implantation triggers a series of body responses which are included in the so-called 'foreign-body reaction', characterized by nonspecific protein adsorption to the scaffold surface and the adhesion of a number of different cells to the scaffold, such as monocytes/macrophages, leukocytes and platelets. If the inflammation persists, the macrophages fuse together to form giant cells, finally leading to the formation of a collagenous capsule surrounding the implant (Ratner and Bryant, 2004). It is therefore clear that to induce successful tissue regeneration in vivo the scaffolds must be able to control the biological response induced by them. One of the most investigated strategies to address this issue has been the modification of the surface properties of porous scaffolds to guide protein adsorption. Initial protein–material interactions are crucial, as they control and guide cell attachment and adhesion processes. Cell adhesion to adsorbed proteins is mediated through integrin and other receptors located within the cell membrane (Garc í a, 2005). Therefore, it is universally recognized that controlling protein adsorption on the surface of biomaterials may be critical in controlling and directing cell response to biomaterials.

Functional porous biomaterials must also be capable of undergoing an active transformation from one state to another in the presence of biological systems. For instance, the transformation from an injectable state to a solid state is highly beneficial for use in minimally invasive surgical procedures to alleviate problems associated with implantation of prefabricated scaffolds. Injectable materials can also be combined with cells and bioactive molecules to improve regeneration.

In vivo implantation of cell-seeded porous scaffolds belongs to the so-called 'cell therapy' and has been proposed as a suitable approach to improve implant bonding and integration to the surrounding tissue, as well as new tissue vascularization. The positive effect of seeding cells within porous scaffolds before implantation has been reported for different scaffolds and tissues, such as bone (Savarino *et al.*, 2007), cartilage (Vinatier *et al.*, 2009) and muscle (Levenberg *et al.*, 2005). For instance, Savarino and co-workers (2007) combined polycaprolactone scaffoldswith bone marrow-derived mesenchymal stem cells for bone regeneration.

Compared to the neat scaffold, the cell-seeded scaffold improved new tissue formation into the macropores of the implant and neo-tissue vascularization after implantation in rabbits. Similarly,

Levenberg and coworkers (2005) demonstrated that mouse myoblasts and endothelial cells can be co-cultured in vitro within a polylactic acid scaffold to improve the in vivo vascularization, blood perfusion and survival of muscle tissue constructs after transplantation in mice. It is important to point out that scaffold-based cell therapies require appropriate cell culture techniques, which are technically demanding, to achieve the desired tissue maturation before implantation.

2.3.2.7. Platforms for the controlled delivery of bioactive agents

Drug delivery systems have already had an enormous impact on medical technology, greatly improving the performance of many existing drugs and enabling the use of entirely new therapies. Polypeptide growth factors are powerful regulators of biological functions. They modulate many cellular functions including migration, proliferation, differentiation and survival. Therefore, additional direction over cell fate, beyond control of biomaterials chemistry, can be achieved through the spatially and temporally controlled incorporation and release of morphogens and growth factors (Sands and Mooney, 2007; Biondi *et al.*, 2008).

Drug encapsulation can be achieved by simply dispersing the bioactive agent inside the matrix, as widely reported in the case of hydrogels. Alternatively, biomaterials can also be modified to interact with bioactive molecules, thereby achieving a better control over their release. For instance, signals can be released upon degradation of a linking tether or the matrix itself that immobilizes the molecule within the biomaterial, as in the case of heparin-binding drugs (Jeon *et al.*, 2007). The number of binding sites, the affinity of the signal for these sites, and the degradation rate of the scaffold, are key parameters controlling the amount of bound signal and its release profile (Biondi *et al.*, 2008; Chan and Mooney, 2008).

Drug delivery technologies can be of help in designing bioactive porous scaffolds in which low or high molecular weight molecules, such as DNA, growth factors and regulators of the inflammation response should be locally released in a chrono-programmed fashion (Shea *et al.*, 1999; Tayalia and Mooney, 2009). Ungaro and co-workers (2006) fabricated drug releasing scaffolds by incorporating poly(lactic-co-glycolic acid) (PLGA) microspheres inside collagen and hyaluronic acid hydrogels. By tuning the pore structure of both microspheres and the

scaffolds, the authors were able to adjust the releasing rate as requested by the specific application. Incorporating drug-loaded microspheres inside a porous matrix also gives the opportunity of a multiple sequential delivery of growth factors, thereby mimicking naturally occurring processes during tissue regeneration and vascularization (Tayalia and Mooney, 2009). Porous synthetic scaffolds have been also fabricated for the controlled release of growth factors able to recruit mesenchymal stem cells from the host and limit scar tissue formation when implanted in vivo for cartilage regeneration (Huang *et al* ., 2002). In principle, this approach can overcome the complex and expensive steps of in vitro cell seeding within porous scaffolds before implantation.

Efforts to miniaturize drug delivery particulate devices from the macroscale (> 1 mm) to the microscale (0.1–100 μ m) or nanoscale (1–100 nm) can potentially allow for the target delivery of precise dose of the drug, reducing the possibility of missing or erring in a dose.

Drug releasing nanoparticles are already in use in several areas of drug delivery and cosmetics. Usually smaller than 100 nm, nanoparticles are obtained by forming nanocrystals or drug–polymer complexes or by creating nanoscale shells (such as liposomes) that entrap drug molecules. Because of their size, they are often taken up by cells, whereas larger particles would be excluded or cleared from the body. Small molecules, peptides, proteins and nucleic acids can be loaded into nanoparticles that are not recognized by the immune system and that can be targeted to particular tissue types (LaVan *et al.*, 2003).

Carbon nanotubes are well-ordered, hollow porous nanomaterials consisting of carbon atoms and can be described as rolled graphene sheets held together by vander Waals interactions. Carbon nanotubes possess outstanding properties and a unique physicochemical architecture, which may serve as an alternative platform for the delivery of various therapeutic molecules.

2.3.2.8. Microscaffolds for *in situ* cell delivery and tissue fabrication

Porous microparticles have been the subject of intensive research by the tissue engineering community in view of their uses, among others, as drug and cell delivery carriers and building blocks for bottom-up scaffold design and tissue fabrication (Biondi *et al.*, 2008; Urciuolo *et al.*, 2010; Salerno *et al.*, 2012). Indeed, microparticles can be fabricated starting from different

biomaterials, while their composition, size, shape, microstructure and drug releasing capability can be controlled, selecting appropriately the fabrication technique and the processing conditions. Furthermore, the recent development of microfluidic techniques holds great promise in both the fields of drug delivery and tissue engineering, allowing for a very precise control, down to a nanoscale resolution, over the biophysical and biochemical properties of microparticles (Marre and Jensen, 2010).

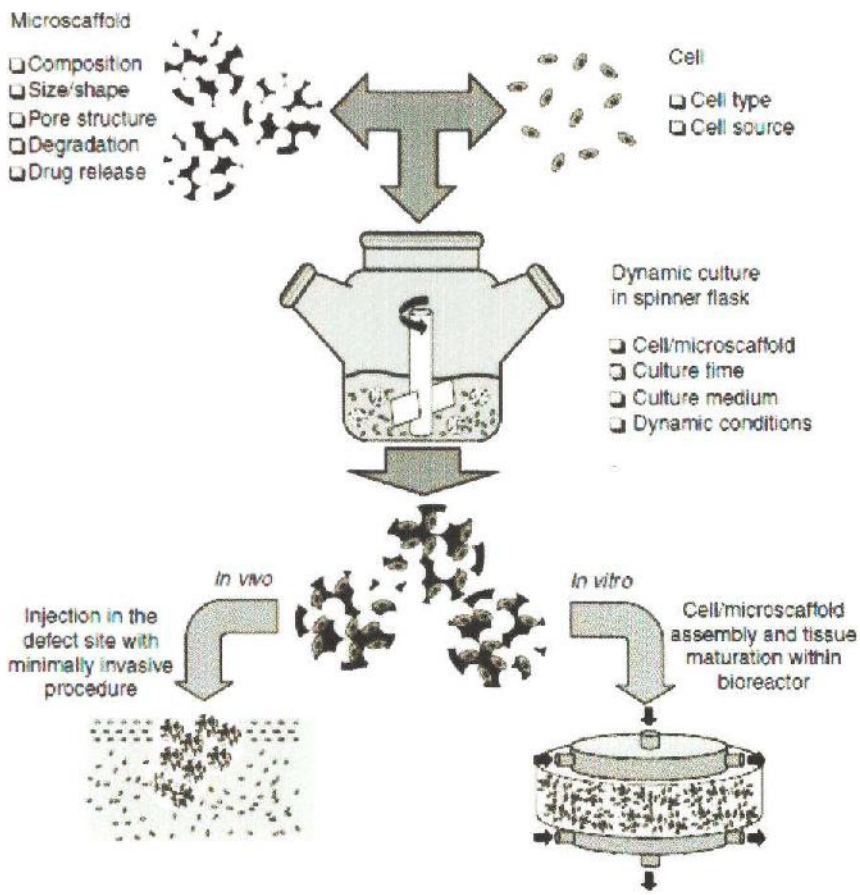


Figure 2.12: Microscaffold approaches for in vitro and in vivo tissue regeneration (Netti *et al.*, 2018)

Microparticulate foams were originally used as carriers for in vitro cell expansion and have since recently been serving as cell delivery systems for cell therapy to regenerate tissue at the site of trauma with minimally invasive procedures (Figure 2.12). Microparticulate foams can be a substrate on which cell populations can attach and migrate, can be implanted with a

combination of specific cell types as a cell delivery vehicle and can also be used as a drug carrier system to activate a specific cellular function in the localized region.

Several studies have highlighted the importance of the pore structure of microscaffolds on their regenerative potential. In vitro cell studies with human keratinocytes and fibroblasts have demonstrated that microparticles with a multicavity surface seem optimal to facilitate cell attachment and proliferation, uniform cell distribution, and ultimately skin regeneration (Huang and Fu, 2010). Similarly, chondrocytes cultured on porous PLGA microscaffolds enhanced significantly in vivo neo-cartilage formation, compared to non-porous ones (Choi *et al.*, 2012). In addition to the formation of a porous structure, a tight control over microscaffold pore size is also essential. Indeed, it has been reported that the increase in pore size from 13 μ m to 36 μ m increased in turn the viability and infiltration of fibroblasts (Choi *et al.*, 2012).

One of the most novel and promising applications of microscaffolds is their use as building blocks for in vitro engineering of viable tissue equivalents (Figure 2.14). In this 'bottom-up' approach, cells are isolated, expanded and seeded onto biodegradable microscaffolds in a dynamic culture. The cell seeded microscaffolds, named microtissues, are then placed in a dynamic culture chamber where they assemble to form a macrotissue (Urciuolo *et al.*, 2010; Chen *et al.*, 2011). Assembling is the result of cell–cell and cell–ECM interactions across the microtissues. The degradation of the biomaterial finally provides the formation of a tailor-made biological tissue.

2.3.2.9. Three-dimensional tumour models

Three-dimensional scaffolds represent highly innovative tools for recreating tumour microenvironmental conditions in culture to study the development and evolution of cancer and to test suitable chemotherapies. Compared to conventional 2D cultures, tumour cells maintained in 3D scaffold-based models exhibit characteristics that are more representative of their behavior in vivo (Fischbach *et al.*, 2007; Pathi *et al.*, 2010). In recent years, 3D tumour cell culture approaches have dramatically improved our understanding of the role of 3D culture on tumour cells. These newly developed tumour models have demonstrated great utility in the investigation of cancer progression and are also used as a new test system for antitumour drugs. Porous

scaffolds prepared starting from natural polymers such as collagen, chitosan and alginate have been investigated as 3D templates for tumour models. For instance, Mitsiades and co-workers (2000) developed a 3D cancer model by co-culturing human osteoblasts and cancer cells within a collagen scaffold. The construct was prepared by mixing osteoblasts with a collagen solution, followed by scaffold setting and subsequent inoculation with cancer cells. In the majority of cases, the inoculation of cancer cells induced a blastic reaction, evidenced by an increased osteoblast proliferation and a higher collagen density. Fischbach and co-workers (2007) used a porous PLGA scaffold prepared via gas foaming and salt leaching to study the angiogenic characteristics of transplanted cancer cells. In vitro culture was optimized in order to induce a central hypoxia within the cell/scaffold construct to mimic 3D tumour-like tissue context. By correlating in vitro and in vivo models, the authors were able to study the angiogenic characteristics of tumour cells and the effect of chemotherapy agents on tumour progression. In order to provide a more reliable model to study bone metastasis, Pathi and co-workers (2010) compared the behaviour of cancer cells within non-mineralized or mineralized polymeric scaffolds. As a result, the authors observed improved tumour cell adhesion, proliferation and secretion of pro-osteoclastic interleukin-8 in mineralized tumour models, demonstrating the role of hydroxyapatite on neoplastic and metastatic growth of cancer cells in bone.

2.3.2.10. Bone tissue engineering in Bangladesh perspective

Since last few years road accidents have been increased dramatically in Bangladesh. In 2013, the number of road accidents across the country was 2,753. In addition, the next year it was 2,713 and 6,582 people were dead and 10,770 people were injured. In 2017, the number of patients admitted was 25,065 furthermore 27,785 patients were operated in NITOR (National Institute of Traumatology & Orthopaedic Rehabilitation) hospital, Bangladesh (Table-2.3). Evidently, annual report of NITOR says, 4486 people were injured in unspecified motor-vehicle accident, 2,182 were injured in collision between car and pick-up truck or van, fracture of bone following insertion of orthopedic implants, joint prosthesis, or bone plate were 2,050, biomechanical lesions 1,280, other maltreatment syndromes were 370, injury of spinal cord were 235, osteomyelitis were 144 (NITOR annual report, 2017).

Table 2.3 National Institute of Truamatology & Orthopaedic Rehabilitation (NITOR) annual report, 2011- 2017

Yearly Patient Statement- 2011 to 2017			
Year	**Patient attendance**	**Patient admission**	**Total operation**
2011	117903	20144	24560
2012	130667	21001	25994
2013	135609	17410	25515
2014	135537	19947	31443
2015	155303	21698	27920
2016	162602	22787	28203
2017	178862	25065	27785

This huge population of Bangladesh is suffering from bone disorders every year either by road accidents or other fatal causes. In comparison to this vast population disorders, only a few hospitals are facilitated with orthopedic treatment strategies. They can hardly provide accommodation and appropriate treatment to these people. Besides, the expense of the treatment is beyond patients' affordability. Therefore, death rate and bone abnormalities are increasing exponentially day by day. Bangladesh Atomic Energy Commission has taken a step forward to meet this problem and started applying grafting method for bone treatment. At present more than two hundred hospitals and clinics in Bangladesh are using the graft materials in tissue transplant surgery and this is increasing day by day. To meet this increasing demand of graft materials, Institute of Tissue Banking and Biomaterial Research (ITBBR) of Bangladesh Atomic Energy Commission conducts tissue banking activities throughout the country. It is the only tissue bank in Bangladesh regularly providing radiation sterilized amnion membrane and bone allograft to different hospitals and clinics that have been using successfully in different types of clinical disorders and injuries, such as bone cancer, degenerative bone diseases, congenital deformities, bone fractures, gap non-union from traumatic accidents, oral and maxillofacial defects etc. At present, research is mainly focused on tissue engineering for bone tissue related surgeries. As a part of this, the institute is working on the fabrication of homogenous biocompatible scaffolds for tissue engineering. They also process freeze dried radiation sterilized cancellous bone allografts to treat osseous defects for skeletal regeneration. To prepare CBA (Cancellous bone allograft), raw bones (femoral heads and condyles) were accumulated from clinically acceptable live donors undergoing surgical treatment. Bone tissues were pasteurized, processed, radiation

sterilized and preserved according to the protocol set by ITBBR based on guidelines of International Atomic Energy Agency (IAEA), the European Association of Tissue Banks (EATB) and the American Association of Tissue Banks (AATB).From July 2016 to June 2017, 833 raw bone tissues were accumulated from different hospitals and freeze dried radiation sterilized bone allografts were prepared for clinical use in orthopedic reconstruction.

As a part of their research, the institute also process frozen irradiated cortical bone allografts for reconstruction of massive bone defects. Clinical situations associated with large bone bone loss brings in the process where cortical bones such as femur, tibia, fibula, cranial bone etc. were collected from seronegative live donor after total knee replacement (TKR) operation, corrective osteotomy, primary traumatic limb amputation surgery etc. and processed with gamma irradiation and finally transferred to hospitals after proper packaging. During the reporting period, 3 massive bones were supplied for clinical use in limb salvage surgery. From July 2015 to June 2016, using bone allografts 284 patients suffering from different orthopedic complications, such as giant cell tumor, bone cyst, spinal defects, bone fracture, osteolytic lesion, fibrous dysplasia etc. were treated successfully. During this period 11704 cc bone grafts were supplied to the different hospitals and clinics throughout the country.

ITBBR also process demineralized bone granules for the treatment of oral and maxillofacial bone defects. For demineralized bone granule preparation, pasteurized bones were cut into pieces (cortico-cancellous and cancellous bone pieces) and washed with sterile distilled water. The bone pieces were then defatted by treating with chloroform: methanol (1:1) solution, crushed, demineralized with 0.6 N hydrochloric acid (HCl) and washed with phosphate buffer solution (pH 7.0) to neutralize the activity of acid followed by washing again several times with sterile distilled water. The granules were then freeze dried at –50°C for approximately 24 hours. Bone granules were then dispensed in 2 cc plastic vials; the vials were wrapped in polyethylene pouches (triple layered), labeled, and sterilized by gamma irradiation (25 kGy). During the period, 16 vial demineralized bone granule were prepared for clinical use in oral and maxillofacial surgery.

Different types of composite scaffolds have been fabricated by ITBBR using different different mineral and polymer compositions with various solvents using thermally induced phase separation (TIPS) technique and freeze drying. The composite scaffolds were characterized to

determine porosity, density, swelling kinetics, biodegradability, morphology and biocompatibility. The composites were compared to human cancellous bone allografts, prepared in ITBBR. The upshot of this research might have significant effects in the development of scaffolds which will be used in clinical trials as replacement of bone allograft to treat bone defects. As a consequence the institute will be able to provide better support for the treatment of bone defects and hopefully for the socio-economic development of our country (BAEC annual report, 2015-2016, 2016-2017).

As a part of these initiatives to fabricate optimized scaffold composite, we have experimented with type 1 collagen-hydroxyapatite-chitosan based scaffold with a goal to achieve the reproducible optimized ratio of composite to increase both cell proliferation and ultimately clinical practices.

CHAPTER THREE

MATERIALS AND METHODS

3.1 Working Place

The research work entitled **"Study on the Fabrication, Optimization of Processing Parameters and Characterization of Collagen Based Vascularized Scaffolds for Biomedical Application"** was designed and carried out in the Institute of Tissue Banking and Biomaterial Research (ITBBR), Atomic Energy Research Establishment (AERE), Savar, Dhaka from July, 2018 to August, 2019. An outline of this research has been depicted as a flowchart and schematic diagram in figure 3.1 and 3.2 respectively. All the chemicals and equipment used in this study are given in Appendix I and II.

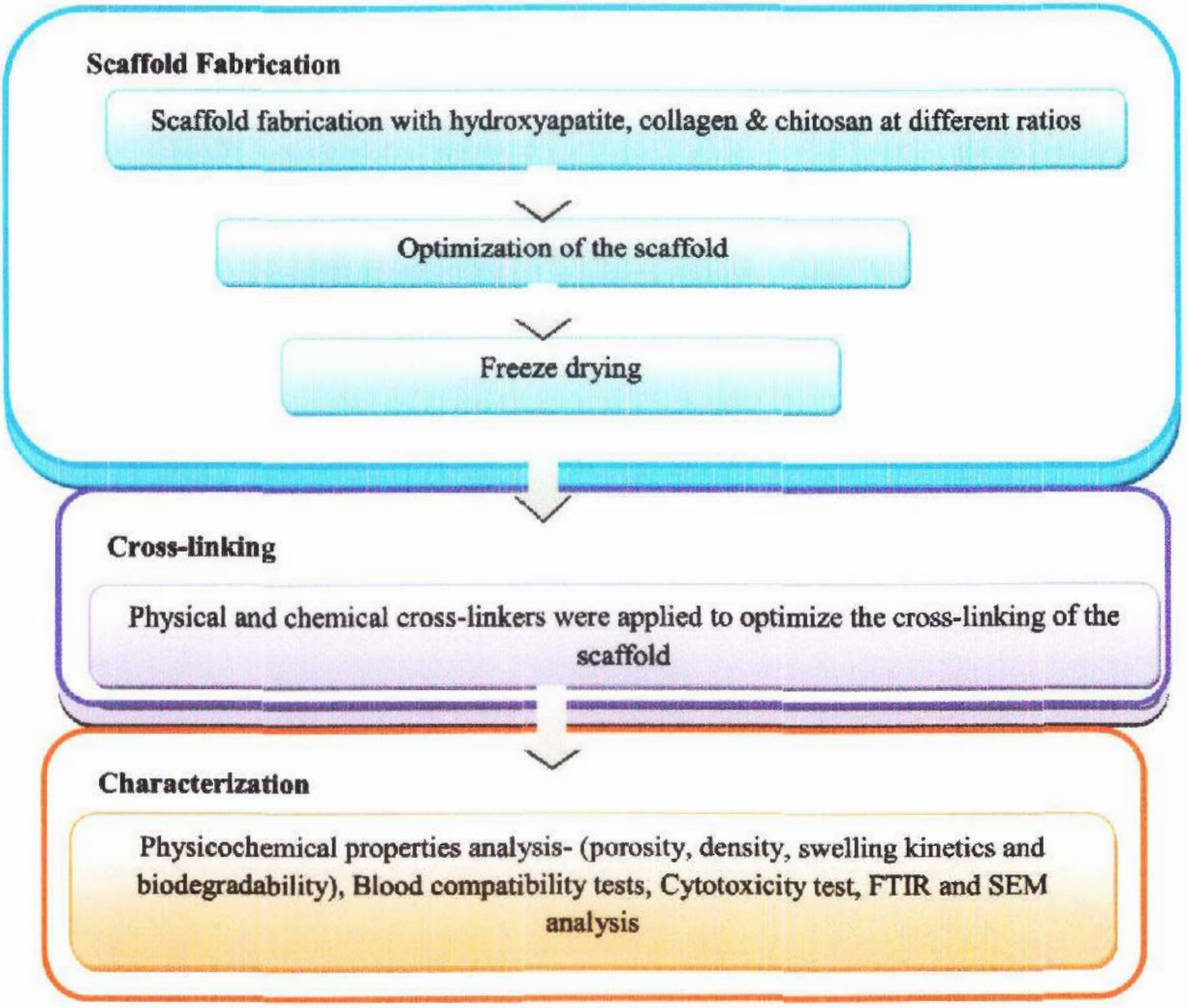


Figure 3.1: Flow Chart of Experimental Design

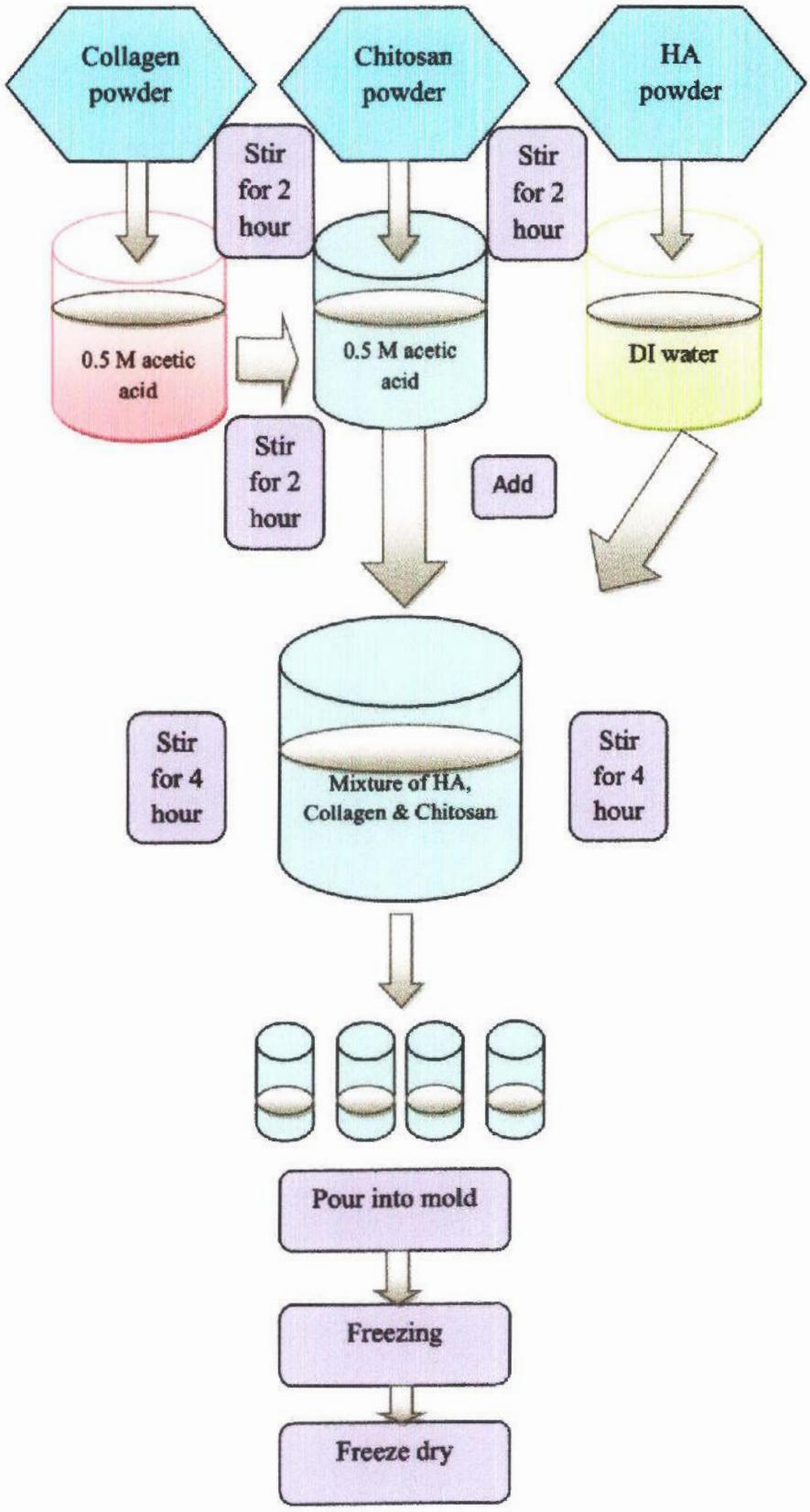


Figure 3.2: Schematic Diagram of Experimental Design

3.2. Extraction of collagen

The extraction process was performed according to the Martinez-Ortiz et al. with some modification (Figure 3.3A-F). Pretreated skins were cut into small pieces (approximately 1 cm^2 and suspended in 0.05 M acetic acid solution at a solid-to-solvent ratio of 1:10 (w/v). The sample was in a shaking incubator (Phoenix Instruments Inc., USA) at 200 rpm for 24 hours at room temperature (22 ± 2°c). After this time the sample was filtered and the liquid portion was called 'acid extraction'.

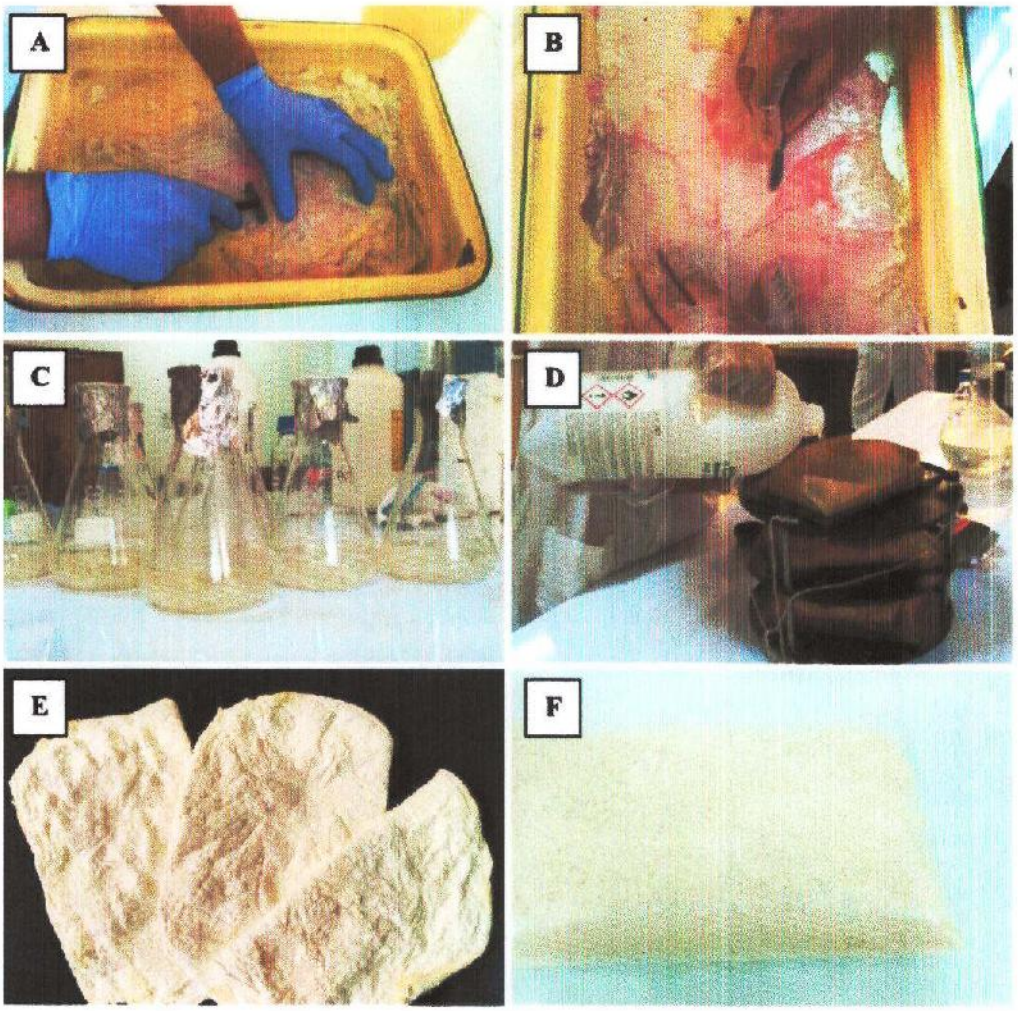


Figure 3.3: Extraction of collagen: (A) Removed hair; (B) Defatting of skin; (C) Mince & Shaking; (D) Plating; (E) Freeze dry collagen; (F) Mashing collagen powder.

After this time, the acid extraction, the non-dissolved residue was used for pepsin soluble collagen extraction as follow: the residues were re-suspended in a new solution of 0.5 M acetic acid at a concentration of 1:10 (w/v) and pepsin at a concentration of 1 g/L. This solution was placed in a shaker machine at the same speed as described above for 48 hours; this process is referred to as 'enzymatic treatment'.

All the samples were filtered and stored at 4°C at the end of every single extraction. Acid and enzymatic collagens were precipitated with a solution of 2.6 M sodium chloride. The precipitated material was centrifuged for 30 minutes at a relative centrifugal force of 10,000 rpm in a centrifuge (Model 6800, Kubota, Japan). The samples were re-suspended in five volumes of 0.5 M acetic acid and dialysed for 48 hours in distilled water and dialysis membrane tubing with 6–8 kDa molecular weight cut-off. The resulted dialysed material was freeze-dried and the collagen was powdered (figure 3.3).

3.3. Preparation of hydroxyapatite powder

To fabricate a porous bone tissue scaffold, firstly hydroxyapatite was prepared chemically. The protocol developed by ITBBR of AERE. Prepare 0.15 M $Na_2HPO_4.2H_2O$ (A) and 0.25 M $Ca(NO_3)_2.4H_2O$ (B) Solution. A and B solution mixed into 2 liters deionized water separately. 0.8 M NaOH was added in solution A for increasing pH (pH ~ 11.0). Then solution B mixed into solution A slowly. The mix solution was boiling in micro-oven at least 20 minutes. Afterward, the boiled solution filtrated with 200nm pore size filter paper. After filtration process the retentate was washed by deionized water at least three times. The aqueous retentate dried at 50^0C for 24 hours and then crushed with mortar- pestle. The crush powder was cantering at 800^0C for 2 hours at 3^0C/min rate. Then the power was crushed again, added ethanol at 70:30 radio and transferred boll milling machine (Figure 3.4). Ethanol was evaporated from liquid HA solution by drying overnight at dryer and then crushed with mortar- pestle.

KHULNA UNIVERSITY Central Library KHULNA

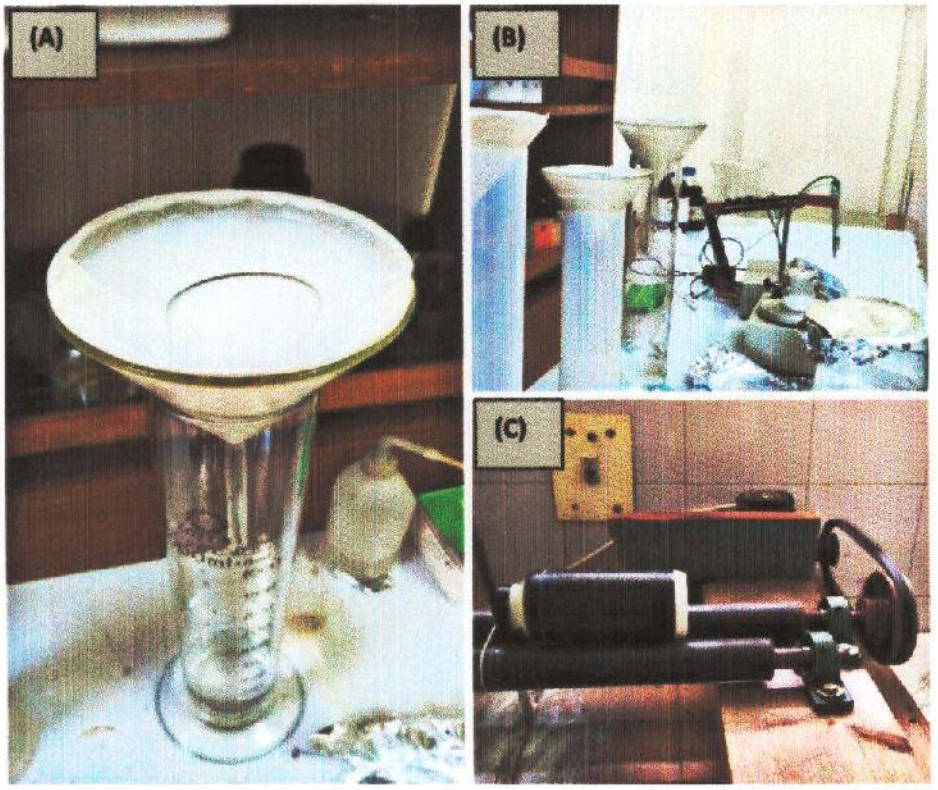


Figure 3.4: Preparation of hydroxyapatite powder: (A) Filtration; (B) Control pH; (C) Boll milling.

3.4. Fabrication of Hydroxyapatite-Collagen-Chitosan scaffolds

Scaffolds were fabricated according to the protocol of Teng *et al.*, 2015, Chan *et al.*, 2012, Luo *et al.*, 2011 with modifications. Hydroxyapatite-Collagen-Chitosan scaffolds were prepared using thermally induced phase separation technique. To fabricate a porous bone tissue scaffold, firstly hydroxyapatite was prepared chemically from $Na_2HPO_4.2H_2O$ and 0.25 M $Ca(NO_3)_2.4H_2O$ chemical compounds (briefly described 3.2.2). Type I collagen was extracted from rabbit skin according to the Martinez-Ortiz *et al* (briefly described 3.2.1).

Collagen and chitosan powder was weighed as per required and dissolved in 0.5M acetic acid solution in 200ml beaker each. The mixture was stirred for 2 hours at room temperature until the collagen and chitosan powder was thoroughly dispersed in 0.5M acetic acid solution. Then HA powder was weighed as per required and dissolved in distill water. Three solutions were mixed together and stirred for 4 hours at room temperature to achieve a complete uniform mixture. The resultant solutions was transferred to mold and frozen at -20^{0}C for 24 hours. The samples were

then freeze dried at -50^{0}C to -60^{0}C to obtain porous scaffolds. The solid to liquid ratio varied from 6:94 to 15:85 in order to optimize the standard scaffold concentration for further tests. The mineral to polymer ratio was maintained as 70:30, 60:40, 50:50, 40:60 and 30:70 respectively. Polymer-polymer ratio also maintained as 1:1, 1:2 and 2:1 respectively. For example, in the case of solid:liquid ratio of 10:90, mineral:polymer ratio of 60:40 and Polymer-polymer ratio 1:2, for 100 ml fabrication 1.33g collagen was dissolved in 20 ml 0.5M acetic acid solution under agitation and stirred for 2 hours. At the same time 2.66g chitosan was dissolved in 60 ml 0.5M acetic acid and 6g HA was dissolved 20 ml distill water. Once the collagen & chitosan were completely dispersed in 0.5M acetic acid solution, and then mixed three solutions together. Thereafter, the mixture was poured in a mold and frozen at -40^{0}C and finally freeze dried for further characterizations.

3.5. Addition of Cross-Linkers

After observing the initial physical properties such as porosity, densities, swelling kinetics and biodegradability, the most suitable lyophilized porous scaffolds were stabilized via cross-linking with physical and chemical cross-linking agents. The chemical cross-linkers were glutaraldehyde (GTA) solution (1.5%) and 1-ethyl-3–3-dimethyl aminopropylcarbodiimide (EDAC)/N-hydroxysuccinimide (NHS) using a concentration of 6 mM EDAC $g^{-1}$of collagen and a 5:2 M ratio of EDAC:NHS, while dehydrothermal (DHT) treatment in a vacuum oven at 105^{0}C temperature under a vacuum of 0.05 bar for 24 h and irradiation at different doses (5-30 kGy) were used as physical cross-linking methods.

3.5.1. Addition of Chemical Cross-Linkers

Scaffolds were cut into same sized cubic pieces and immersed into chemical cross-linkers such as GTA solution (1.5%) and EDAC/NHS using a concentration of 6 mM EDAC $g^{-1}$of collagen and a 5:2 M ratio of EDAC:NHS for 4 and 2 hours respectively and then washed with deionized water for at least 1.5 hours changing the water after every 15 minutes to eliminate the excess chemicals and reaction by products (urea) from the scaffolds. The scaffolds were then frozen at -40^{0}C for 24 hours and finally lyophilized in a freeze dryer to obtain porous HA-collagen-chitosan composite scaffolds.

3.5.2. Addition of Physical Cross-Linkers

The scaffolds were physically cross-linked via DHT treatment in a vacuum oven at 105^{0}C temperature under a vacuum of 0.05 bar for 24 h and irradiated at different doses (5-30 kGy) in order to stabilize the binding strength among the components of the scaffolds.

3.6. Scaffold characterization

The fabricated final samples and resultant structures of porous bone scaffolds were characterized by analyzing their physical, chemical and biological properties.

3.6.1. Porosity and Density Determination

The liquid displacement method was used to determine the porosity and density of the prepared scaffolds. A solvent other than deionized water should be used in this test. Ethanol was taken as the displacement liquid as it permeates the scaffolds without swelling or shrinking the matrix.

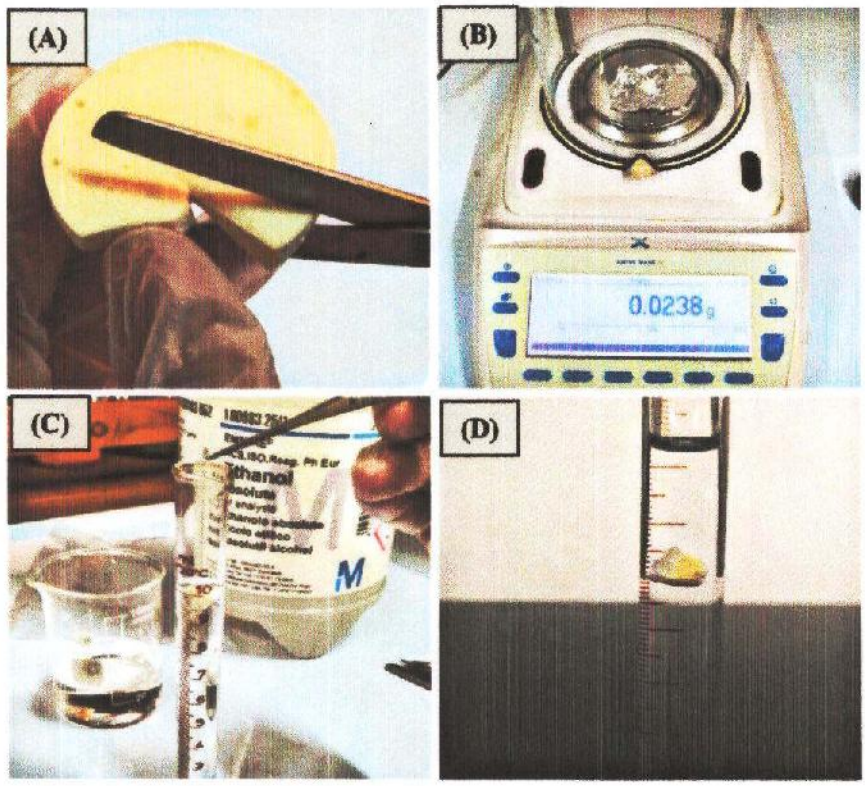


Figure 3.5: Porosity and Density Determination: (A) Cut into small pieces; (B) Measurement its weight; (C) Immersed into ethanol; (D) Observation.

To conduct this test, scaffolds were cut into pieces of weight W and immersed into a graded cylinder containing a known volume (V_1) of ethanol for five minutes. The cylinder was placed in a vacuum in order to force ethanol into the pieces of scaffold until no air bubble emerged from the scaffold. The total volume of ethanol and scaffold was recorded as V_2. The volume difference ($V_2 - V_1$) was the volume of the framework of the scaffold. The scaffold was removed from the ethanol and the remaining ethanol volume was measured as V_3 (Figure 3.5). The total volume of the scaffold, V, was then, $V = V_2 - V_3$

$$\textbf{Porosity (\%)} = (V_1 - V_3)/(V_2 - V_3)$$

The apparent density of the scaffold, ρ was evaluated using,

$$\textbf{Density, } \rho = W/(V_2 - V_3)$$

3.6.2. Swelling Kinetics test

Swelling ability was determined by the percentage of water absorption. Dry weight of the scaffold was denoted as W_d. Then, porous scaffolds were immersed in PBS buffer (Phosphate-buffered saline) solution with pH 7.4 at 37°C for 24 hours. Afterward, the scaffolds were taken out from PBS buffer solution and its wet weight was measured, denoted as W_w (Figure 3.6). The ratio of swelling will be calculated using equation,

$$\textbf{Swelling ratio (\%)} = ((W_w - W_d)/W_d) \times 100$$

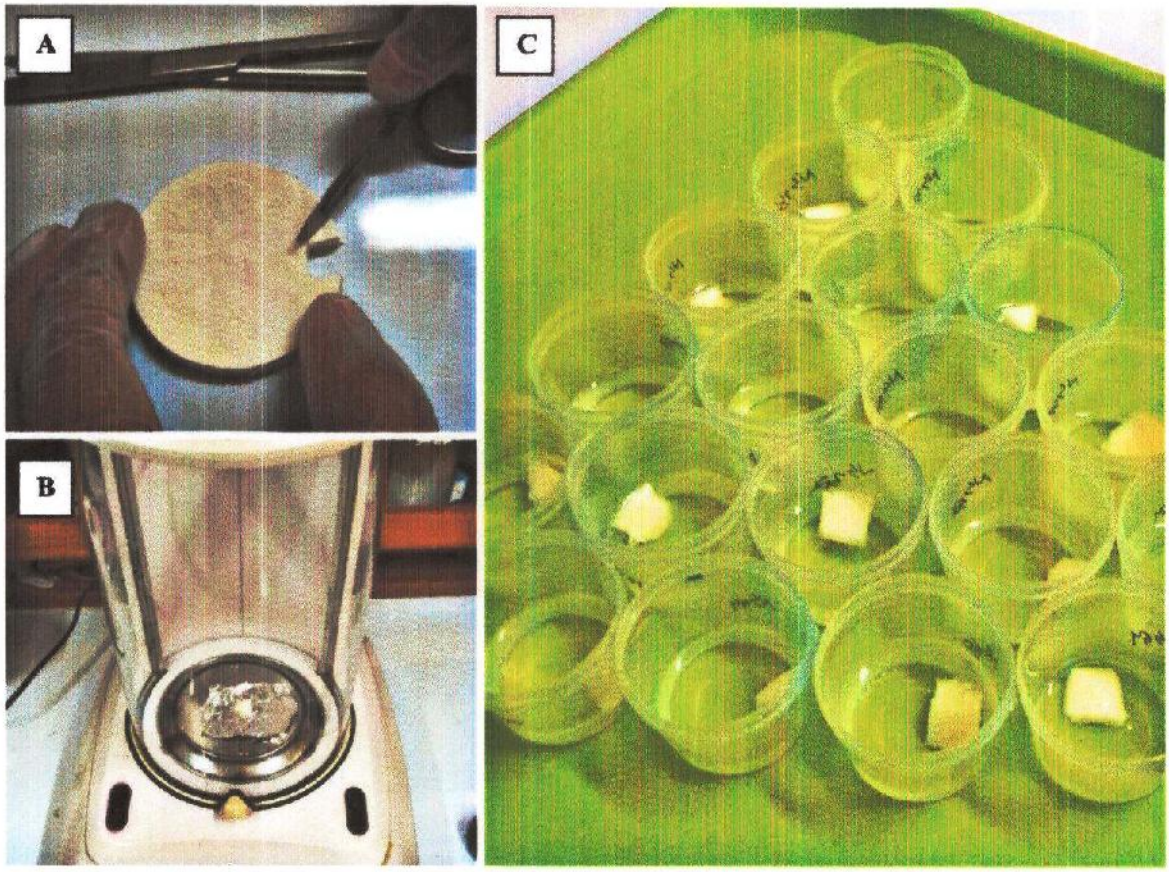


Figure 3.6: Swelling Kinetics test: (A) Cut into small pieces; (B) Measurement its weight; (C) Immersed into PBS buffer.

3.6.3. Biodegradation Test

Biodegradability of the scaffolds were characterized by in vitro study. The scaffolds were immersed in SBF buffer (Simulated body fluid) medium at 37 °C for 7, 14, 21 and 28 days (Figure 3.7). The initial scaffold weight was denoted as W_0. After selected days, the scaffolds were washed in deionized water to eliminate ions adsorbed on the surface and then freeze-dried. The dry weight of the scaffold was denoted as W_t. The degradation of the scaffold was calculated using equation,

$$\textbf{Biodegradability (\%)} = ((W_0 - W_t)/W_0) \times 100$$

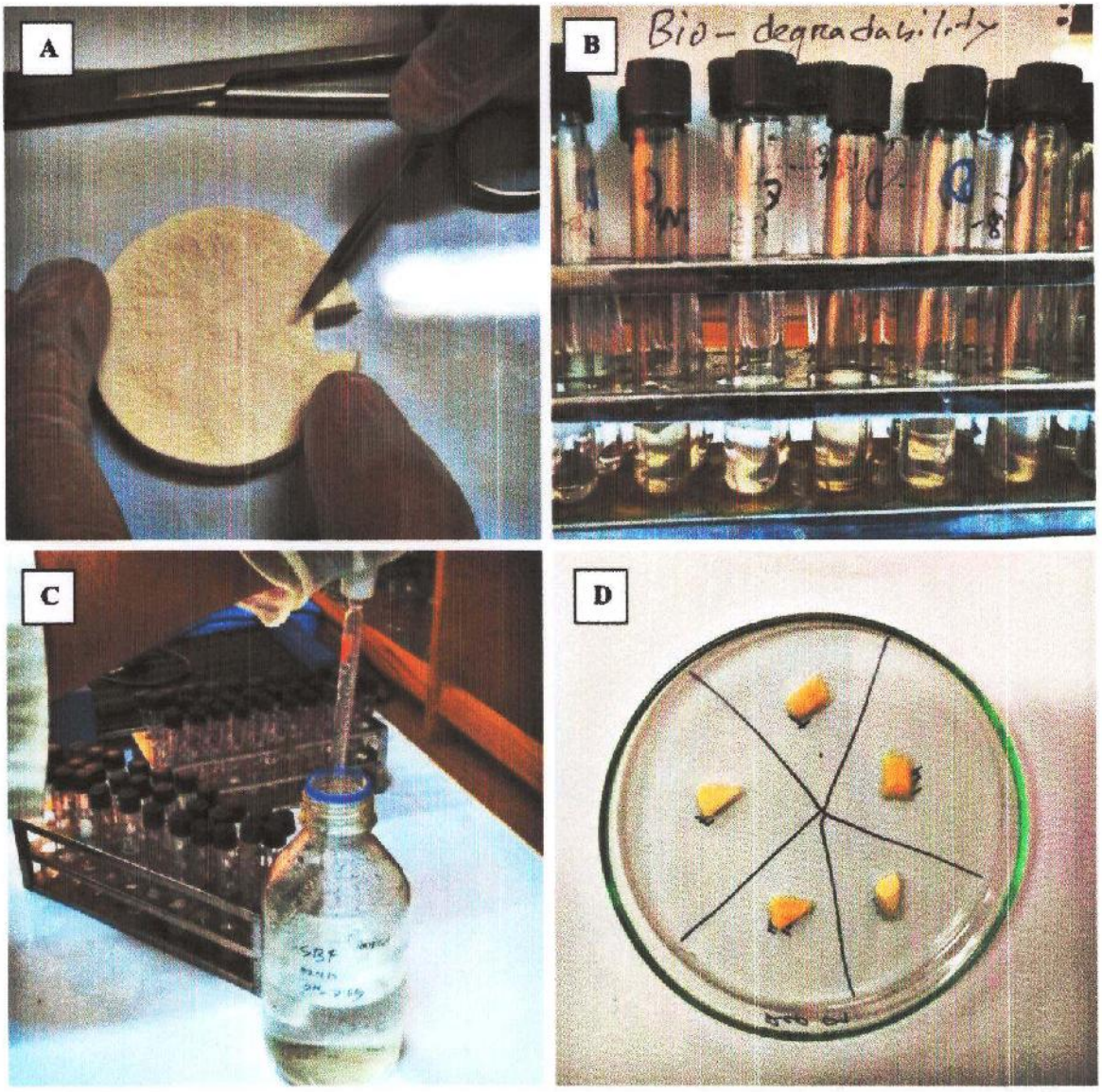


Figure 3.7: Biodegradation Test: (A) Cut into small pieces; (B) Immersed into SBF buffer; (C) Changed buffer every day ; (D) Dry the pieces of scaffold.

3.7. Vascularization of Scaffold

Bone engineering has been an active field of research for several decades now. However, the amount of clinical applications in the field of bone engineering is still limited. One of the current limitations of bone engineering is its inability to provide sufficient blood supply in the initial phase after implantation. Insufficient vascularization can lead to improper cell integration or cell death in tissue-engineered constructs. Several strategies for enhancing vascularization are currently under investigation. We designed several shape of mold. Among them the cylinder like structure performed well with its high rigidity and stability. To make vascular scaffold we used hygienic cupper fiber. Liquate composite were poured into specially designed mold that contain cupper fiber vascular network. After freeze dry the cupper fibers were dragged off carefully from the pours HA-collagen-chitosan scaffold. The cupper fiber reformed a vascular network into composite.

3.8. *In Vitro* Cytotoxicity Test

In vitro cytotoxicity test was performed using brine shrimp lethality bioassay method as showed in Figure 3.8 (Bundela and Bajpai, 2008). Brine shrimps (*Artemiasalina*) were hatched using brine shrimp eggs in a conical shaped vessel (1L), filled with sterile artificial seawater and pH was adjusted at 8.5 using 0.1N NaOH under constant aeration for 48 hours.

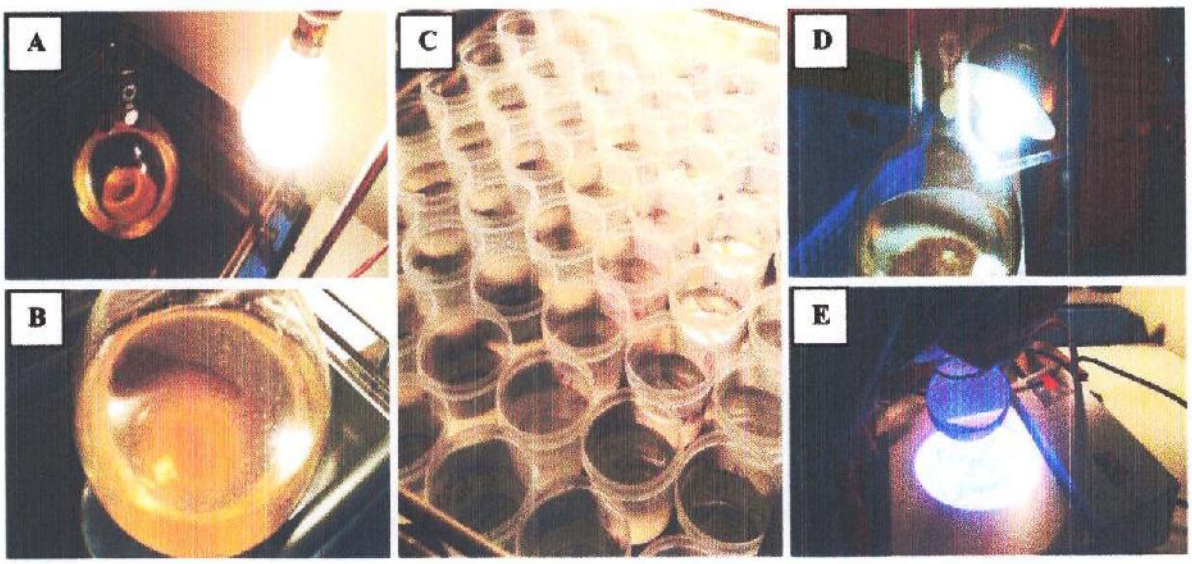


Figure 3.8: *In Vitro* Cytotoxicity Test of Scaffold on Brine Shrimp: Hatching of Brine Shrimp (A); Hatched Brine Shrimp (Nauplii) (B); Inoculation of Nauplii in Artificial Seawater (C); Counting of Live Nauplii (D); Counting Nauplii after incubation (E).

After hatching, active nauplii free from egg shells were collected from brighter portion of hatching chamber and used for the assay. The scaffold composites were dissolved in artificial seawater at different concentrations and taken in a sample container where the active nauplii were inoculated. After overnight incubation, the nauplii were counted. Here, 0.5 mg/ml of Colchicines (an anti-cancer drug) was used as positive control (figure 3.8).

3.9. Blood Compatibility

A biomaterial composite is a substance used as medical devices in contact with the living body for the intended method of application and a certain time period. To acquire biocompatibility, the materials used in medical applications must meet certain regulatory requirements. The surface of biomaterials is believed to play an important role in determining biocompatibility. For the biomaterials come into contact with blood, clot formation is the most undesirable but frequently occurring event that restricts the clinical acceptance of a scaffold to be used as biomaterial.

3.9.1. Clot Formation Testing

The anti-thrombogenic potential of the scaffold composite surface was determined by the blood-clot formation test (Bundela and Bajpai, 2008). In brief, the specimens were equilibrated with saline water (0.9% w/v NaCl) at 37°C for 24 h in a constant temperature bath. To these swollen samples was added 0.5 ml of ACD blood followed by the addition of 0.03 ml of $CaCl_2$ solution (4 mol/L) to start the thrombus formation. Adding 4.0 ml of deionized water stopped the reaction and the thrombus formed was separated by soaking in water for 10 min at room temperature and then fixed in 36% formaldehyde solution (2.0 ml) for another 10 min. The fixed clot was placed in water for 10 min and after drying, its weight was recorded. The same procedure was repeated for the composites of varying compositions and respective weights of thrombus formed were recorded (Figure 3.9).

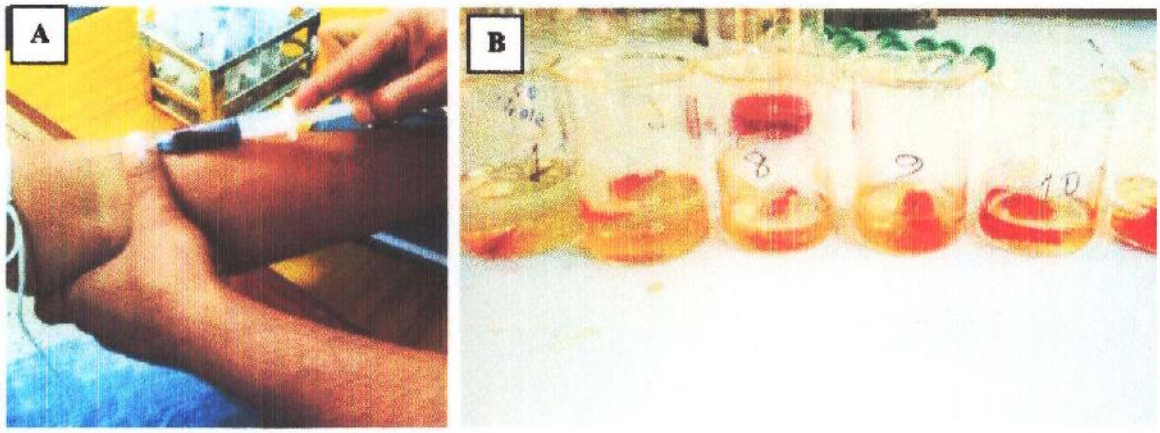


Figure 3.9: Blood Clot Formation Test of scaffold composites: (A) Collection of Blood; (B) ACD Blood Containing Sample.

3.9.2. Degree of Hemolysis Test

Haemolysis experiments were performed on the surfaces of prepared PAm-gelatin-HA composites (Bundela and Bajpai, 2008). In a typical experiment, dry composite pieces (4 cm^2) were equilibrated in normal saline water (0.9% w/v NaCl) at 37°C for 24 h and human ACD (acid citrate dextrose) blood (0.25 ml) was added into the composites. After that, 2.0 ml of saline water was added into the specimens to stop haemolysis and the samples were incubated for 60 min at 37°C. Positive and negative controls were obtained by adding 0.25 ml of human ACD blood to 2.0 ml of doubly distilled water and 0.9% NaCl respectively. Incubated samples were centrifuged for 45 min at 100×g, the supernatant was taken and its absorbance at 540 nm was recorded using a spectrophotometer. The percentage of haemolysis was calculated using the following relationship, given in equation below, where A is the absorbance.

$$\text{Hemolysis (\%)} = (A_{\text{test sample}} - A_{(-)\text{control}})/(A_{(+)\text{control}} - A_{(-)\text{control}})$$

3.10. Fourier Transform Infrared Spectroscopy (FTIR) Analysis

FTIR Spectroscopy is an analytical technique used to identify organic, polymeric and in some cases, inorganic materials. The FTIR analysis method (figure 3.10) uses infrared light to scan test samples and observe chemical properties. For obtaining FTIR spectra, samples were directly placed in sample holder (Model: IRprestige21, Shimadzu, Japan). FTIR spectra were recorded with FT-IR 8400S Shimadzu Spectrophotometer in the range 4000-700cm^{-1}, Resolution 4cm^{-1}, No of scan : 20 times. An image of FTIR machine used for this study is shown here,

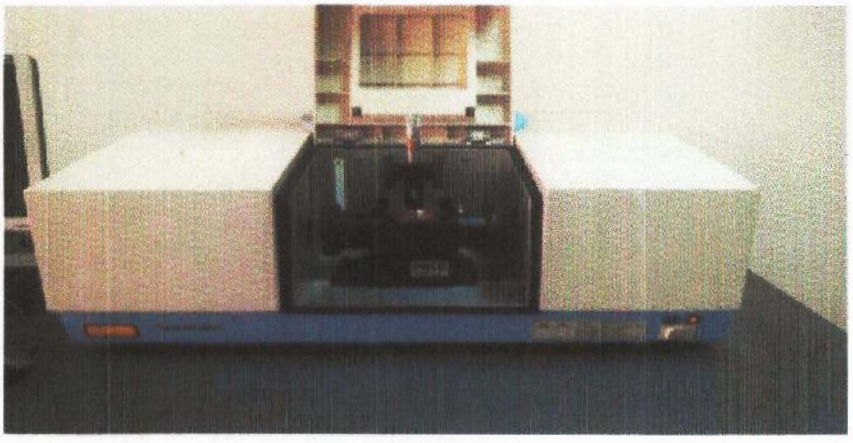


Figure 3.10: Fourier Transform Infrared Spectroscopy

3.11. Mechanical Properties of Scaffold

When scaffolds are implanted into the human body, it must have adequate mechanical strength to efficiently support the growth of cells. For each application, different requirements of mechanical properties are needed and thus, different testing's have been utilized. In this case, scaffold applied compression test that was performed (figure 3.11) by UTM (Universal testing machine). Stress was calculated by this equation:

$$\textbf{Stress } (\sigma) = F/A = m \times g / l \times r$$

Where, F= the force applied to the sample

g= gravity

l= length of scaffold

r= radius of scaffold

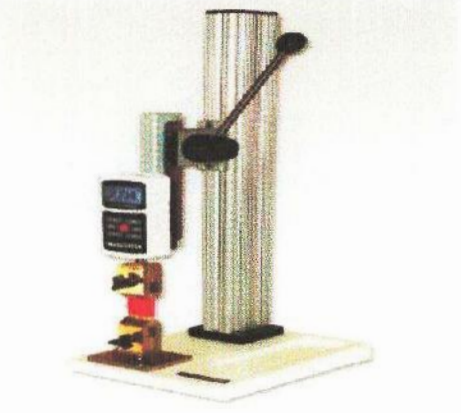


Figure 3.11: Universal Testing Machine

CHAPTER FOUR

RESULTS

Tissue engineering is an ever expanding field of biomedical arena, especially, bone tissue augmentation and repair by artificial bone material, and their scaffolds are prevalent to replace the damaged or diseased bone. From the literature review, it is evident that hydroxyapatite, collagen and chitosan are potential biomaterials for their high biocompatibility, biodegradability and other bio-functional properties in bone tissue engineering applications. The study was therefore planned, to fabricate and characterize of HA based biocompatible scaffold for bone tissue engineering that could be analogous to human bone. This research was conducted using thermally induced phase separation technique, which offers a simple, cost effective, time saving and easy to scale up method for the fabrication of porous scaffold. Keeping this aspect in mind we had endeavor to fabricate a 3D scaffold for the implementation of bone tissue engineering and the obtained results are delineated in this chapter as below:

4.1 Selection of Hydroxyapatite-Collagen-Chitosan Based Scaffold Composition

To obtain an ideal composition of 3D bone tissue scaffold, we reviewed lots of articles and selected hydroxyapatite-collagen-chitosan based on a number of advantageous properties they possess. We designed a series of liquid to solid (L:S) ratios (85:15, 90:10, 92:8; 94:6) and fabricated scaffold at different mineral to polymers (M:P) concentrations (70:30, 60:40, 50:50, 40:60; 30:70) along with different polymer to polymer (1:1, 2:1; 1:2) ratios depicted in Table 4.1. Thereafter we performed different tests including porosity, density and swelling kinetics to characterize the scaffold. The highest value of porosity (95.01%) was obtained at 94:6 liquid to solid ratio while the mineral to polymer concentration ratio was maintained as 1:2. However, the density was lower (0,09g/cm^3) along with a high percentage of swelling kinetics (783%). On the contrary, the lowest value of porosity (68.02%) was found at 85:15 liquid to solid ratios with 70:30 mineral to polymer concentrations. And the density was higher (0.30g/cm^3) in this case with a lower percentage of swelling kinetics (300%).

Table 4.1: Study of Hydroxyapatite-Collagen-Chitosan (HCC) scaffold

Components	Liquid – Solid ratio (w/v)	Mineral-polymer ratio (w/w)	Polymer-polymer ratio (w/w)	Sample ID.	Porosity (%)	Density	Swelling ratio (%)	Comment
HCC	85:15	70:30	1:1	NS_1	68.02	0.30	300	Hard/crack
			1:2	NS_2	68.55	0.28	345	Hard/crack
			2:1	NS_3	68.23	0.28	315	Hard/crack
		60:40	1:1	NS_4	74.19	0.27	148	Hard
			1:2	NS_5	75.22	0.27	185	Hard
			2:1	NS_6	73.24	0.25	165	Hard
		50:50	1:1	NS_7	84.33	0.24	168	Porous/crack
			1:2	NS_8	84.44	0.24	170	Porous/crack
			2:1	NS_9	84.96	0.24	250	Porous/crack
		40:60	1:1	NS_{10}	84.71	0.17	288	Porous
			1:2	NS_{11}	85.98	0.16	301	Porous
			2:1	NS_{12}	85.18	0.16	299	Porous
		30:70	1:1	NS_{13}	87.34	0.16	421	Porous
			1:2	NS_{14}	88.76	0.16	447	Porous
			2:1	NS_{15}	87.08	0.15	419	Porous
HCC	90:10	70:30	1:1	NS_{16}	70.98	0.20	470	Hard/crack
			1:2	NS_{17}	74.66	0.20	485	Hard/crack
			2:1	NS_{18}	72.60	0.19	472	Hard/crack
		60:40	1:1	NS_{19}	85.68	0.18	310	Hard/porous
			1:2	NS_{20}	86.65	0.18	355	Hard/porous
			2:1	NS_{21}	85.76	0.16	311	Hard
		50:50	1:1	NS_{22}	89.21	0.15	380	Hard
			1:2	NS_{23}	90.33	0.15	401	Porous/crack
			2:1	NS_{24}	89.00	0.14	390	Porous/crack
		40:60	1:1	NS_{25}	89.88	0.14	490	Porous
			1:2	NS_{26}	90.44	0.14	455	Porous
			2:1	NS_{27}	90.35	0.13	300	Porous
		30:70	1:1	NS_{28}	92.62	0.12	355	Porous
			1:2	NS_{29}	93.01	0.12	385	Porous
			2:1	NS_{30}	91.55	0.12	375	Porous
HCC	92:8	70:30	1:1	NS_{31}	89.91	0.14	785	Hard/crack
			1:2	NS_{32}	90.22	0.14	815	Hard/crack
			2:1	NS_{33}	90.08	0.14	780	Hard
		60:40	1:1	NS_{34}	90.44	0.13	700	Hard
			1:2	NS_{35}	90.60	0.13	755	Hard
			2:1	NS_{36}	90.54	0.12	680	Hard
		50:50	1:1	NS_{37}	90.31	0.13	650	Hard/porous
			1:2	NS_{38}	90.81	0.13	665	Hard/porous
			2:1	NS_{39}	90.91	0.12	645	Hard/porous
		40:60	1:1	NS_{40}	91.81	0.13	650	Porous
			1:2	NS_{41}	92.22	0.13	677	Porous
			2:1	NS_{42}	92.07	0.12	644	Porous
		30:70	1:1	NS_{43}	93.37	0.11	700	Spongy/porous
			1:2	NS_{44}	94.01	0.11	738	Spongy/porous
			2:1	NS_{45}	93.22	0.11	698	Spongy/porous

4.2.1 Optimization of NS_{19} Scaffold through Cross-linking

Selected scaffold NS_{19} (Liquid –Solid 90:10, Mineral-Polymer 60:40, Polymer-Polymer 1:1) was cross-linked through dehydrothermal (DHT) treatment at 105°C and radiation at 5, 10, 15, 20, 25 and 30kGy. In chemical cross-linking treatment, two chemical cross-linkers (gluteraldehyde (GTA) and EDAC with NHS were separately added to scaffolds. Furthermore, scaffolds were also cross-linked by first EDAC and NHS and then through DHT. Each data was repeated three times for obtaining more authentic and accurate observation. Then its mean and standard deviation were calculated (Table 4.2A-B).

Table 4.2(A): Effect of cross-linking on the porosity (%) of NS_{19} scaffold

Cross-linker (%)		Porosity (%)				
		R1	R2	R3	Mean	SD
Without Cross-linker		84.86	84.61	83.8	84.42	0.452
Radiation	5 kGy	82.81	82.7	82.19	82.57	0.270
	10 kGy	79.9	78.19	78.13	78.74	0.820
	15 kGy	76.71	76.81	76.07	76.53	0.327
	20 kGy	75.92	75.08	75.72	75.57	0.358
	25 kGy	74.29	74.04	74.8	74.38	0.316
	30 kGy	72.44	72	72.6	72.35	0.253
DHT		72.46	72.73	71.46	72.22	0.546
EDAC/NHS		82.88	82.31	81.88	82.36	0.409
1.5% GTA		76.52	76.3	75.52	76.11	0.429
EDAC/NHS+DHT		79.01	78.86	78.89	78.92	0.064

Analyzed data of NS_{19} scaffold is given in Figure 4.2 (A-D). Data from Figure 4.2(A) shows that porosity of NS_9 scaffold varied in different ways because of the addition of different cross-linkers. As shown in Figure 4.2(A), the scaffold without cross-linker showed the highest value of porosity which was 84.42%, however addition of different cross-linkers decreased the porosity of the scaffold.



Figure 4.2(A): Effect of cross-linking on the porosity (%)±SD of NS_{19} scaffold

The lowest porosity 72.22%, was found in the case of scaffold treated with DHT. Irradiated scaffold had 82.57% porosity at 5 kGy and it was gradually decreasing in state of increasing irradiation dose. The porosity of EDAC and NHS cross-linked scaffold reduced a little bit to 82.36% and remained almost similar to that of the raw NS_{19} scaffold.

Table 4.2(B): Effect of cross-linking on the density (%) of NS_{19} scaffold

Cross-linker (%)		Density (%)				
		R1	R2	R3	Mean	SD
Without Cross-linker		0.17	0.17	0.18	0.17	0.004
Radiation	5 kGy	0.18	0.17	0.17	0.17	0.004
	10 kGy	0.19	0.19	0.18	0.19	0.004
	15 kGy	0.2	0.19	0.2	0.20	0.004
	20 kGy	0.21	0.2	0.2	0.20	0.004
	25 kGy	0.2	0.21	0.2	0.20	0.004
	30 kGy	0.21	0.21	0.23	0.22	0.009
DHT		0.2	0.21	0.21	0.21	0.004
EDAC/NHS		0.18	0.18	0.19	0.18	0.004
1.5% GTA		0.19	0.19	0.18	0.19	0.004
EDAC/NHS+DHT		0.21	0.21	0.22	0.21	0.004

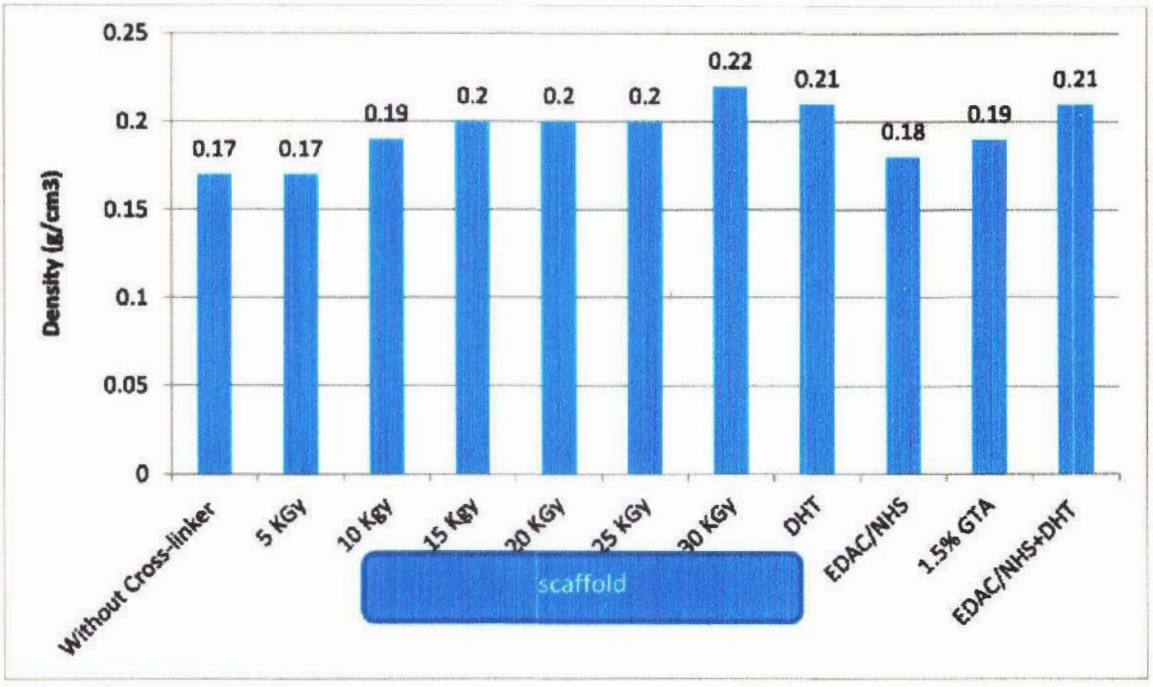


Figure 4.2(B): Effect of cross-linking on the density (%)±SD of NS_{19} scaffold

Figure 4.2(B) shows that lowest density (0.17 g/cm^3) was found for the raw NS_{19} scaffold which had the highest porosity and cross-linking of the scaffold increased its density. The density of the scaffold cross-linked through 30 kGy was 0.22 g/cm^{3}which was the highest among the density of all NS_{19} scaffold. However, the density of the DHT treated scaffold was 0.21 g/cm^3 and for EDAC/NHS cross-linked scaffold, it was 0.18 g/cm^3. Increasing radiation dose also increased the density of the scaffold. While the density of the scaffold cross-linked with 5kGy radiation was 0.17 g/cm^3, it was increased to 0.22 g/cm^3 in the case of 30kGy radiation dose. The density of EDAC, NHS and DHT treated scaffold was 0.21 g/cm^3.

The swelling rate (%) test was performed at 2, 24 and 48 hours. Each data was repeated three times for obtaining more authentic and accurate observation. Then its mean and standard deviation were calculated (Table 4.2.C1-C3).

Table 4.2(C1): Effect of cross-linking on the swelling rate (%) of NS_{19} scaffold.

Cross-linker (%)		Swelling rate (%) 2 hours				
		R1	R2	R3	Mean	SD
Without Cross-linker		77.06	76.42	76.68	76.72	0.262
Radiation	5 kGy	77.40	75.86	76.37	76.54	0.640
	10 kGy	73.19	73.78	71.81	72.93	0.825
	15 kGy	70.57	70.55	68.83	69.98	0.815
	20 kGy	65.96	64.88	66.51	65.78	0.677
	25 kGy	64.08	63.9	63.64	63.87	0.180
	30 kGy	61.81	61.68	59.85	61.11	0.894
DHT		60.05	59.62	59.56	59.74	0.218
EDAC/NHS		97.67	95.94	97.58	97.06	0.795
1.5% GTA		80.19	79.71	80.2	80.03	0.228
EDAC/NHS+DHT		73.33	71.6	73.58	72.84	0.880

From figure 4.2(C1), it can be seen that the highest swelling rate (97.06%) was found in the case of NHS/EDAC treated NS_{19} scaffold, however the addition of different cross-linkers reduced the swelling rate of the scaffolds. Swelling rate of the scaffold treated with DHT was 59.74%, which was the lowest. The swelling rate of 1.5% GTA cross-linked scaffold was 80.03%.



Figure 4.2(C1): Effect of cross-linking on the swelling rate (%)±SD of NS_{19} scaffold

Table 4.2(C2): Effect of cross-linking on the swelling rate (%) of NS_{19} scaffold.

Cross-linker (%)		Swelling rate (%) 24 hours				
		R1	R2	R3	Mean	SD
Without Cross-linker		82.16	81.62	82.08	81.95	0.237
Radiation	5 kGy	81.5	80.06	80.67	80.74	0.590
	10 kGy	78.29	78.98	77.11	78.13	0.772
	15 kGy	74.67	74.75	73.13	74.18	0.745
	20 kGy	71.06	70.08	71.85	71.00	0.723
	25 kGy	68.18	68.19	67.94	68.10	0.115
	30 kGy	66.9	66.88	65.15	66.31	0.820
DHT		64.18	63.82	64.86	64.29	0.431
EDAC/NHS		102.77	101.14	101.88	101.93	0.666
1.5% GTA		84.29	84.91	84.5	84.57	0.257
EDAC/NHS+DHT		78.43	76.8	77.54	77.59	0.666

From Figure 4.2(C1) we can see that increasing radiation dose decreased the swelling rate of scaffold. Scaffold cross-linked with 5kGy had 76.54% swelling rate which was highest and it decreased 61.11% in the case of scaffold cross-linked with 30kGy radiation dose. The scaffold cross-linked with EDAC, NHS and DHT had 72.84% swelling rate.

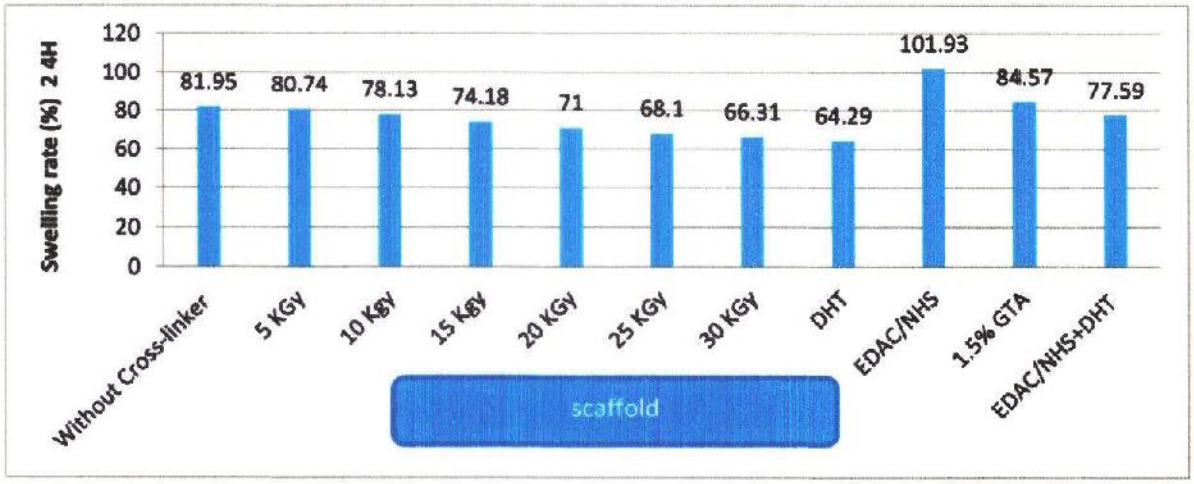


Figure 4.2(C2): Effect of cross-linking on the swelling rate (%)±SD of NS_{19} scaffold

From figure 4.2(C2), it can be found that the highest swelling rate (101.93%) was found in the case of NHS/EDAC treated NS_{19} scaffold, however the addition of different cross-linkers

KHULNA UNIVERSITY Central Library KHULNA.

reduced the swelling rate of the scaffolds. Swelling rate of the scaffold treated with DHT was 64.29%, which was the lowest. We also observed that increasing radiation dose decreased the swelling rate of scaffold. Scaffold cross-linked with 5kGy had 80.74% swelling rate which was highest and it decreased 66.31% in the case of scaffold cross-linked with 30kGy radiation dose. The swelling rate of 1.5% GTA cross-linked scaffold was 84.57%. The scaffold cross-linked with EDAC, NHS and DHT had 77.59% swelling rate.

Table 4.2(C3): Effect of cross-linking on the swelling rate (%) of NS_{19} scaffold

Cross-linker (%)		Swelling rate (%) 48 hours				
		R1	R2	R3	Mean	SD
Without Cross-linker		84.36	83.92	84.48	84.25	0.240
Radiation	5 kGy	83.00	81.66	82.67	82.44	0.570
	10 kGy	80.29	81.88	82.97	81.71	1.100
	15 kGy	76.17	76.35	76.35	76.29	0.084
	20 kGy	73.16	72.28	72.28	72.57	0.414
	25 kGy	69.68	69.79	69.79	69.75	0.051
	30 kGy	69.1	69.18	69.18	69.15	0.037
DHT		65.68	65.42	65.42	65.51	0.122
EDAC/NHS		104.87	103.34	103.34	103.85	0.721
1.5% GTA		85.79	86.51	86.51	86.27	0.339
EDAC/NHS+DHT		80.53	79	79.84	79.79	0.625

From figure 4.2(C3), it can be seen that the highest swelling rate (103.85%) was found in the case of NHS/EDAC treated NS_{19} scaffold, however the addition of different cross-linkers reduced the swelling rate of the scaffolds. Swelling rate of the scaffold treated with DHT was 65.51%, which was the lowest. The swelling rate of 1.5% GTA cross-linked scaffold was 86.27%. From Figure 4.2(C3) we can see that increasing radiation dose decreased the swelling rate of scaffold. Scaffold cross-linked with 5kGy had 82.44% swelling rate which was highest and it decreased 69.15% in the case of scaffold cross-linked with 30kGy radiation dose. The scaffold cross-linked with EDAC, NHS and DHT had 79.79% swelling rate.

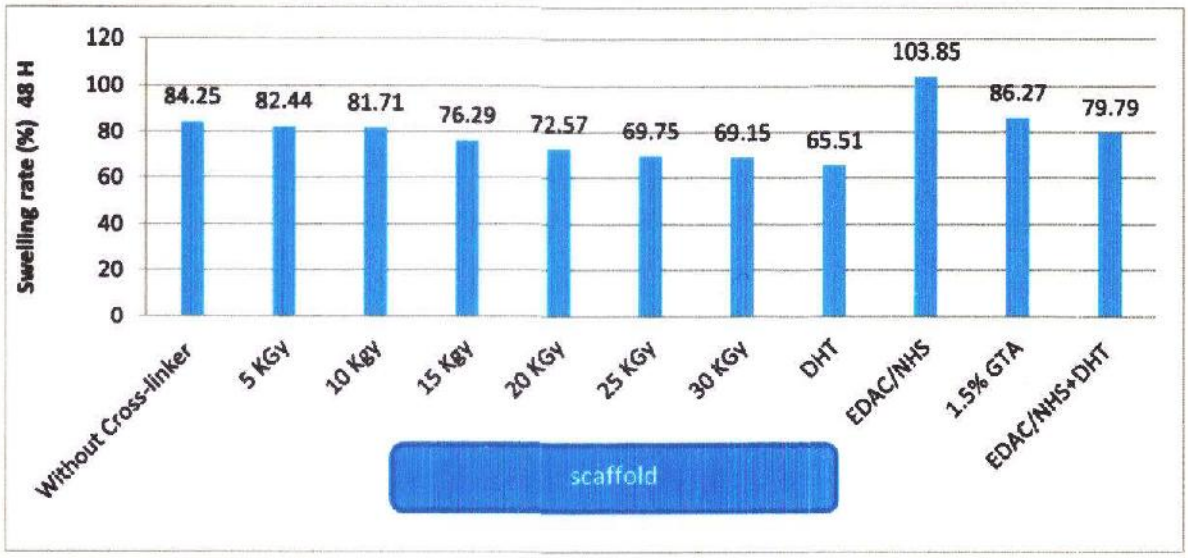


Figure 4.2(C3): Effect of cross-linking on the swelling rate (%)±SD of NS_{19} scaffold

The biodegradability test was performed at 7, 14, 21 and 28 days. Each data was repeated three times for obtaining more authentic and accurate observation. Then its mean and standard deviation were calculated (Table 4.2.D1-D4).

Table 4.2(D1): Effect of cross-linking on the Biodegradability (%) of NS_{19} scaffold

Cross-linker (%)		Biodegradability(%) after 7 days				
		R1	R2	R3	Mean	SD
Without Cross-linker		32.7	32.96	33.96	33.21	0.543
Radiation	5 kGy	30.08	31.82	30.17	30.69	0.799
	10 kGy	29.88	29.75	28.87	29.50	0.448
	15 kGy	28.11	27.77	28.8	28.23	0.428
	20 kGy	28.70	28.91	27.73	28.45	0.513
	25 kGy	27.10	28.12	26.07	27.10	0.836
	30 kGy	25.28	24.81	25.95	25.35	0.467
DHT		30.90	29.69	30.11	30.23	0.501
EDAC/NHS		10.91	10.1	12.07	10.69	0.331
1.5% GTA		4.13	4.30	4.80	4.41	0.284
EDAC/NHS+DHT		6.73	6.10	6.07	6.30	0.304

Table 4.2(D2): Effect of cross-linking on the Biodegradability (%) of NS_{19} scaffold

Cross-linker (%)		Biodegradability(%) after 14days				
		R1	R2	R3	Mean	SD
Without Cross-linker		35.61	34.7	35.17	35.16	0.371
Radiation	5 kGy	34.77	35.14	34.08	34.66	0.439
	10 kGy	33.38	33.11	34.23	33.57	0.477
	15 kGy	33.81	33.09	34.1	33.67	0.424
	20 kGy	32.98	32.88	33.17	33.01	0.120
	25 kGy	32.82	32.27	32.1	32.40	0.307
	30 kGy	31.48	31.12	31.03	31.21	0.194
DHT		34.13	34.04	34.5	34.22	0.199
EDAC/NHS		16.47	14.91	16.70	16.36	0.424
1.5% GTA		6.54	8.09	6.88	6.84	0.226
EDAC/NHS+DHT		10.49	10.14	10.54	10.39	0.177

Table 4.2(D3): Effect of cross-linking on the Biodegradability (%) of NS_{19} scaffold

Cross-linker (%)		Biodegradability(%) after 21days				
		R1	R2	R3	Mean	SD
Without Cross-linker		39.75	38.12	38.03	38.63	0.790
Radiation	5 kGy	38.58	37.13	37.04	37.58	0.705
	10 kGy	38.09	37.9	37.28	37.76	0.345
	15 kGy	37.42	36.25	36.53	36.73	0.498
	20 kGy	36.11	35.22	35.4	35.58	0.384
	25 kGy	35.23	34.05	34.6	34.63	0.482
	30 kGy	34.55	33.1	34.1	33.92	0.605
DHT		36.95	35.6	35.08	35.88	0.788
EDAC/NHS		17.30	16.03	16.35	16.56	0.539
1.5% GTA		10.56	10.64	8.45	10.22	0.543
EDAC/NHS+DHT		14.38	14.13	14.43	14.31	0.131

Table 4.2(D4): Effect of cross-linking on the Biodegradability (%) of NS_{19} scaffold

Cross-linker (%)		Biodegradability(%) after 28days				
		R1	R2	R3	Mean	SD
Without Cross-linker		42.45	41.09	41.91	41.82	0.559
Radiation	5 kGy	41.09	40.9	40.11	40.70	0.424
	10 kGy	40.81	39.13	39.4	39.78	0.736
	15 kGy	39.88	38.64	38.48	39.00	0.625
	20 kGy	38.29	37.11	38.09	37.83	0.515
	25 kGy	38.23	37.5	38.55	38.09	0.439
	30 kGy	37.05	36.67	36.7	36.81	0.172
DHT		39.05	40.14	39.5	39.56	0.447
EDAC/NHS		20.92	20.28	19.91	20.37	0.417
1.5% GTA		14.58	16.84	16.04	16.15	0.520
EDAC/NHS+DHT		18.9	18.36	19.99	18.75	0.827

The biodegradability test was performed at 7, 14, 21 and 28 days. From figure 4.2(D1-D11), it can be seen that the raw NS_{19} scaffold had the highest degradation rate among all the samples. The degradation rate of raw NS_{19} scaffold was from 33.21 to 41.82% over the fixed time period. However, both physical and chemical crosslinking made the scaffold more stable and less degradable. It has been observed that increasing the dose of irradiation decreased degradation rate and made the scaffold much more stable. The sample degradation rate varied from 37.58 to 33.92% at 21 days for 5 to 30 kGy irradiation dose.

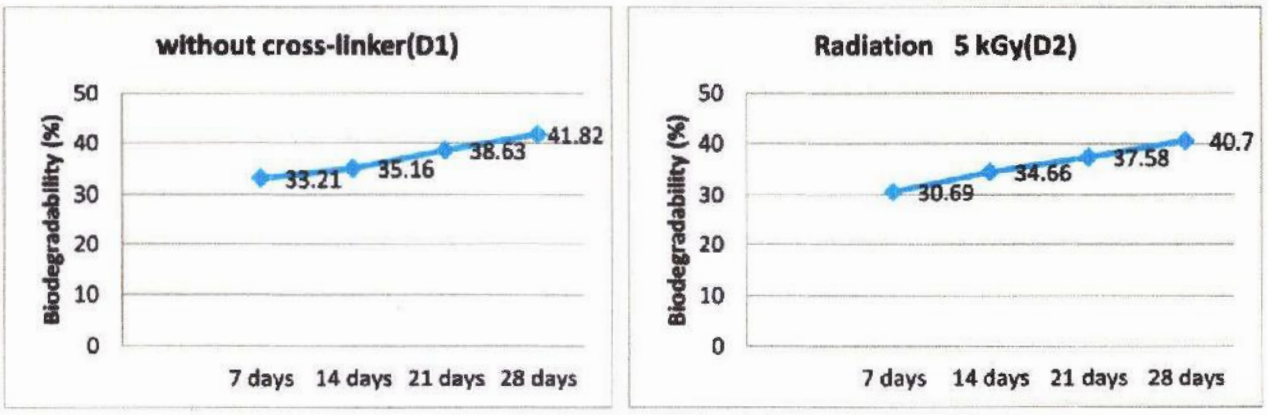
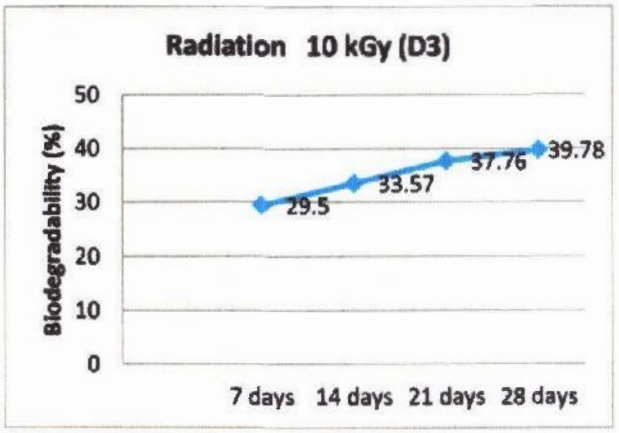
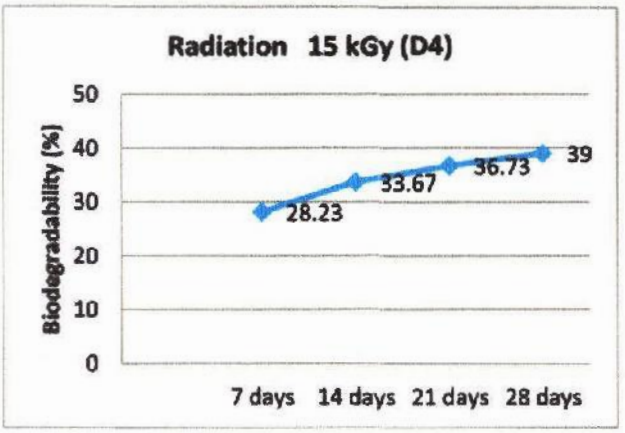
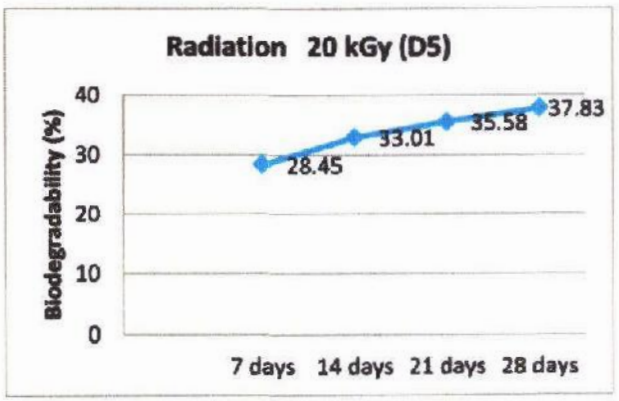
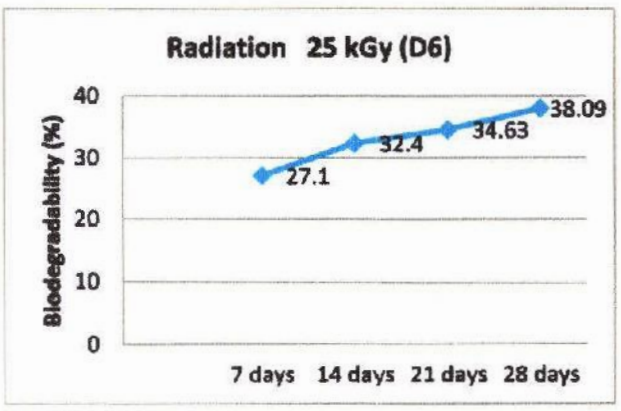


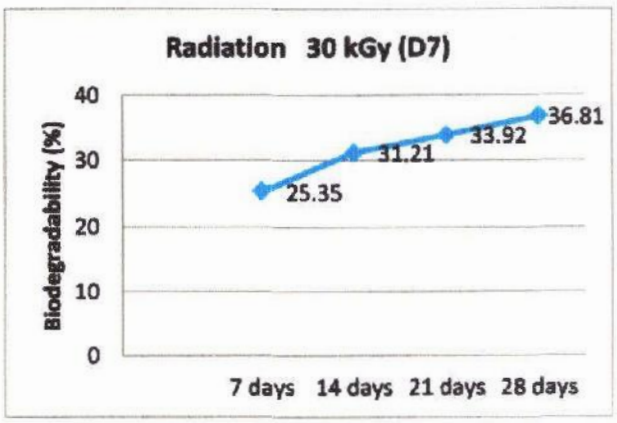
Figure 4.2(D): Day vs. Biodegradability (%)±SD Curve; D1: NS_{19} Scaffold without Crosslinking; D2: NS_{19} Irradiated at 5 kGy











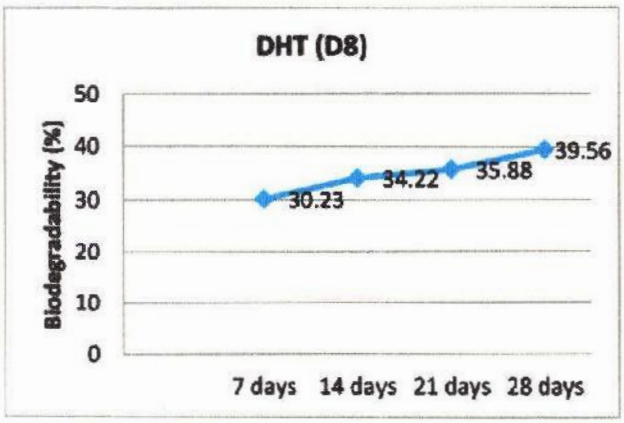


Figure 4.2(D): Day vs. Biodegradability (%)±SD Curve; D3: NS_{19} Irradiated at 10 kGy; D4: NS_{19} Irradiated at 15 kGy; D5: NS_{19} Irradiated at 20 kGy; D6: NS_{19} Irradiated at 25 kGy; D7: NS_{19} Irradiated at 30 kGy; D8: NS_{19}+DHT

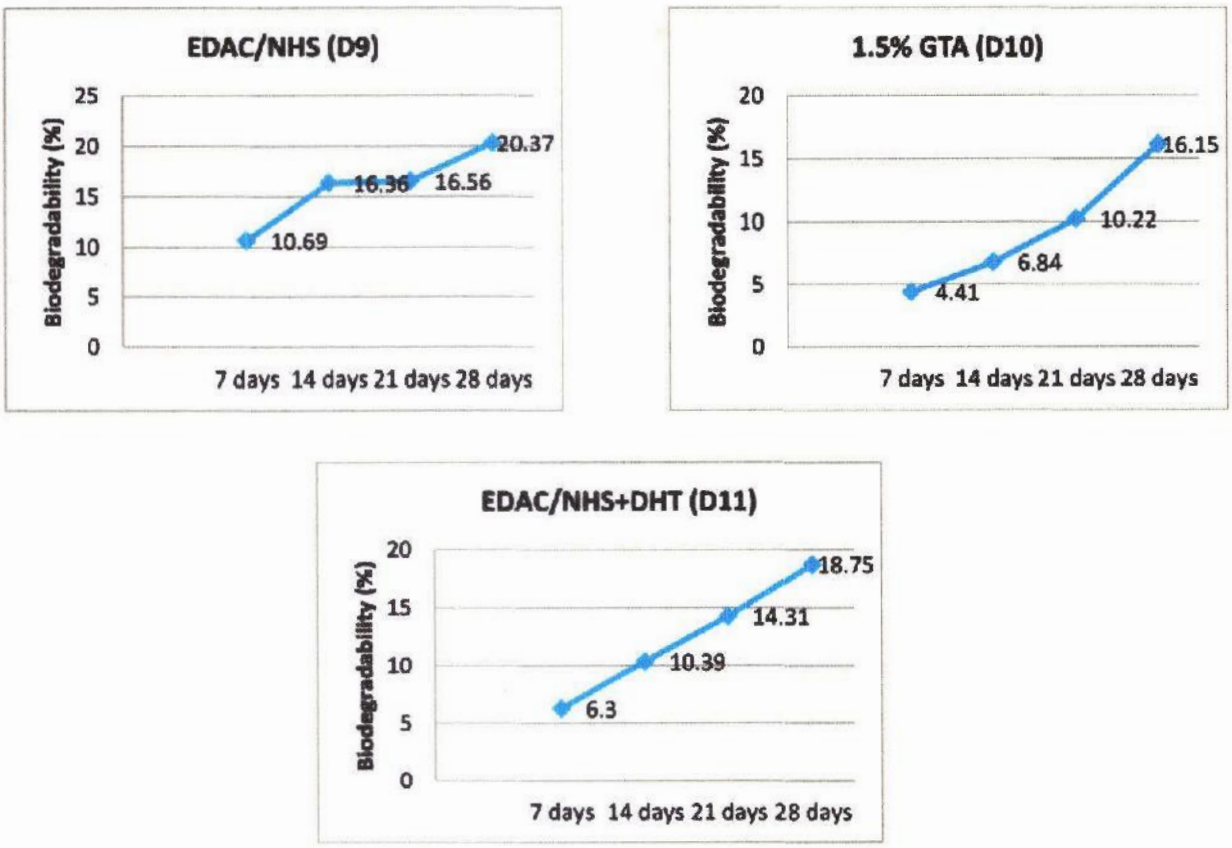


Figure 4.2(D): Day vs. Biodegradability (%)±SD Curve; D9: NS_{19}+EDAC/NHS; D10: NS_{19}+1.5% GTA; D11: NS_{19}+EDAC/NHS+DHT

The DHT treated scaffold had degradation rate from 30.23 to 39.56% over the fixed time period which was almost same to that of the 30kGy radiation treated scaffold. Scaffold cross-linked with EDAC and NHS had degradation rate from 10.69 to 20.37% over the fixed time.

The 1.5% GTA treated scaffold had degradation rate from 4.41 to 16.15% over the fixed time period stable. From figure 4.2(D), it is evident that 1.5% GTA cross-linked scaffold was the most stable scaffold and most suitable for *in vivo* implantation among all of the NS_{19} samples. The degradation rate of the scaffold was almost zero till third day and its degradation rate at 7, 14, 21 and 28 days was 2.41, 3.84, 5.22 and 8.15 respectively. By analyzing the data from figure 4.2(D), it can be said that the rate of biodegradation was found to be increasing in each time period, however most degradation occur till 7 days, after that the degradation occur slowly.

4.2.2 Optimization of NS_{48} Scaffold through Cross-linking

Selected scaffold NS_{48} (Liquid –Solid 92:8, Mineral-Polymer 70:30, Polymer-Polymer 2:1) was cross-linked through radiation at 5, 10, 15, 20, 25; 30 kGy and dehydrothermal (DHT) treatment at 105°C. In chemical cross-linking treatment, two chemical cross-linkers (gluteraldehyde (GTA) and EDAC with NHS were separately added to scaffolds. Furthermore, scaffolds were also cross-linked by first EDAC and NHS and then through DHT. Each data was repeated three times for obtaining more authentic and accurate observation. Then its mean and standard deviation were calculated (Table 4.3A-B).

Table 4.3(A): Effect of cross-linking on the porosity (%) of NS_{48} scaffold

Cross-linker (%)		Porosity (%)				
		R1	R2	R3	Mean	SD
Without Cross-linker		90.55	89.1	90.12	89.92	0.608
Radiation	5 kGy	88.5	87.56	87.9	87.99	0.388
	10 kGy	85.59	84.14	85.5	85.08	0.663
	15 kGy	82.4	82.05	82.57	82.34	0.216
	20 kGy	81.61	80.75	81.58	81.31	0.398
	25 kGy	79.98	79.17	79.72	79.62	0.337
	30 kGy	78.13	78.45	78.95	78.51	0.337
DHT		78.1	77.02	78.72	77.95	0.702
EDAC/NHS		85.54	84.02	84.44	84.67	0.640
1.5% GTA		82.21	81.25	82.11	81.86	0.430
EDAC/NHS+DHT		72.54	71.05	72.41	72.00	0.673

As shown in Figure 4.3(A), the highest value of porosity (89.92%) was found for the scaffold without cross-linker, however addition of different cross-linkers reduced the porosity of the scaffold. Irradiated scaffold had 87.99% porosity at 5 kGy and it was gradually decreasing in state of increasing irradiation dose. In addition, at 30 kGy radiation, the porosity stands 78.51 that was the third lowest value. Porosity of the scaffold treated with DHT was 77.95%. The porosity of EDAC and NHS cross-linked scaffold also decreased to 84.67%, however it remained very close to the porosity of raw NS_{48} scaffold.



Figure 4.3(A): Effect of cross-linking on the porosity (%)±SD of NS_{48} scaffold

The lowest porosity 75.76%, was found in the case of scaffold cross-linked with EDAC, NHS and DHT. After analyzing mentioned data, we can say that just like NS_{19}, in the case of NS_{48} scaffold, reduction of porosity due to physical crosslinking was also a bit larger than that of the chemical crosslinking, however increasing the concentration of chemical cross-linker also increased this reduction.

Table 4.3(B): Effect of cross-linking on the density (%) of NS_{19} scaffold

Cross-linker (%)		Dencity (%)				
		R1	R2	R3	Mean	SD
Without Cross-linker		0.12	0.13	0.13	0.13	0.004
Radiation	5 kGy	0.13	0.13	0.13	0.13	0
	10 kGy	0.13	0.14	0.13	0.13	0.004
	15 kGy	0.14	0.14	0.15	0.14	0.004
	20 kGy	0.15	0.15	0.16	0.15	0.004
	25 kGy	0.16	0.16	0.17	0.16	0.004
	30 kGy	0.17	0.17	0.16	0.17	0.004
DHT		0.15	0.16	0.16	0.16	0.004
EDAC/NHS		0.13	0.13	0.12	0.13	0.004
1.5% GTA		0.14	0.14	0.14	0.14	0
EDAC/NHS+DHT		0.2	0.2	0.21	0.20	0.004

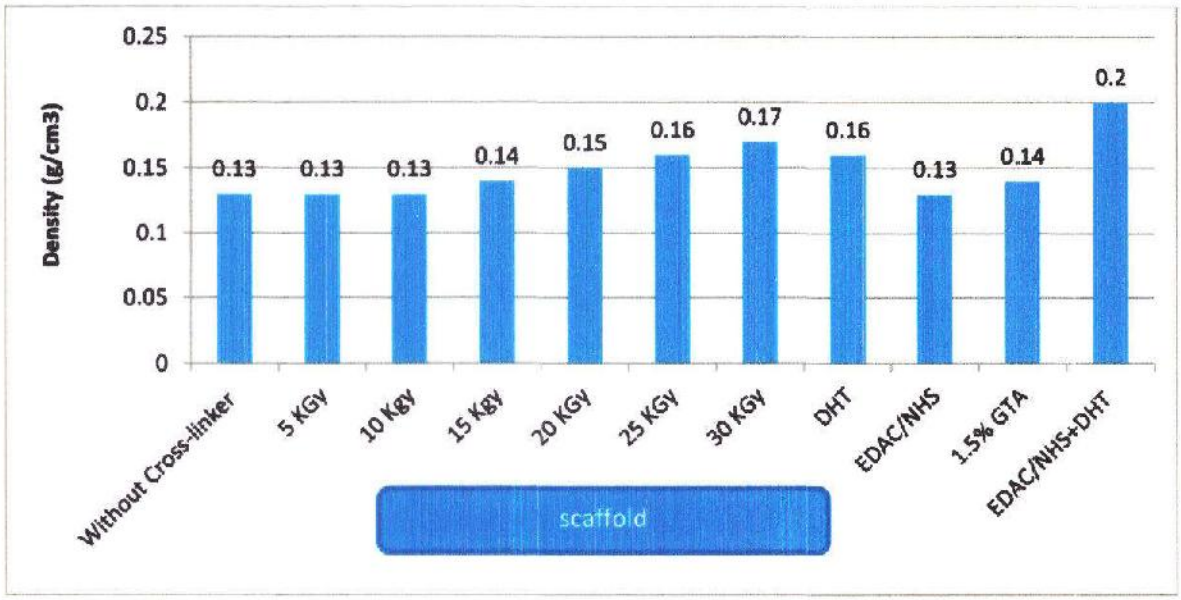


Figure 4.3(B): Effect of cross-linking on the density (%)±SD of NS_{48} scaffold

On the other hand, figure 4.3(B) shows that the raw NS_{48} scaffold had the lowest density which was 0.13 g/cm^3 and cross-linking of the scaffold increased its density. Increasing dose of irradiation also increased the density of the scaffold. While the density of the scaffold cross-linked with 5kGy radiation was 0.13 g/cm^3, it was increased to 0.17 g/cm^3 in the case of 30 kGy radiation. The density of the scaffold cross-linked through DHT was 0.16 g/cm^3 and for EDAC and NHS cross-linked scaffold it was 0.13 g/cm^3, which was as same as NS_{48} raw scaffold. The highest value of density (0.20 g/cm^3) was found from EDAC, NHS and DHT treated scaffold which also had the lowest porosity.

The swelling rate (%) test was performed at 2, 24 and 48 hours. Each data was repeated three times for obtaining more authentic and accurate observation. Then its mean and standard deviation were calculated (Table 4.3.C1-C3).

As shown in figure 4.3(C1), swelling rate was highest for the raw NS_{48} scaffold without any crosslinking which was 90.66%, however the addition of different cross-linkers reduced the swelling rate of the scaffolds.

Table 4.3(C1): Effect of cross-linking on the swelling rate (%) of NS_{48} scaffold

Cross-linker (%)		Swelling rate (%) 2 hours				
		R1	R2	R3	Mean	SD
Without Cross-linker		91.41	88.98	91.60	90.66	1.192
Radiation	5 kGy	88.50	89.68	87.80	88.66	0.775
	10 kGy	85.58	87.48	85.35	86.14	0.954
	15 kGy	85.98	86.05	86.01	86.01	0.028
	20 kGy	86.63	85.18	85.01	85.61	0.726
	25 kGy	82.92	83.74	83.08	83.25	0.354
	30 kGy	80.38	80.65	80.81	80.61	0.177
DHT		79.03	77.19	77.75	77.99	0.770
EDAC/NHS		89.40	88.36	88.72	88.83	0.431
1.5% GTA		67.44	68.20	66.48	67.37	0.703
EDAC/NHS+DHT		55.40	53.59	54.72	54.57	0.746

We observed that increasing radiation dose decreased the swelling rate of scaffold. Scaffold cross-linked with 5kGy had 88.66% swelling rate and it decreased 80.81% in the case of scaffold cross-linked with 30kGy radiation. Swelling rate of the scaffold



Figure 4.3(C1): Effect of cross-linking on the swelling rate (%)±SD of NS_{48} scaffold

treated with DHT was 77.99%. The swelling rate of EDAC and NHS cross-linked scaffold was 88.83% which was the highest among cross-linked scaffolds. In addition at 1.5% GTA concentration it was 67.37%. However, scaffold cross-linked with EDAC, NHS and DHT had 54.57% swelling rate which was the lowest swelling rate among all NS_{48} scaffolds.

Table 4.3(C2): Effect of cross-linking on the swelling rate (%) of NS_{48} scaffold

Cross-linker (%)		Swelling rate (%) 24 hours				
		R1	R2	R3	Mean	SD
Without Cross-linker		95.51	94.18	95.9	95.20	0.736
Radiation	5 kGy	93.6	93.8	93.1	93.50	0.294
	10 kGy	90.68	91.58	90.13	90.80	0.597
	15 kGy	91.08	90.15	91.65	90.96	0.618
	20 kGy	90.73	90.38	90.11	90.41	0.253
	25 kGy	88.12	88.24	87.18	87.85	0.473
	30 kGy	85.48	84.85	85.31	85.21	0.266
DHT		83.23	82.39	83.05	82.89	0.361
EDAC/NHS		94.6	93.66	94.12	94.13	0.383
1.5% GTA		72.54	72.4	71.08	72.01	0.657
EDAC/NHS+DHT		59.83	58.89	59.35	59.36	0.383

As shown in figure 4.3(C2), swelling rate was highest for the raw NS_{48} scaffold without any crosslinking which was 95.20%, however the addition of different cross-linkers reduced the swelling rate of the scaffolds. We observed that increasing radiation dose decreased the swelling rate of scaffold. Scaffold cross-linked with 5kGy had 93.50% swelling rate and it decreased 85.21% in the case of scaffold cross-linked with 30kGy radiation.

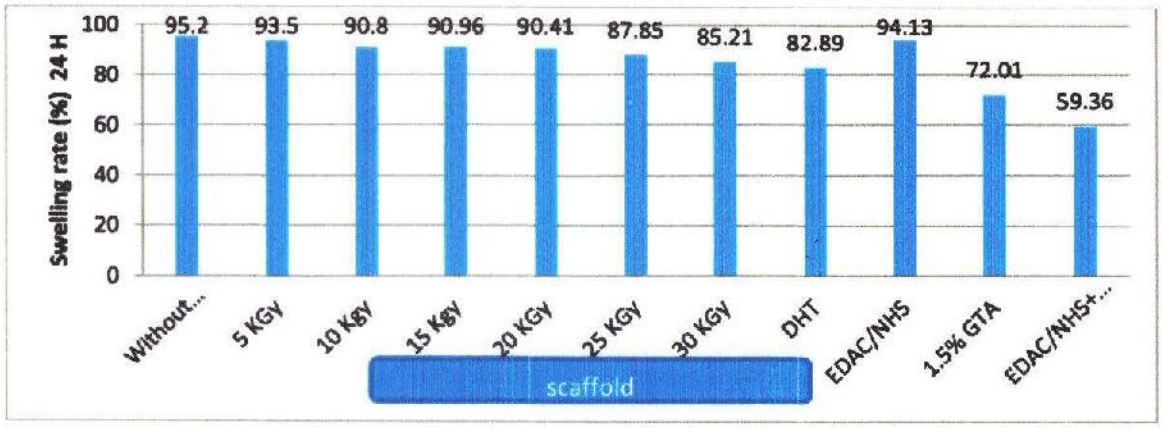


Figure 4.3(C2): Effect of cross-linking on the swelling rate (%)±SD of NS_{48} scaffold

Table 4.3(C3): Effect of cross-linking on the swelling rate (%) of NS_{48} scaffold

Cross-linker (%)		Swelling rate (%) 48 hours				
		R1	R2	R3	Mean	SD
Without Cross-linker		97.61	96.48	98.3	97.46	0.750
Radiation	5 kGy	95.1	95.4	94.7	95.07	0.286
	10 kGy	92.78	93.88	92.43	93.03	0.617
	15 kGy	92.58	91.75	93.35	92.56	0.653
	20 kGy	92.83	92.58	92.41	92.61	0.172
	25 kGy	89.62	89.84	88.98	89.48	0.364
	30 kGy	87.58	87.05	87.61	87.41	0.257
DHT		84.73	83.99	84.85	84.52	0.380
EDAC/NHS		96.7	95.86	96.42	96.33	0.349
1.5% GTA		74.04	74	72.88	73.64	0.537
EDAC/NHS+DHT		61.93	61.09	61.65	61.56	0.349

Swelling rate of the scaffold treated with DHT was 82.89%. The swelling rate of EDAC and NHS cross-linked scaffold was 94.13% which was the highest among cross-linked scaffolds. In addition at 1.5% GTA concentration it was 72.01%. However, scaffold cross-linked with EDAC, NHS and DHT had 59.36% swelling rate which was the lowest swelling rate among all NS_{48} scaffolds.

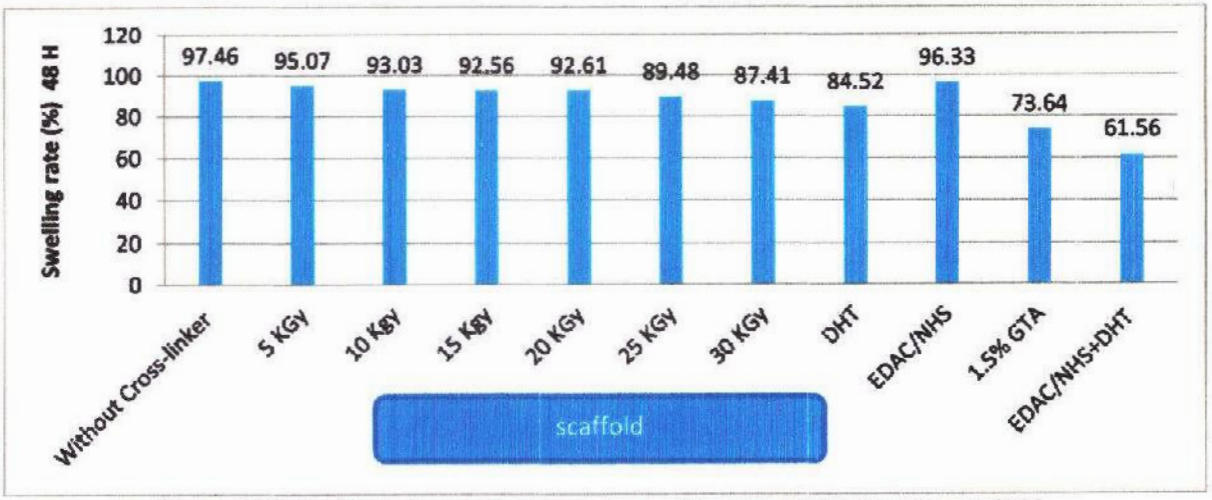


Figure 4.3(C3): Effect of cross-linking on the swelling rate (%)±SD of NS_{48} scaffold

The biodegradability test was performed at 7, 14, 21 and 28 days. Each data was repeated three times for obtaining more authentic and accurate observation. Then its mean and standard deviation were calculated (Table 4.3.D1-D4).

Table 4.3(D1): Effect of cross-linking on the Biodegradability (%) of NS_{48} scaffold

Cross-linker (%)		Biodegradability(%) after 7 days				
		R1	R2	R3	Mean	SD
Without Cross-linker		32.7	32.96	33.96	33.21	0.543
Radiation	5 kGy	30.08	31.82	30.17	30.69	0.799
	10 kGy	29.88	29.75	28.87	29.50	0.448
	15 kGy	28.11	27.77	28.8	28.23	0.428
	20 kGy	28.7	28.91	27.73	28.45	0.513
	25 kGy	27.1	28.12	26.07	27.10	0.836
	30 kGy	25.28	24.81	25.95	25.35	0.467
DHT		30.9	29.69	30.11	30.23	0.501
EDAC/NHS		10.91	10.10	12.07	10.69	0.331
1.5% GTA		4.13	4.3	4.8	4.41	0.284
EDAC/NHS+DHT		6.73	6.10	6.07	6.30	0.304

Table 4.3(D2): Effect of cross-linking on the Biodegradability (%) of NS_{48} scaffold

Cross-linker (%)		Biodegradability(%) after 14days				
		R1	R2	R3	Mean	SD
Without Cross-linker		35.61	34.7	35.17	35.16	0.371
Radiation	5 kGy	34.77	35.14	34.08	34.66	0.439
	10 kGy	33.38	33.11	34.23	33.57	0.477
	15 kGy	33.81	33.09	34.1	33.67	0.424
	20 kGy	32.98	32.88	33.17	33.01	0.120
	25 kGy	32.82	32.27	32.1	32.40	0.307
	30 kGy	31.48	31.12	31.03	31.21	0.194
DHT		34.13	34.04	34.5	34.22	0.199
EDAC/NHS		16.47	14.91	16.70	16.36	0.424
1.5% GTA		6.54	5.09	6.88	6.84	0.226
EDAC/NHS+DHT		10.49	10.14	10.54	10.39	0.177

Table 4.3(D3): Effect of cross-linking on the Biodegradability (%) of NS_{48} scaffold

Cross-linker (%)		Biodegradability(%) after 21days				
		R1	R2	R3	Mean	SD
Without Cross-linker		39.75	38.12	38.03	38.63	0.790
Radiation	5 kGy	38.58	37.13	37.04	37.58	0.705
	10 kGy	38.09	37.9	37.28	37.76	0.345
	15 kGy	37.42	36.25	36.53	36.73	0.498
	20 kGy	36.11	35.22	35.4	35.58	0.384
	25 kGy	35.23	34.05	34.6	34.63	0.482
	30 kGy	34.55	33.1	34.1	33.92	0.605
DHT		36.95	35.6	35.08	35.88	0.788
EDAC/NHS		32.3	34.03	32.35	32.56	0.539
1.5% GTA		10.56	10.64	8.45	10.22	0.543
EDAC/NHS+DHT		14.38	14.13	14.43	14.31	0.131

Table 4.3(D4): Effect of cross-linking on the Biodegradability (%) of NS_{48} scaffold

Cross-linker (%)		Biodegradability(%) after 28days				
		R1	R2	R3	Mean	SD
Without Cross-linker		42.45	41.09	41.91	41.82	0.559
Radiation	5 kGy	41.09	40.9	40.11	40.70	0.424
	10 kGy	40.81	39.13	39.4	39.78	0.736
	15 kGy	39.88	38.64	38.48	39.00	0.625
	20 kGy	38.29	37.11	38.09	37.83	0.515
	25 kGy	38.23	37.5	38.55	38.09	0.439
	30 kGy	37.05	36.67	36.7	36.81	0.172
DHT		39.05	40.14	39.5	39.56	0.447
EDAC/NHS		38.92	36.28	37.91	37.70	0.417
1.5% GTA		14.58	16.84	16.04	16.15	0.520
EDAC/NHS+DHT		22.90	20.36	18.99	20.75	0.827

The biodegradability test was performed at 7, 14, 21 and 28 days. From figure 4.3(D1-D11), it can be seen that the NS_{48} scaffold without any crosslinking degraded the most among all the samples. The degradation rate of raw NS_{48} scaffold was from 27.05 to 37.70% over the fixed time period. However, both physical and chemical crosslinking made the scaffold more stable and less degradable.

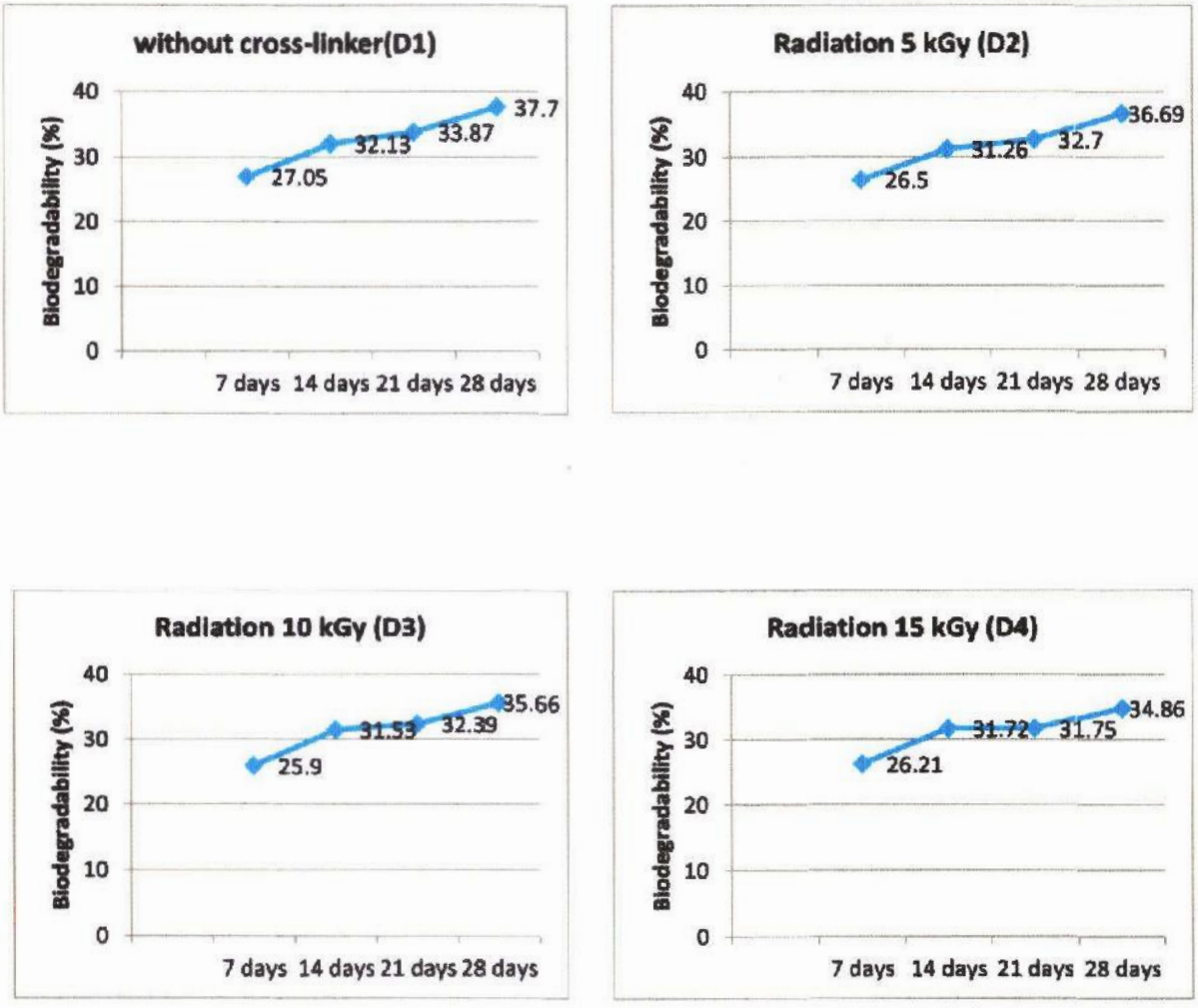


Figure 4.3(D): Day vs. Biodegradability (%)±SD Curve; D1: NS_{48} Scaffold without Crosslinking; D2: NS_{48} Irradiated at 5 kGy; D3: NS_{48} Irradiated at 10 kGy; D4: NS_{48} Irradiated at 15 kGy

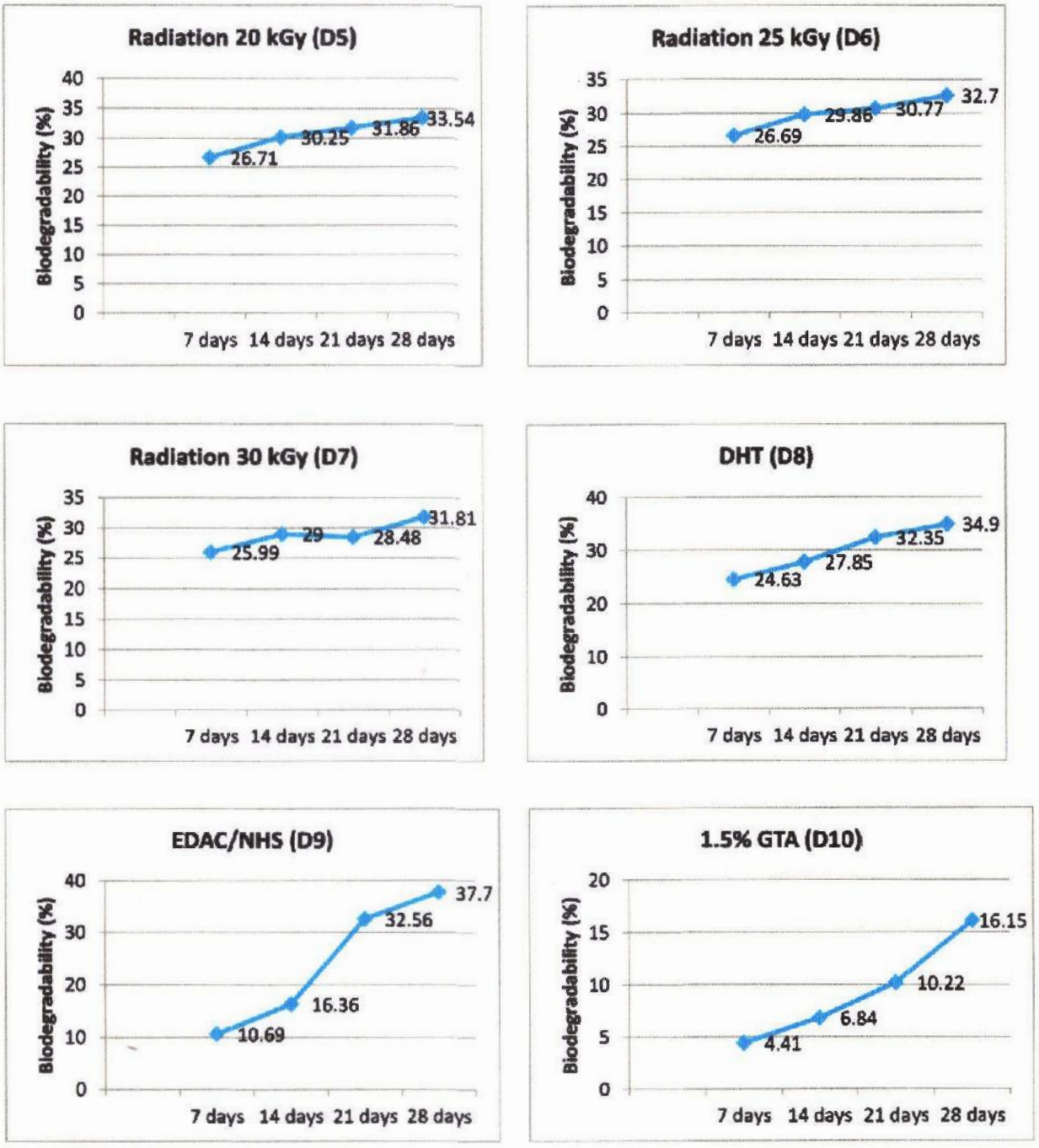


Figure 4.3(D): Day vs. Biodegradability (%)±SD Curve D5: NS_{48} Irradiated at 20 kGy; D6: NS_{48} Irradiated at 25 kGy; D7: NS_{48} Irradiated at 30 kGy; D8: NS_{48}+DHT; D9: NS_{48}+EDAC/NHS; D10: NS_{48}+1.5% GTA

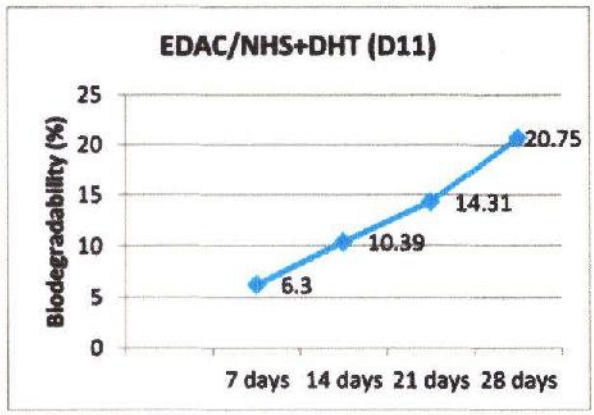


Figure 4.3(D): Day vs. Biodegradability (%)±SD Curve; D11: NS_{48}+EDAC/NHS+DHT

It has been observed that increasing the dose of irradiation decreased degradation rate and made the scaffold much more stable. The sample degradation rate varied from 36.69 to 31.81% at 28 days for 5 to 30 kGy irradiation dose. The DHT treated scaffold had degradation rate from 24.63 to 34.90% over the fixed time period which was almost same to that of the 30kGy radiation treated scaffold. Scaffold cross-linked with EDAC and NHS had degradation rate from 10.69 to 37.70% over the fixed time.

The NHS/EDAC+DHT treated scaffold had degradation rate from 6.30 to 20.75% over the fixed time period stable. From figure 4.3(D), it is evident that NHS/EDAC+DHT cross-linked scaffold was the most stable scaffold and most suitable for *in vivo* implantation among all of the NS_{48} samples. The degradation rate of the scaffold was almost zero till third day and its degradation rate at 7, 14, 21 and 28 days was 1.94, 3.56, 5.51 and 7.34 respectively. By analyzing the data from figure 4.3(D), it can be said that the rate of biodegradation was found to be increasing in each time period, however most degradation occur till 7 days, after that the degradation occur slowly.

4.3. Fourier Transform Infrared Spectroscopy (FTIR) Analysis

Fourier Transform Infrared Spectroscopy is an analytical technique used to identify organic, polymeric, and, in some cases, inorganic materials. The FTIR analysis method uses infrared light to scan test samples and observe chemical properties. In this case, we use it to find inter molecular interaction of selected NS_{19} and NS_{48} scaffold.

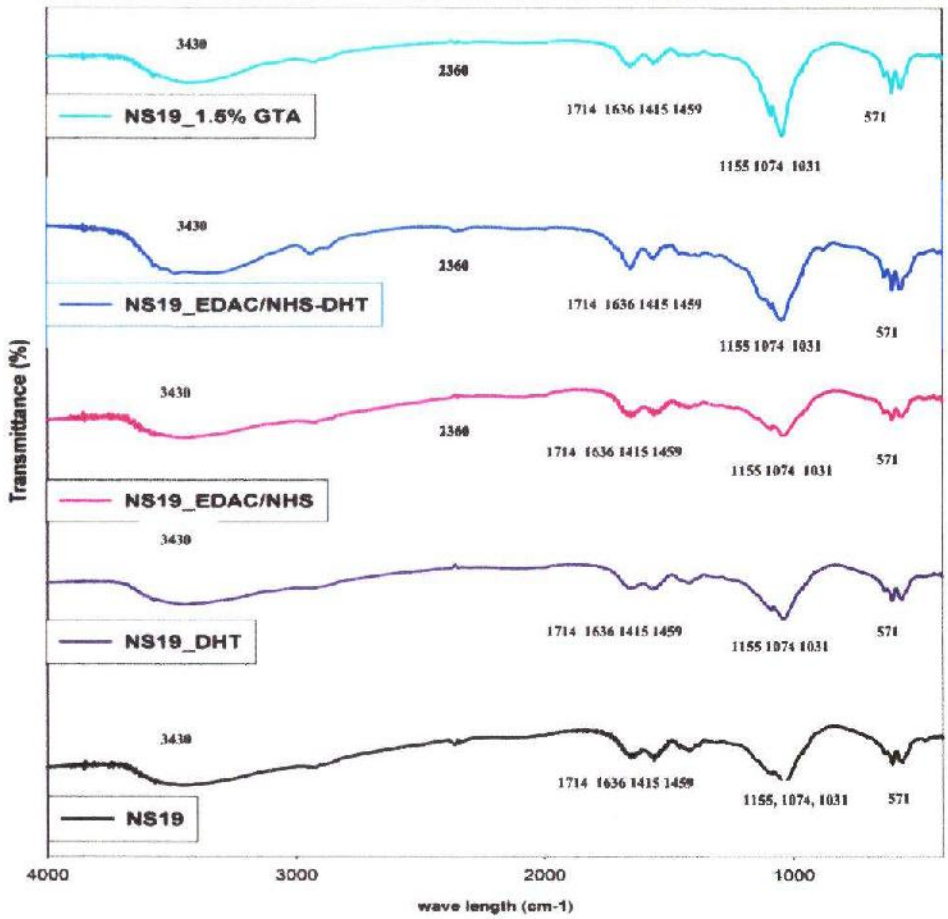


Figure 4.4: FTIR analysis of NS_{19} scaffold with its chemical cross-linker

As Figure 4.4 was illustrated , the spectrum showed typical characteristic absorption bands of chitosan as peak around 3430 cm^{-1} attributed to the combined stretching vibration of OH and N-H groups, whereas at 1647 and 1606 cm^{-1} are the characteristic peaks of amide I and amide II, respectively. Moreover, C-H stretching of rock and bending mode were observed at 1412 and 1385 cm^{-1}, respectively, and pyranose C-O-C stretching mode at 1155, 1074, and 1031 cm^{-1},

respectively. The spectra of HA resulted in several characteristic absorption bands are PO_4^{3-} stretching at 1050–1089 cm^{-1}, PO_4^{3-} at 962 cm^{-1}, PO_4^{3-} asymmetric bending stretched at 571 cm^{-1}, and CO_3^{2-} at 1415 and 1459 cm^{-1}. A sharp band was observed at 3571 cm-^{1}, which corresponds to OH. Traditionally speaking, collagen diversity makes significant existence and appearance in IR spectrum as characteristic peaks ranging from 1100 to 1400 cm^{-1}, which are significant to the corresponding fibrillar and nonfibrillar collagens. These peaks are consistent and correlated with the previously reported IR spectrum of collagens. The major absorption peaks of all scaffold, were the amide I absorptions. The amide I absorption (1600–1700 cm^{-1}) arises predominantly from protein amide C=O stretching vibrations, which was observed at 1636 and 1714 cm^{-1}. These absorptions peaks correlated with the previous reports on type I collagen (1032–1338 cm^{-1}), indicating that most of the absorptions in the obtained spectra are attributed to the presence of collagen. Additional frequencies that were observed between 1300 and 1400 cm^{-1} were characteristically specific of intermolecular hydrogen bonding, which suggests the intermolecular hydrogen bonding between collagen chains with chitosan and HA.

However, for the uncross-linked scaffold there was no band at 2400-2120cm^{-1}, but cross-linked scaffolds (except for DHT) showed a sharp band at 2360 cm^{-1} which was due to C-N triple bond (nitrile group) and there was another band at ~2152cm^{-1}in all of the cross-linked scaffolds which represent C-C triple bond. The spectra showed a band at 2360 cm^{-1} because in the case of EDAC and EDAC/DHT treated scaffolds the band represents the nitrile group of the EDAC itself, however in GTA cross-linked and irradiated scaffolds the nitrile group was formed due to crosslinking. These two bonds were formed due to cross-linking of the scaffold.

Nevertheless, for uncross-linked (figure 4.5) scaffold there was no band at 2400-2120 cm^{-1}, but irradiated scaffolds showed a sharp band at 2360 cm^{-1} which was due to C-N triple bond and there was another band at ~2152cm^{-1} which represent C-C triple bond. These two bonds were formed due to radiation. For every scaffold, there was a band at ~2000cm^{-1} which represent bending of C-H bond in aromatic compounds which in this case are histidine and phenylalanine of collagen molecule. The spectra showed that there was a band of amide I stretching at ~1635 cm^{-1} for uncross-linked and irradiated scaffolds (5-20 kGy), however the band shifted to 1636 cm^{-1} at high radiation dose (25 and 30 kGy).

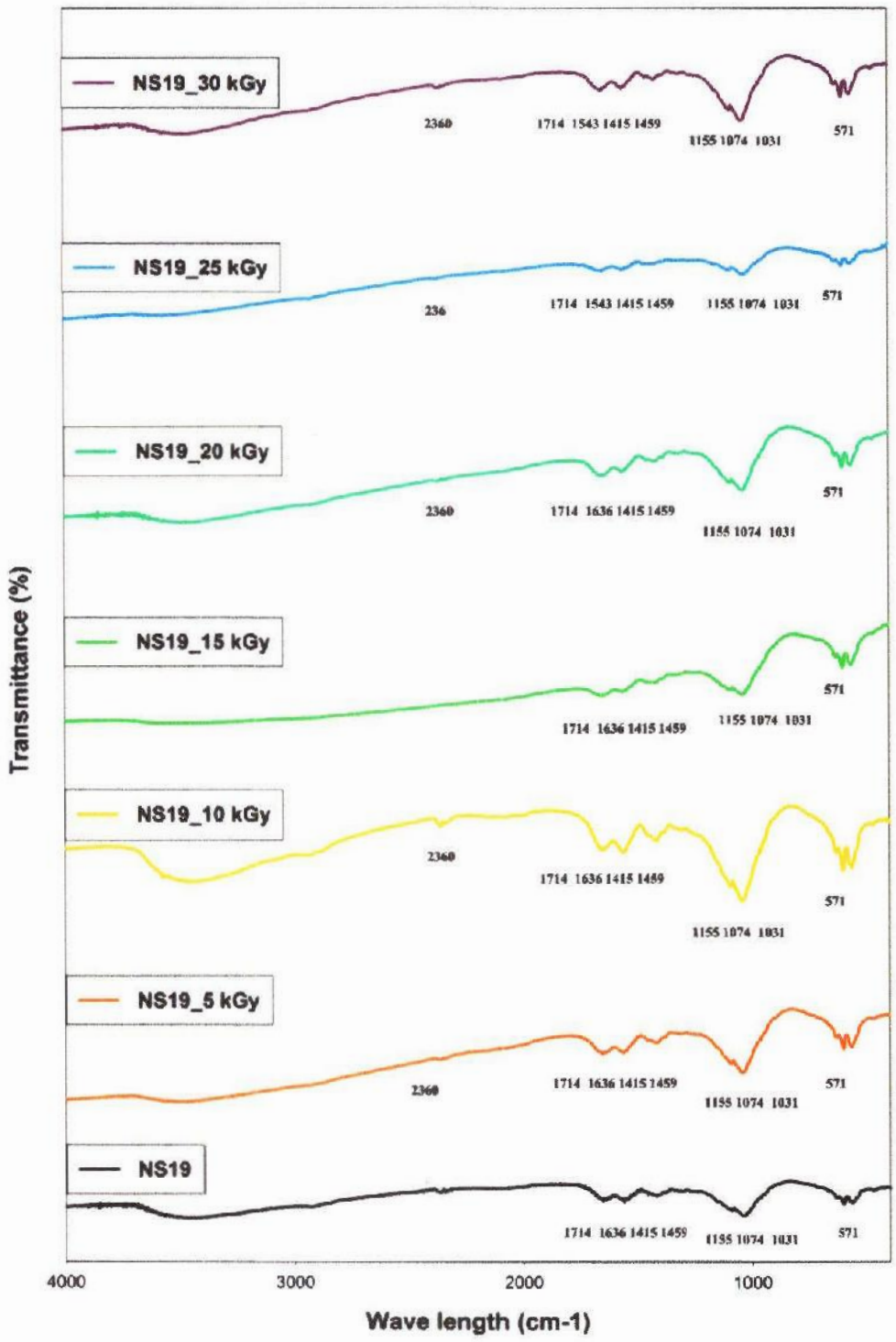
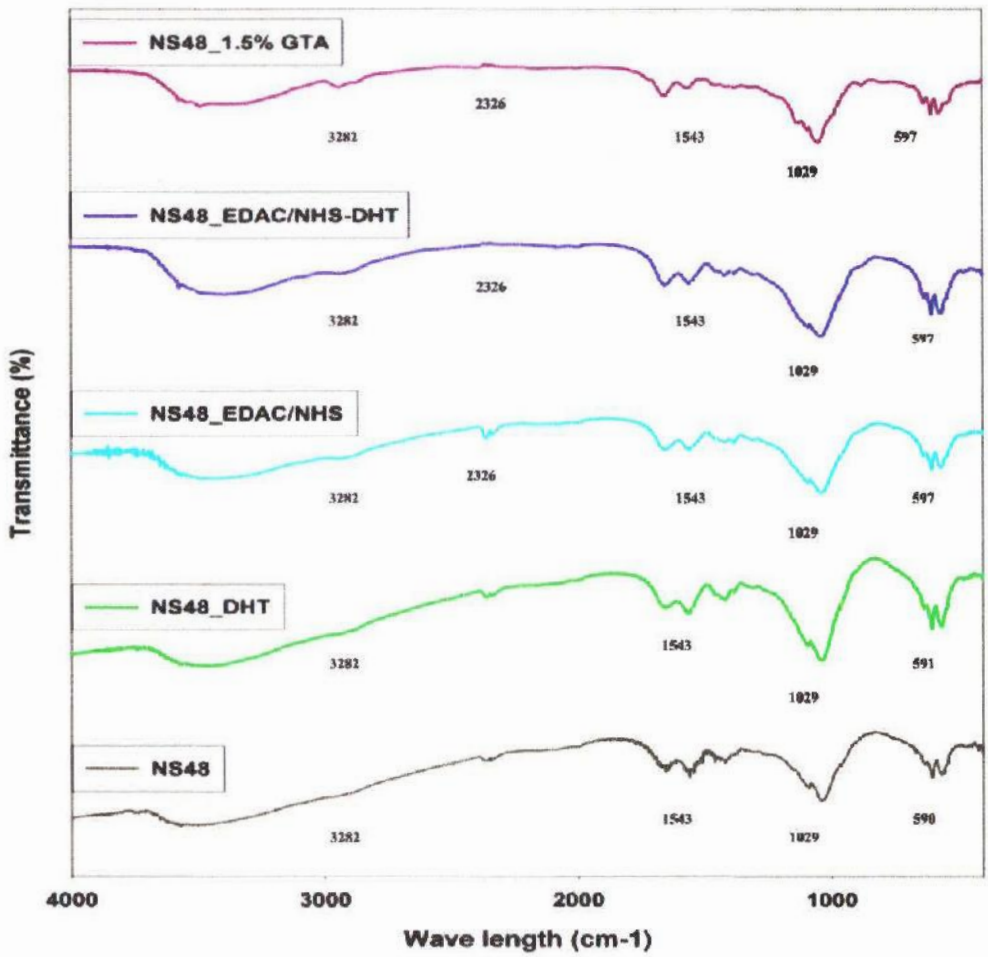


Figure 4.5: FTIR analysis of NS_{19} scaffold with its physical cross-linker

As shown in Figure 4.6 NS_{48} scaffold showed the characteristic bands (1543, 1029, 597) of chitosan collagen and HA. The spectra also showed that N-H stretching generated a broad band from~3200-3400 cm^{-1} due to the hydrogen bonding between N-H of secondary amide and –OH of acetic acid in the case of all of the scaffolds. This is a characteristic band of collagen which represent amide A band resulting from a Fermi resonance between the N-H stretch fundamental band and the overtone of amide II. However, for the uncross-linked scaffold there was no band at 2400-2120cm^{-1}, but cross-linked scaffolds (except for DHT) showed a band at 2360 cm^{-1} which was due to C-N triple bond (nitrile group) and there was another band at ~2152cm^{-1}in all of the cross-linked scaffolds which represent C-C triple bond.



KHULNA UNIVERSITY Central Library KHULNA

Figure 4.6: FTIR analysis of NS_{48} scaffold with its chemical cross-linker.

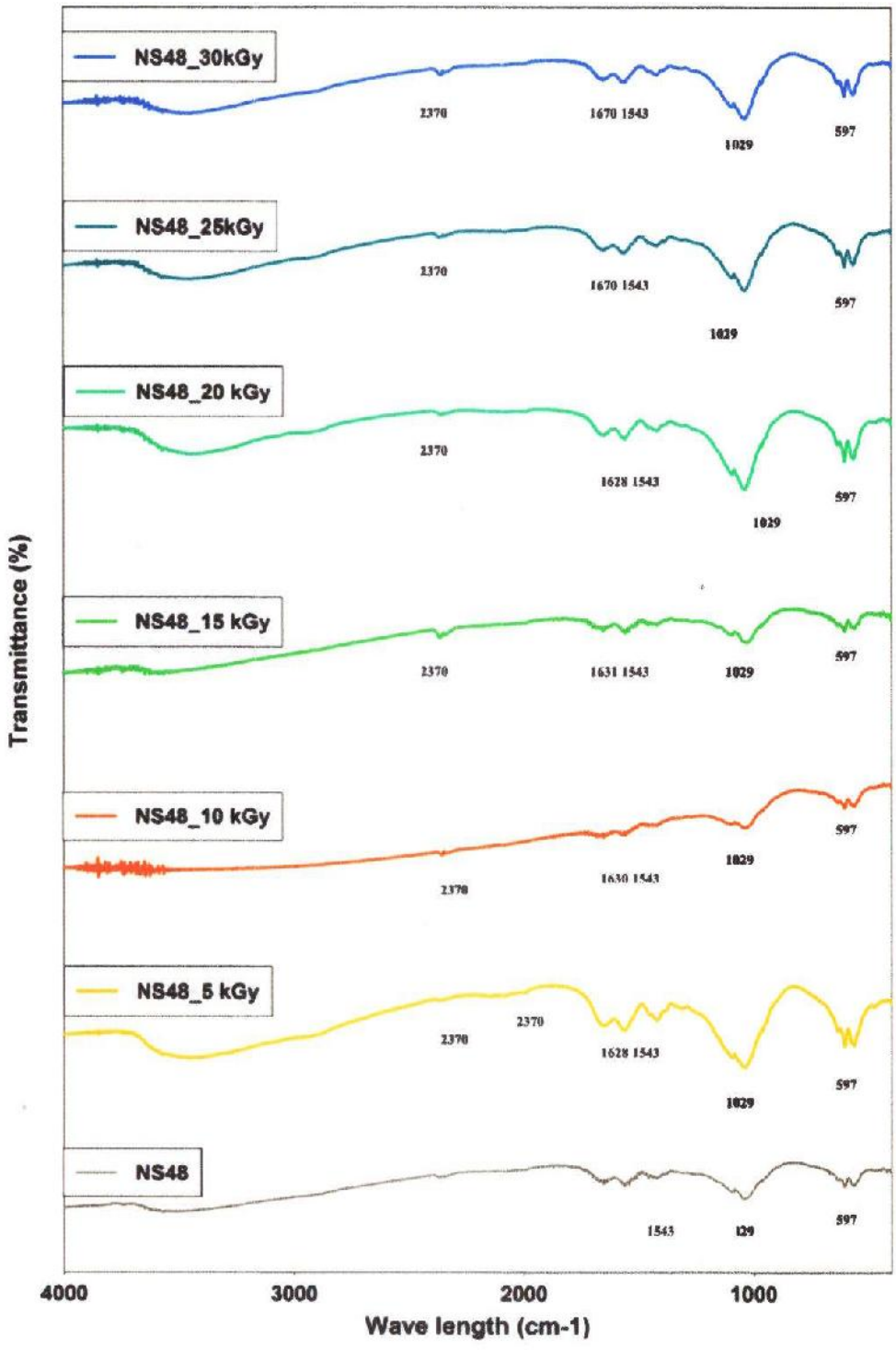


Figure 4.7: FTIR analysis of NS_{48} scaffold with its physical cross-linker.

As shown in Figure 4.7 NS_{48} scaffold showed the characteristic bands (1543, 1029, 597) of chitosan collagen and HA. However, for uncross-linked scaffold there was no band at 2400-2120 cm^{-1}, but irradiated scaffolds showed a sharp band at 2370 cm^{-1} which was due to C-N triple bond and there was another band at ~2152cm^{-1} which represent C-C triple bond. These two bonds were formed due to radiation. For every scaffold, there was a band at ~2000cm^{-1} which represent bending of C-H bond in aromatic compounds which in this case are histidine and phenylalanine of collagen molecule. The spectra showed that there was a band of amide I stretching at ~1630 cm^{-1} for uncross-linked and irradiated scaffolds (5-20 kGy), however the band shifted to 1670 cm^{-1} at high radiation dose (25 and 30 kGy).

4.4. Vascularization of Scaffold

One of the current limitations of bone engineering is its inability to provide sufficient blood supply in the initial phase after implantation. Insufficient vascularization can lead to improper cell integration or cell death in tissue-engineered constructs. Several strategies for enhancing vascularization are currently under investigation. We designed several shape of mold. Among them the cylinder like structure performed well with its high rigidity and stability. To make vascular scaffold we used hygienic cupper fiber. Liquate composite were poured into specially designed mold that contain cupper fiber vascular network. After freeze dry the cupper fibers were dragged off carefully from the pours HA-collagen-chitosan scaffold. The cupper fiber reformed a vascular network into composite.

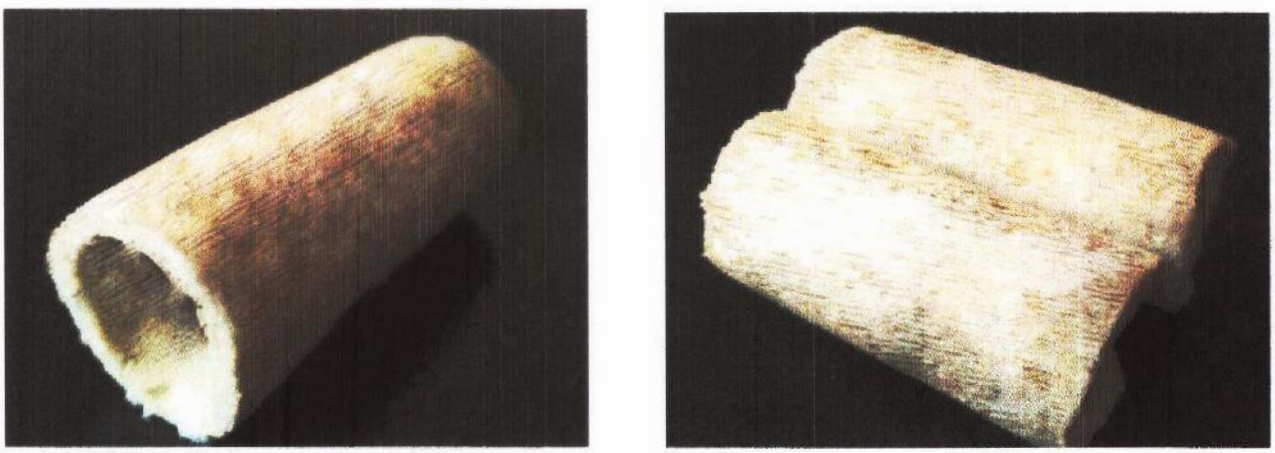


Figure 4.8: Vascularization of Scaffold

4.5. Comparison between NS_{19} and NS_{48} scaffold and select one scaffold for biocompatibility test

By analyzing the various characteristics (porosity, density, swelling kinetics and biodegradability) of all two scaffolds (NS_{19}, NS_{48}), it can be concluded that increasing porosity increases the swelling rate and biodegradability of the scaffold, however it decreases the density of the scaffold. In the case of each of two scaffolds, porosity was highest for the uncross-linked sample and further crosslinking reduced the porosity. Comparing among two scaffold, NS_{48} shows more porous condition than NS_{19} scaffold.

The apparent density of a porous scaffold can influence its mechanical strength, permeability, and presence of structural defects. In the case of density, the uncross-linked scaffolds had lower density compared to the cross-linked ones and among the two selected scaffolds NS_{19} shows the higher density.

In the case of swelling rate, among all two selected scaffolds NS_{48} had the highest swelling rate, however it decreased with the increase in solid content. However addition of cross-linker decreased the swelling rate for each of two scaffolds. Physical cross-linking reduced the swelling rate of all two scaffolds to a great extant as they eliminate water molecule and shrink the intermolecular space in the case of DHT treatment and irradiation can cause breakage of hydrogen bond either of which reduced the swelling rate. EDAC treated scaffolds had slightly higher swelling porosity than GTA treated scaffolds this is because EDAC only cross-link the adjacent collagen molecule which give it the chance to absorb water a little more than GTA which can cross-link both adjacent and distant collagen molecules.

Degradation was observed at 7, 14, 21 and 28 days. In the case degradation, the uncross-linked scaffold degraded the most for all two scaffolds. The result revels that the greatest loss of mass occurred within the first seven days of incubation and there was no more large weight loss in further time. Both of the physical crosslinking methods (DHT and radiation) reduced the scaffold degradation rate to very small extant. Comparing among two scaffold, NS_{48} shows more stable condition than NS_{19} scaffold.

By analyzing the porosity, density, swelling kinetics and biodegradability of NS_{19} and NS_{48} scaffolds, selected NS_{48} scaffold for biocompatibility test.

4.6. Mechanical Properties of Scaffold

Mechanical Properties of Scaffold were measured by Universal testing machine (UTM). Finally selected six scaffolds were performed by this action. The results are given bellow-

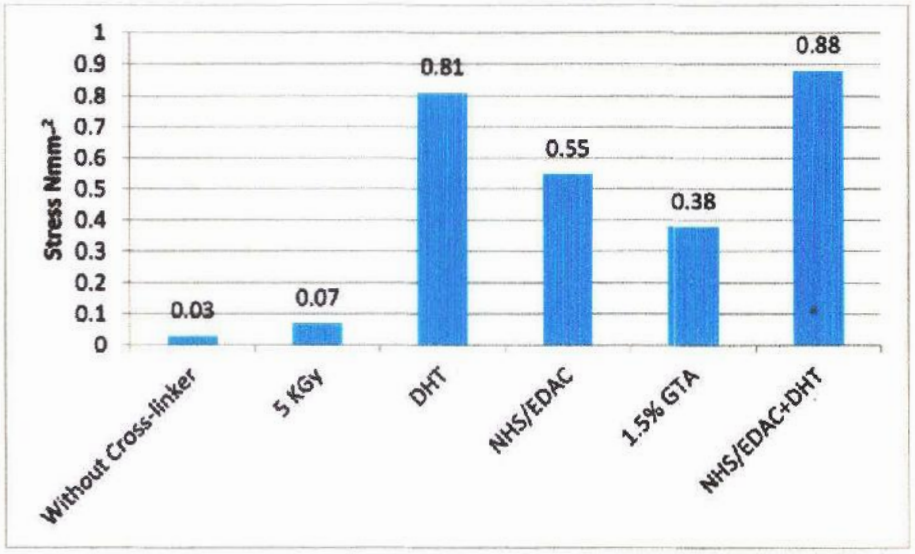


Figure 4.9: Mechanical Properties of Scaffold

Figure 4.9 shows that the raw NS_{48} scaffold had the lowest value which was 0.03 N/mm^{-2} and cross-linking of the scaffold increased its mechanical strength. Increasing dose of irradiation also increased the stress value of the scaffold. The stress value of the scaffold cross-linked with 5kGy radiation was 0.07 N/mm^{-2}. The value of the scaffold cross-linked through DHT was 0.81 N/mm^{-2} and for EDAC and NHS cross-linked scaffold it was 0.55 N/mm^{-2}. The highest value of density (0.88 N/mm^{-2}) was found from EDAC, NHS and DHT treated scaffold.

4.7. Cytotoxicity Testing of Scaffolds using Brine Shrimp Lethal Assay

The brine shrimp bioassay method was used to observe the cytotoxic effect of the fabricated scaffolds as depicted in Table 4.4. The scaffolds were dissolved in artificial sea water in which 20 nauplii (larvae of brine shrimp in number) were inoculated in each vessel. Colchicine was used as a positive control at certain dose.

Table 4.4: Number and Percentage of Mortality of Nauplii after the Cytotoxicity Test

Sample Name	Dose (mg/ml)	No. of Nauplii present after incubation	Mortality (%)
(+)ve control	0.5	0	100
(-)ve control	-	20	0
NS_{48}	0.25	20	0
	0.50	20	0
	1.00	20	0
	1.50	20	0
	2.00	19	5
NS_{48} + 25kGy	0.25	20	0
	0.50	20	0
	1.00	20	0
	1.50	20	0
	2.00	19	5
NS_{48} + DHT	0.25	20	0
	0.50	20	0
	1.00	20	0
	1.50	19	5
	2.00	18	10
NS_{48}+EDAC /NHS	0.25	20	0
	0.50	19	5
	1.00	19	5
	1.50	17	15
	2.00	17	15
NS_{48} + 1.5% GTA	0.25	19	5
	0.50	19	5
	1.00	18	10
	1.50	16	20
	2.00	16	20
NS_{48}+EDAC /NHS+DHT	0.25	20	0
	0.50	20	0
	1.00	19	5
	1.50	19	5
	2.00	18	10

The results suggested that there was no death of the nauplii, not even at higher doses of scaffolds except for the scaffold treated with EDAC, NHS and DHT. In the case of EDAC, NHS and DHT treated scaffold, there was no death of the nauplii at low doses (0.25 mg/ml, 0.50 mg/ml, 1 mg/ml and 2 mg/ml) of the scaffold. Furthermore, there was very small rate of death of the nauplii at high dose (2 mg/ml) of the scaffold. To be exact, the rate of death of nauplii at higher

dose (1 mg/ml) of the scaffold was only 5%. However, in the present study, the possibility of nauplii death due to cytotoxicity of the scaffold is very low as the number of death was zero at lower concentrations, suggesting no cytotoxic effect of the scaffold. Moreover, there was lowest mortal rate of nauplii in the case of EDAC and NHS cross-linked scaffold, not even at the highest dose. The highest mortality showed at 1.5% GTA treated scaffold with 2 mg/ml concentration dose (20% mortality). As there were no cytotoxic effect of EDAC+NHS and DHT treated scaffolds individually, the possibility of EDAC, NHS and DHT treated scaffold having cytotoxic effect is very low.

4.8. Clot Formation Test

The scaffolds showed a superior level of blood compatibility in the *in vitro* blood clot formation test. The results of the test are given in Figure 4.10.

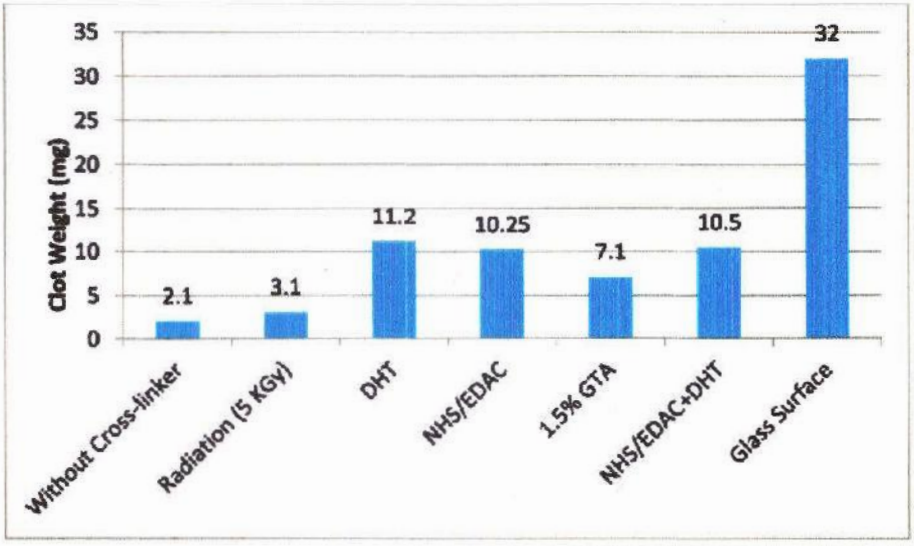


Figure 4.10: Blood Clot Weight Determination on Scaffold Surface: Clot Weight vs. Scaffold Curve

It is evident from the data that in the case of NS_{48} scaffold without cross-linking we found the lowest amount of clot and the value was 2.1 mg. This is because the mineral and polymer used in the scaffold are highly biocompatible as they are part of native bone and the scaffold had a smooth surface resist blood clotting. However, crosslinking of scaffold increased clot formation. The value of clotted weight increased to 11.20 mg in the case of DHT treated sample which was

the highest among the values for scaffolds. However, it decreases in the case of irradiated samples; the value of clotted weight was 3.1 mg in the case of 5 kGy.

Irradiated scaffolds showed a little increased clotting compared to that of the uncross-linked scaffold yet amount of clotting was minor which is also due to their smooth surface. For EDAC and NHS cross-linked scaffolds the weight of dried blood clot was 10.25, which further poorly increased to 10.50 mg in the case of EDAC, NHS and DHT treated scaffold. The dried blood clot weight was 7.1 mg for 1.5% GTA treated scaffold which was lower than that of the scaffold treated with another pair of chemical cross-linkers (EDAC and NHS) which can be contributed to the smooth surface of GTA cross-linked scaffold. As EDAC crosslinking made the scaffold surface a little bit rough which contributes to its little increased amount of blood clotting. Addition of DHT to already EDAC cross-linked scaffold further increased clot formation. This is because during DHT treatment, water molecules were eliminated from scaffold and as a result the scaffold shrinks which left the surface rough. However as the scaffold was previously cross-linked with a pair of strong chemical crosslinking agents, DHT cannot shrink the scaffold much. On the other hand only DHT treated scaffold had rough surface which caused makes large clot. However the highest value (32.0 mg) was seen in glass surface.

4.9. Degree of Hemolysis Test

The degree of hemolysis in bone tissue engineering is a delicate indicator of the extant of erythrocyte damage due to exposure to scaffold samples. In the present study *in vitro* hemolysis tests were applied to observe the blood biocompatibility of fabricated composites (Table 4.5).

Table 4.5: Percentage (%) of Hemolysis Test (Measured at 545 nm)

Sample	NS_{48}	NS_{48} + 5kGy	NS_{48} + DHT	NS_{48} +EDAC + NHS	NS_{48} + 1.5% GTA	NS_{48} + EDAC + NHS + DHT	(+) ve control	(-) ve control
Hemolysis (%)	0.22	0.57	4.94	0.57	0.27	2.20	100	0

From the result it can be seen that the measured optical density (at 545 nm) of blood sample exposed to raw NS_{48} scaffold, positive and negative control was 0.101±0.01, 0.176±0.01 and

CHAPTER FIVE

DISCUSSION

Tissue engineering is an ever growing field of biomedical arena, especially, bone tissue augmentation and repair by artificial bone material, and their scaffolds are prevalent to replace the damaged or diseased bone. For decades tissue engineering, which applies methods from engineering and life sciences to create artificial constructs to direct tissue regeneration, has fascinated many scientists and surgeons with a hope to treat patients in a minimally invasive and less painful way. Recent advances in composite biomaterials have directed to a paradigm shift towards biomimetic tissue engineering scaffolds for use in the regeneration of bone tissue defects. Researchers have been studying the effect of incorporation of hydroxyapatite (HA) as mineral within polymeric matrix to produce biomimetic composite bone scaffold and impact of the HA properties on bone cells behavior. Generally, fabrication of a scaffold with HA and natural polymer exhibits useful effects on the seeding, proliferation, osteoconductivity, differentiation and mineral desposition of stem cells (osteoblasts or mesenchymal) (Gleeson *et al.*, 2010).

Researchers have showed that incorporation of HA as mineral phase improves stiffness, interconnectivity and in vitro bioactivity. It also improves surface properties of composite scaffolds by increasing the roughness, hydrophobicity, protein adsorption (Deng *et al.*, 2010). After a detailed study on various materials, we have selected type I collagen and Chitosan as the polymer phase and HA as the mineral phase of the scaffold. As native bone is predominantly composed of type I collagen and hydroxyapatite, these materials are an obvious choice for the basis for a composite biomaterial capable of supporting and promoting the bone regenerative process (Wahl & Czernuszka, 2006). Recent studies have shown that improvements in the interaction between osteoblasts and PLLA scaffolds can be improved by the application of a collagen-HA coating (Li *et al.*, 2010) clearly demonstrating the potential of a composite material composed of only collagen and hydroxyapatite for use as a bioactive bone graft. Additionally, collagen has good biocompatibility and it causes no irritation or toxicity after implantation in the human body. It can promote cell proliferation and accelerate wound healing. Furthermore, collagen is biodegradable and can be absorbed by the human body. Its degradation products are non-toxic and cause no unwanted side effects. Due to its excellent biocompatibility,

degradability, and abundance in the body, collagen is highly desirable as a scaffold material in tissue engineering. In addition, collagen binds with most integrins for enhanced cell adhesion (Pashuck *et al.*, 2012). Chitosan (Chi) has been considerably used as a scaffold in orthopedic and other biomedical applications due to its high biocompatibility, biodegradability, porous structure, suitability for cell ingrowth, and intrinsic antibacterial nature (Vande Vord *et al.*, 2002, Martino *et al.*, 2005, Muzzarelli, 2011). Chi based composite biomaterials of low interconnected porosity for cell attachment and optimum mechanical strength need to be improved. Hence, instead of single component system that cannot assist and mimic all the properties of natural bone, an alternative multicomponent system has to be developed for bone repair and tissue engineering. Therefore, choosing these components results in a great outcome on the prepared scaffolds.

In the first phase of this research work, effort was given to optimize the solid to liquid ratio in order to obtain highly porous scaffold. Liquid to solid ratio plays a vital role in determining the properties of the prepared scaffolds, such as porosity, density, swelling ratio, mechanical strength, phase formation and *in vivo* responses. We have fabricated scaffolds at different liquid to solid (L:S) ratios (94:6 to 85:15) and observed the property changes along with the change in liquid to solid ratio (Table 4.1). Scaffolds with higher liquid content showed higher porosity, however HA precipitated indicating lacking of adequate bonding between the components. It has been evident that, when hydrated with phosphate buffer solution (PBS), the different Ca-P phases of HA undergo acid-base reaction causing dissolution of Ca-P phases and precipitation of interlocked HA (Verma & Sinha, 2013). In our study, as we increase the liquid (94%), the strength of the scaffold decreased, however the scaffold appeared spongy and the porosity and swelling rate increased. The swelling rate became very high at higher liquid percentage which could lead to the degradation of the scaffold shortly after its implementation into human body. However, under a bit excess fluid or blood flow HA has been reported to wash away in short time, either caused by physiology of the particular site of application or minor surgical procedural mistake (Burguer *et al.*, 2008). To overcome this problem, different liquid to solid ratios were incorporated to fabricate HA based composite scaffolds to make them suitable for bone regeneration.

Later on, we fabricated scaffolds at different mineral to polymer (M:P) ratios (30:70, 40:60, 50:50, 60:40 and 70:30) along with a series of liquid to solid (L:S) ratios (94:6 to 85:15). While

at high liquid percentage porosity of the scaffolds was high, lowering the liquid content to a great extent resulted in scaffolds with crack on surface. Moreover, the density of the scaffold became so high that the porosity became much lower (68.02% at 85:15 liquid to liquid ratio) than the expectation. Furthermore, reducing the liquid percentage left the solution very viscous which interrupt proper stirring. Besides, as with differing liquid to solid ratio, at different mineral to polymer ratio the scaffolds were also found to show different porosity, density and biodegradation rate. At 60:40 mineral to polymer ratios porosity and density of the scaffolds were much desirable, however at 50:50 mineral to polymer ratios these properties were also satisfactory. Lowering the mineral content less than 50% showed noticeable decrease in the porosity and adhesiveness of the scaffold (Table 4.1) (Nie *et al.,* 2012). On the other hand, Narbat *et al.,* (2006) showed increasing mineral content to 70% or more result in brittleness of HA. This is because water absorption of composite reduced with increasing HA content due to formation of a temporary HA barrier preventing water permeability into the scaffold and retaining porosity of the scaffold while high HA may be brittle (Narbat *et al.,* 2006). However, at 60% mineral content, the scaffolds showed homogenous porosity throughout the whole surface. This may be due to low solubility of collagen even in acidic solution, thus reducing the collagen content permits its maximum solubility (Telis *et al.,* 2006).

Sometimes short time mixing wasn't enough to bring the homogeneity into the mixture and after freeze drying the scaffold was found to be non-homogenous. This happened especially in the case of scaffolds with high solid and polymer content. Hence, we had to stir the solution for a long time to first mix collagen and then to mix it with HA. The next step was to evaluate the properties of the prepared scaffolds. As mentioned earlier, with increase in solid content porosity and decreased swelling rate decreased but density increased (Table 4.1). At 94:6 liquid to solid ratio, scaffold showed 94.98% porosity while 0.10 g/cm^3 density, porosity decreased to 93.22% and density increased to 0.11 g/cm^3 in the case of scaffold with 92:8 liquid to solid ratio. At 85:15 liquid to solid ratio, the scaffold demonstrated significantly low porosity, though there was a high density, most importantly there was creak on the surface of scaffold. So we stopped further increasing the solid content and focused on selecting few compositions on the basis of their porosity mainly for further study. At 94:6 liquid to solid ratio, both the 40:60 and 60:40 mineral to polymer ratio showed a suitable porosity (~90%) with 0.11 to 0.13 g/cm^3 density which was similar to the apparent density of human cancellous bone which typically ranges from

0.05 to 1.1 g/cm^3 whereas the apparent density of trabecular bone ranges from 0.14 to 1.10 g/cm^3 (average: 0.62 ± 0.11 g/cm^3) (Evans *et al.*, 1992).

We selected two scaffolds (NS_{19} and NS_{48}) on the basis of their analyzed properties and cross-linked them through both physical and chemical methods to stabilize them and further studied their properties. As physical crosslinking method we used DHT (105°C) and radiation (5-30 kGy), while as chemical method we used EDAC and NHS cross-linker pair and gluteraldehyde (GTA) at 1.5% concentrations. Again scaffolds were cross-linked first with EDAC and NHS cross-linker pair and then through DHT. In the case of each of two scaffolds, porosity was highest for the uncross-linked sample and further crosslinking reduced the porosity. Among the all cross-linked scaffolds irradiated ones had porosity closer to that of the uncross-linked sample. This is because irradiation at such low dose (5 kGy) is not sufficient for crosslinking collagen molecule and however porosity was reduced due to the reduction of intermolecular space in polymer structural space because of irradiation (Islam *et al.*, 2014). In the case of the scaffold treated with DHT, it also had lower porosity compared to the uncross-linked scaffold. This is because DHT treatment eliminates water from the collagen molecules, causing the formation of intermolecular cross-links through condensation reactions which results in reduction in intermolecular space (Khor, 1997). However, from this study it can be seen that the chemical cross-linkers were much more effective in reducing porosity than the physical ones. In the case of EDAC and NHS cross-linked porosity was lower than the scaffold without crosslinking, however it was higher than that of the GTA cross-linked scaffolds. This is because EDAC generates ''zero length'' cross-links, which are chemically analogous to those generated during DHT treatment and can only cross-link collagen molecules that are directly adjacent to each other (1nm) (Zeeman *et al.*, 1999). On the other hand, GTA cross-linked scaffolds had porosity even lower than that of EDAC and NHS treated scaffolds. This is because GTA cross-links take the form of long polymer chains and can cross-link molecules that are separated by a distance (Powell and Boyce, 2006). Furthermore, the porosity of GTA cross-linked scaffolds continued to reduce with the increase in GTA concentration. Bundela and Bajpai (2008) also found similar result where increasing cross-linker concentration decreased the porosity which is because increased number of crosslinks make polymer network more compact which results in the lower mesh size and decreased porosity (Bundela and Bajpai, 2008). For maximum case, the lowest porosity was found from the scaffold cross-linked first with EDAC and NHS pair and then

through DHT. This is probably because EDAC and NHS first reduced its porosity by primary forces like covalent bond formation and again exposure to high temperature further reduced its porosity through secondary force such as hydrogen bonding (intermolecular/intramolecular) interaction (Mane *et al.*, 2015). In the case of two selected uncross-linked scaffolds, the highest porosity was found in the case of NS_{48} scaffold and it gradually reduced in the case of NS_{19} scaffolds. This reduction in porosity among two scaffolds is due to the difference in mineral and solid content among them (Bundela and Bajpai, 2008). This is may be because addition of more solid content results in more dense and thicker pore walls which in turn lower porosity.

The apparent density of a porous scaffold can influence its mechanical strength, permeability, and presence of structural defects. In the case of density, the uncross-linked scaffolds had lower density compared to the cross-linked ones and among the two selected scaffolds NS_{19} had the highest porosity and it reduced further in the case of NS_{48} scaffold. This difference in density among two scaffolds is due to the difference in mineral and solid content among them (Bundela and Bajpai, 2008). This is may be because addition of more HA content results in more dense and thicker pore walls which in turn increase the density. It is also evident that density increases with the decrease. Since a higher density of a scaffold usually leads to higher mechanical strength while a high porosity provides a favorable biological environment, a balance between the porosity and density for a scaffold must be established for the specific application. In the case of cross-linked scaffolds the density increased due to the reduction of intermolecular space between collagen molecules. The physical crosslinking agents had increased density compared to the uncross-linked scaffolds for each of two scaffolds, additionally it was even higher than the scaffolds treated with chemical cross-linkers. This is because physical cross-linkers crosslink by elimination of water molecules (DHT) from the composite and by reducing the intermolecular space (irradiation), in which case result in a denser morphology (Mane *et al.*, 2015). In the case of scaffolds cross-linked with EDAC and NHS, the density of the scaffold was higher than that of the uncross-linked scaffold for each of two scaffolds, however it was lower than that of the GTA treated scaffolds. This is because EDAC can only cross-link collagen molecules that are directly adjacent to each other (1nm) (Zeeman *et al.*, 1999), while GTA can cross-link molecules that are separated by a distance (Powell and Boyce, 2006). As a result crosslinking with GTA resulted in denser morphology than EDAC. Additionally, increasing GTA concentration increased the density of the scaffold which is because increasing GTA increased number of

crosslinks which make polymer network more compact and thus results in more dense morphology (Bundela and Bajpai, 2008). However, the highest value of density was found for the scaffolds cross-linked first with EDAC and NHS pair and then through DHT which is because due to double crosslinking intermolecular space was reduced significantly which lead to higher density.

In the case of density, among all two selected scaffolds NS_{48} had the highest swelling rate, however it decreased with the increase in solid content. However addition of cross-linker decreased the swelling rate for each of two scaffolds. Physical cross-linking reduced the swelling rate of all two scaffolds to a great extant as they eliminate water molecule and shrink the intermolecular space in the case of DHT treatment and irradiation can cause breakage of hydrogen bond either of which reduced the swelling rate. EDAC treated scaffolds had slightly higher swelling porosity than GTA treated scaffolds this is because EDAC only cross-link the adjacent collagen molecule which give it the chance to absorb water a little more than GTA which can cross-link both adjacent and distant collagen molecules. Additionally, increasing GTA concentration decreased swelling rate as higher polymer cross-linking lower its swelling and vice-versa for lower crosslink polymer. This is mainly because of lower cross-link polymers have longer chain length and easy to expand. In contrast, in higher cross-link polymer, chain length is smaller and difficult to swell (Mane *et al.*, 2015). In the case of EDAC and DHT treated scaffold, swelling reduced to a great extant due to double crosslinking.

Degradation was observed at 7, 14, 21 and 28 days. In the case degradation, the uncross-linked scaffold degraded the most for all two scaffolds. The result revels that the greatest loss of mass occurred within the first seven days of incubation and there was no more large weight loss in further time. Both of the physical crosslinking methods (DHT and radiation) reduced the scaffold degradation rate to very small extant. In the case of DHT although the process is done in vacuum but at such high temperature some of the collagen degraded which accelerates the degradation on the other hand the amide and ester crosslinks formed by DHT resist the degradation (Salvatore *et al.*, 2014). That's why DHT treated scaffolds had degradation rate similar to that of the uncross-linked scaffold. Irradiation of scaffolds although crosslinks polymers but also breaks hydrogen bonds between them which accelerates the degradation. However chemical cross-linkers are much more effective in stabilizing scaffolds. This is because chemical cross-linking is a function

of primary forces like covalent bond formation whereas physical cross-linking is a function of secondary forces such as ionic, hydrophobic, hydrogen bonding (intermolecular/intramolecular) interaction, stereo-complexation, supra-molecular chemistry. Chemical cross-linking is much stronger and stable towards heat, mechanical, or any other action (Gulrez *et al.*, 2011). However among chemically cross-linked scaffolds, EDAC treated scaffolds had slightly higher degradation rate compared to GTA cross-linked scaffolds this is because EDAC form peptide and ester linkages among the adjacent collagen macromolecules while GTA form peptide and ester linkages among both distant and adjacent collagen macromolecules which make GTA cross-linked scaffolds much more stable and more resistant to degradation compared to EDAC treated scaffolds (Salvatore *et al.*, 2014). However EDAC and DHT treated scaffolds also have very low degradation rate due to double crosslinking.

FTIR analysis is an important tool to determine the chemical changes at molecular level. The width and intensity of spectral bands as well as position of peaks are all sensitive to chemical changes and to conformations of macromolecule. All selected scaffold showed the characteristic bands of both collagen, HA and chitosan. The spectra showed that N-H stretching generated a broad band from~3200-3400 cm^{-1} due to the hydrogen bonding between N-H of secondary amide and –OH of acetic acid in the case of all of the scaffolds. This is a characteristic band of collagen which represent amide-A band resulting from a Fermi resonance between the N-H stretch fundamental band and the overtone of amide II (Lee *et al.*, 1999). However, for the uncross-linked scaffold there was no band at 2400-2120 cm^{-1}, but cross-linked scaffolds (except for DHT) showed a sharp band at 2360 cm^{-1} which was due to C-N triple bond (nitrile group) and there was another band at ~2152 cm^{-1} in all of the cross-linked scaffolds which represent C-C triple bond.

The spectra showed a band at 2360 cm^{-1} because in the case of EDAC and EDAC/DHT treated scaffolds the band represents the nitrile group of the EDAC itself, however in GTA cross-linked and irradiated scaffolds the nitrile group was formed due to crosslinking. These two bonds were formed due to cross-linking of the scaffold. For every scaffold, there was a band at ~2000cm-1 which represent bending of C-H bond in aromatic compounds which in this case are histidine and phenylalanine of collagen molecule. There was no further significant change in the spectra due to crosslinking. All of the scaffolds showed bands of amide I, amide II stretching at ~1635

cm^{-1} and 1543 cm^{-1} respectively. C-H stretching of methyl group of collagen was found at ~1454 cm^{-1} for all scaffolds (uncross-linked and cross-linked). There no significant change in Amide III stretching of collagen and it was found at ~1234 cm^{-1} for all scaffolds. Asymmetric (v3) stretching of phosphate group of HA was found at ~1029 cm^{-1} for all scaffolds (uncross-linked and crosslinked). In particular, the bands at 557 and 600 cm^{-1} correspond mainly to v4 PO_4^{3-} bending vibrations, despite some minor contribution from collagen (amide bands) in that region which was present in all scaffolds (uncross-linked and irradiated). In general there was no significant change in the mineral phase of the scaffold due to radiation, however new bonds (C-N triple bond and C-C triple bond) were formed in the polymer phase of the scaffold.

The spectra showed that N-H stretching generated a broad band from 3200-3400 cm^{-1} due to the hydrogen bonding between N-H of secondary amide and –OH of acetic acid in the case of all of the scaffolds. However, for uncross-linked scaffold there was no band at 2400-2120 cm^{-1} but irradiated scaffolds showed a sharp band at 2360 cm^{-1} which was due to C-N triple bond and there was another band at ~2152 cm^{-1} which represent C-C triple bond. These two bonds were formed due to radiation. For every scaffold, there was a band at ~2000 cm^{-1} which represent bending of C-H bond in aromatic compounds which in this case are histidine and phenylalanine of collagen molecule. The spectra showed that there was a band of amide I stretching at ~1635 cm-1 for uncross-linked and irradiated scaffolds (5-20 kGy), however the band shifted to 1643 cm-1 at high radiation dose (25 and 30 kGy). But the amide II stretch at 1543 cm-1 was stable in all of the scaffolds which means radiation has no impact on amide II bond. C-H stretching of methyl group of collagen was found at 1454 cm^{-1} for all scaffolds (uncross-linked and irradiated). There no significant change in Amide III stretching of collagen and it was found at ~1234 cm^{-1} for all scaffolds. Asymmetric (v3) stretching of phosphate group of HA was found at ~1029 cm^{-1} for all scaffolds (uncross-linked and irradiated). In particular, the bands at 557 and 600 cm^{-1} correspond mainly to v4 PO_4^{3-} bending vibrations, despite some minor contribution from collagen (amide bands) in that region which was present in all scaffolds (uncross-linked and irradiated). In general there was no significant change in the mineral phase of the scaffold due to radiation, however new bonds (C-N triple bond and C-C triple bond) were formed in the polymer phase of the scaffold.

By analyzing the various characteristics (porosity, density, swelling kinetics and biodegradability) of all two scaffolds (NS_{19} and NS_{48}), it can be seen that NS_{48} scaffold had the highest porosity among all two scaffold and its degradation rate is little bit higher than other scaffolds, at the same time it is quite stable while cross-linked. So we had selected NS_{48} scaffold on the basis of its properties for further study.

Later on we selected NS_{48} uncross-linked scaffold and scaffolds cross-linked through DHT, EDAC & NHS, EDAC, NHS & DHT, 1.5% GTA, irradiation at 5 and 25 kGy in order to perform cytotoxicity and blood compatibility tests to evaluate the scaffold property.

After thorough study, the cytotoxicity test was performed based on brine shrimp lethal assay where colchicine was used as a positive control at certain dose and artificial seawater as negative control. The result of cytotoxicity testing of the scaffold suggested that there was no death of the nauplii, not even at higher doses of scaffolds except for the scaffold treated with EDAC, NHS and DHT. In the case of EDAC, NHS and DHT treated scaffold, there was no death of the nauplii at low doses (0.25 mg/ml, 0.50 mg/ml) of the scaffold. Furthermore, there was very small rate of death of the nauplii at high dose (1 mg/ml, 1.5 mg/ml, 2 mg/ml) of the scaffold. A number of causes may attribute to the death of Nauplii such as, the cytotoxic effect of the scaffold, formation of viscous layer on the gills of nauplii, and the reduction in the dissolved oxygen concentration of the artificial sea water. However, in the present study, the possibility of nauplii death due to cytotoxicity of the scaffold is very low as the number of death was zero at lower concentrations, suggesting no cytotoxic effect of the scaffold. Moreover, there was no death of nauplii in the case of EDAC and NHS cross-linked scaffold, not even at the highest dose. The same phenomenon happened in the cased DHT treated scaffold. As there were no cytotoxic effect of EDAC+NHS and DHT treated scaffolds individually, the possibility of EDAC, NHS and DHT treated scaffold having cytotoxic effect is very low. Hence the most possible causes for the death of nauplii are (1) the formation of the viscous layer on the gills of the nauplii as the highly concentrated solution of the composite led to high viscosity, and (2) the formation of a gel-like structure on the gills which eventually inhibited oxygen dissolution (Bundela and Bajpai, 2008).

However, in the case of blood compatibility the scaffolds showed a less clot formation compared glass surface. The uncross-linked NS_{48} scaffold formed the least clot amongst all of the scaffolds

KHULNA UNIVERSITY Central Library KHULNA

this is because the mineral and polymer used in the scaffold are highly biocompatible as they are part of native bone and the scaffold had a smooth surface resist blood clotting. Irradiated scaffolds (both at 5 and 25 kGy) and GTA cross-linked of scaffold showed a little increased clotting compared to that of the uncross-linked scaffold yet amount of clotting was minor which is also due to their smooth surface. However, EDAC cross-linked scaffold formed greater clot compared to the GTA cross-linked one as EDAC crosslinking made the scaffold surface a little bit rough which contributes to its little increased amount of blood clotting. Addition of DHT to already EDAC cross-linked scaffold further increased clot formation. This is because during DHT treatment, water molecules were eliminated from scaffold and as a result the scaffold shrink which left the surface rough. However as the scaffold was previously cross-linked with a pair of strong chemical crosslinking agents, DHT cannot shrink the scaffold much. On the other hand only DHT treated scaffold had rough surface which caused it to form large clot. In fact, the highest clot formation among the scaffold was observed for DHT treated scaffold (Bundela and Bajpai, 2008). However, the highest clot was observed on the glass surface only which was way too high compared to that of the scaffolds which indicate the compatibility of scaffold composition towards blood.

The prepared composites were tested for hemolytic activity. The degree of hemolysis is a sensitive indicator of the extent of damage to erythrocytes and the results obtained are quite satisfactory. Generally, a usable biomaterial should yield less than 2% hemolysis (Liu *et al.*, 2007). A higher degree of hemolysis indicates poor hemo-compatibility of the biomaterial. Percent hemolysis is maximum (100%) for a distilled water–water-added blood sample (positive control).In our study most of the scaffolds less than one percent hemolysis which indicates good hemo-compatible nature of the scaffolds. This is because of the smooth scaffold surface which resist lysis of RBC. However, hemolysis increased only a bit (2.20 %) compared to the standard level in the case of EDAC, NHS and DHT treated scaffold which is also acceptable. Among all the samples, DHT treated scaffold showed high degree of hemolysis which is because DHT treatment made the surface rough that encourage the lysis of RBC (Maruyama *et al.*, 2005).

CHAPTER SIX

CONCLUSION

This study sought to identify a proper mixing ratio between chitosan, collagen and HA for developing porous bone scaffold that could yield acceptable biodegradability, porosity and swelling properties for bone grafting based on bone tissue engineering technique. The results showed that degradability of scaffold was decreased with increasing chitosan-collagen and HA concentrations. Porosity increased with decreasing chitosan-collagen and HA concentrations. Swelling increased with increasing chitosan-collagen and decreasing HA concentrations. The scaffolds had desirable physicochemical and biocompatible properties without any cytotoxic effects with the advantage of strong ionic cross-linking interactions among the polymers and mineral content. These findings could be attributed to the bioactive biomaterials mimicking the structural composition of natural human bone. As a future perspective, the scaffolds may be supplemented with growth factors along with stem cell cultures to enhance osteogenesis. Over and above, this research in addition to other *in vitro* experiments on stem cell regeneration using the 3D scaffold might be a milestone in bone tissue engineering.

Reference:

Agrawal, C. M., Ray, R. B. (2001). Biodegradable polymeric scaffolds for musculoskeletal tissue engineering. Journal of Biomedical Materials Research, 55(2): 141-150.

Agrawal, P., Strijkers, G. J., Nicolay, K. (2010). Chitosan-based systems for molecular imaging. Advanced Drug Delivery Reviews, 62: 42-58.

Ahmed, T., Dare, E., Hincke. M., (2008). Fibrin: a versatile scaffold for tissue engineering applications. Tissue Engineering, 14: 199– 215.

Ajir, H., Takahashi, Y., Akashi, M., and Fujiwara, T. (2012). Polylactide block copolymers using trimethylene carbonate with methoxyethoxy side groups for dual modification of hydrophilicity and biodegradability. Macromolecular Biosciences, 12: 1315-1320.

Alaribe, F. N., Manoto, S. L. (2016). Scaffolds from biomaterials: advantages and limitations in bone and tissue engineering. Biologia, 71(4): 353-366.

Ali, F. A. M. (2017). Study of the factors affects the five years survival rate of prostate cancer patient in Sudan. Sudan University of Science and Technology, 18: 629–633.

Ambrosch, K., Manhardt, M., Loth, T., Bernhardt, R., Schultz-Siegmund, M., Hacker, M. C. (2012) Open porous microscaffolds for cellular and tissue engineering by lipid templating. Acta Biomater, 8, 1303–1315.

Baino, F., G. Novajra. (2015). Bioceramics and scaffolds: a winning combination for tissue engineering. Frontiers in bioengineering and biotechnology, 3: 202109–117.

Baino, F., Novajra, G.,Vitale-Brovarone, C. (2015). Bioceramics and Scaffolds: A Winning Combination for Tissue Engineering. Frontiers in Bioengineering and Biotechnology, vol. 3:202.

Barakat, N. A. M., Khil, M. S., Omran, A. M., Sheikh, F. A., Kim, H. Y. (2009). Extraction of pure natural hydroxyapatitefrom, the bovine bones bio waste by three different methods. Journal of Materials Processing Technology, vol. 209(7):3408–3415.

Bell, E., Ehrlich, H. P., Buttle, D. J., Nakatsuji, T. (1981). Living tissue formed *in vitro* and accepted as skin-equivalent tissue of full thickness. Science, 211, 1052–1054.

Ben-Nissan, B., Milev, A. (2004). Morphology of sol–gel derived nano-coated coralline hydroxyapatite. Biomaterials 25(20): 4971-4975.

Bertsch, A., Jiguet, S., Bernhard, D., Renaud, P. (2003). Microstereolithography: a review, Materials Research Society Symposium Proceedings, 758 Rapid Prototyping Technologies Symposium, Boston, Massachusetts, 1–13.

Bhattacharjee, N., Urrios, A. (2016). The upcoming 3D-printing revolution in microfluidics. Lab on a Chip, 16(10): 1720-1742.

Bhattarai, N., Gunn, J., Zhang, M. Q. (2010). Chitosan-based hydrogels for controlled, localized drug delivery. Advanced Drug Delivery Reviews, 62: 83-99.

Biondi, M., Ungaro, F., Quaglia, F., Netti, P. (2008). Controlled drug delivery in tissue engineering. Advance Drug Delivery, 60, 229–242.

Bose, S., Vahabzadeh, S. (2013). Bone tissue engineering using 3D printing. Materials today, 16(12): 496-504.

Brennan, A. B., Kirschner, C. M. (2014). Bio-inspired Materials for Biomedical Engineering. John Wiley & Sons, 60, 229–242.

Browning, W. D., Cho, S. D., Deschepper, E. J. (2012). Effect of a nano-hydroxyapatite paste on bleaching-related tooth sensitivity. Journal of Esthetic and Restorative Dentistry, 24: 268-76.

Bundella, H., Bajpai, A. K. (2008). Designing of hydroxyapatite-gelatin based porous matrix as bone substitute: Correlation with biocompatibility aspects. Polymer Letters, Vol. 2(3):201–213.

Burguer, H., Kasuga, T., Nogami, M., Ueda, M. (2005). Preparation of bone like apatite composite for tissue engineering scaffold. Science & Technology Advance Material, 6: 48–53.

Cai, J., Ruffieux, P. (2010). Atomically precise bottom-up fabrication of graphene nanoribbons. Nature, 466(7305): 470.

Cancedda, R., Giannoni, P. (2007). A tissue engineering approach to bone repair in large animal models and in clinical practice. Biomaterials, 28(29): 4240-4250.

Cao, W., Hench, L. L. (1996). Bioactive materials. Ceramic International, 22, 493–507.

Causa, F., Netti, P. A., Ambrosio, L. (2007). A multi-functional scaffold for tissue regeneration: The need to engineer a tissue analogue. Biomaterials, 28, 5093–5099.

Chan, L. K., Leung, V. Y., Tam, V., Lu, W. W., Sze, K. Y. (2013). Decellularized bovine intervertebral disc as a natural scaffold for xenogenic cell studies. Acta Biomater, 9: 5262–72.

Chan, G., Mooney, D. J. (2008). New materials for tissue engineering: towards greater control over the biological response. Trends Biotechnology, 26, 382–392.

Chang, E., Chang, W. J., Wang, B. C., Yang, C. Y. (1997). Plasma spraying of zirconia-reinforced hydroxyapatite composite coatings on titanium: Part I: Phase, microstructure and bonding strength. Journal of Materials Science: Materials in Medicine, 8: 193-200.

Chapekar, M. S. (2000). Tissue engineering: challenges and opportunities, Journal of Biomedical Materials Research: An Official Journal of The Society for Biomaterials, The Japanese Society for Biomaterials, and The Australian Society for Biomaterials and the Korean Society for Biomaterials 53(6): 617-620.

Chen, G., Ushida, T., Tateishi, T. (2002). Scaffold design for tissue engineering. Macromol Bioscience, 2, 67–77.

Chen, M., Wang, X., Zhang, Y., Zhou, Y., Tan, W. (2011). A modular approach to the engineering of a centimeter-sized bone tissue construct with human amniotic mesenchymal stem cells-laden microcarriers. Biomaterials, 32, 7532–7542.

Chen, M., Wang, X., Ye, Z., Zhang, Y., Zhou, Y., Tan, W. (2011). A modular approach to the engineering of a centimeter-sized bone tissue construct with human amniotic mesenchymal stem cells-laden microcarriers. Biomaterials, 32, 7532–7542.

Chevalier, E., Chulia, D., Pouget, C., Viana, M. (2007). Fabrication of porous substrates: A review of processes using pore forming agents in the biomaterial field. Journal of Pharmaceutical Science, 97, 1135–1154.

Choi, N. W., Cabodi, M., Held, B., Gleghorn, J. P., Bonassar, L. J., Stroock, A. D. (2007). Microfluidic scaffolds for tissue engineering. Nature, 6, 908–915.

Choi, S., Zhang, Y., Yeh, Y., Wooten, A. L., Xia, Y. (2012). Biodegradable porous beads and their potential applications in regenerative medicine. Journal of Material Chemistry, 22, 11442–11451.

Chun, Y. W., Webster, T. J., (2009). The role of nanomedicine in growing tissues. Annals of Biomedical Engineering, 37(10): 2034-2047.

Chung, S. E., Park, W., Shin, S., Lee, S. A., Kwon, S. (2008). Guided and fluidic self-assembly of microstructures using railed microfluidic channels. Nature Material, 7, 581–587.

Cooke, M. N., Fisher, J. P., Dean, D., Rimnac, C., Mikos, A. G. (2003).Use of Stereolithography to manufacture critical-sized 3D biodegradable scaffolds for bone ingrowth. Journal of Biomaterial Science, 64B, 65–69.

Deng, B., Lungwitz, U., Breunig, M., Dennis, A., Blunk, T., Tessmar, J. (2010). Biomimetic polymers in pharmaceutical and biomedical sciences. European Journal of Pharmacy, 58: 385–407.

Dhaliwal, A., (2012). A comprehensive review of methods for 3D cell culture. Material Methods, 2: 162.

Dhariwala, B., Hunt, E., Boland, T. (2004). Rapid prototyping of tissue-engineering constructs, using photopolymerizable hydrogels and stereolithography. Tissue Engineering, 10, 1316–1322.

Di-Martino, A., Sittinger, M., Risbud, M. (2005). Chitosan: A versatile biopolymer for orthopaedic tissue-engineering. Biomaterials, 26: 5983–5990.

Drury, J. L., Mooney, D. J. (2003). Hydrogels for tissue engineering: scaffold design variables and applications. Biomaterials, 24, 4337–4351.

Evans, C. T., Attawia, M., Borden, M. D. (1992). Advancements in tissue engineered bone substitutes. Current Opinion in Orthopaedics, 10: 10445–10451.

Falconnet, D., Csucs, G., Michelle, G. H., Textor, M. (2006). Surface engineering approaches to micropattern surfaces for cell-based assays. Biomaterials, 27(16): 3044-3063.

Fiorina, P., Vergani, A. (2018). Method of preventing and treating type 1 diabetes, allograft rejection and lung fibrosis (by targeting the ATP/P2X7R axis). US Patent Application, 14/786,424.

Fischbach, C., Chen, R., Matsumoto, T., Schmelzle, T., Brugge, J. S., Polverini, P. J., Mooney, D. J. (2007). Engineering tumors with 3D scaffolds. Nature Material, 4, 855–860.

Flemming, R. G., Murphy, C. J., Abrams, G. A., Goodman, S. L., Nealey, P. F. (1999). Effects of synthetic micro- and nano-structured surfaces on cell behavior. Biomaterials, 20(6): 573-588.

Franco, M., Ferronato, G., Santello, T., Martinetti, R., Scarano, A. (2012). Resorption of composite polymer-hydroxyapatite membranes: a time-course study in rabbit. Biomaterials, 20, 545-540.

Frohlich, K. L., Potvin, L., (2008). Transcending the known in public health practice: the inequality paradox: the population approach and vulnerable populations. American journal of public health, 98(2): 216-221.

Gaalen, S. (2008). Tissue engineering of bone. Tissue Engineering, Elsevier Academic Press, San Diego, 559-610.

Gao, C., Deng, Y., Feng, P., Mao, Z., Li, P., Yang, B., Deng, J., Cao, Y., Shuai, C., Peng, S. (2014). Current Progress in Bioactive Ceramic Scaffolds for Bone Repair and Regeneration. International Journal of Molecular Sciences, vol. 15(3):4714–4732.

Garcia, A. J. (2005). Get a grip: integrins in cell–biomaterial interactions. Biomaterials, 26, 7525–7529.

Garg, T., Singh, O., Arora, S., Murthy, R. (2012). Scaffold: anovel carrier for cell and drug delivery. Critical Reviews in Therapy Drug Carrier Systems, 29: 1-63.

Gleeson, A., Franco, M., Ferronato, G., Santello, M. T., Martinetti, R., Scarano, A. (2010). Resorption of composite polymer-hydroxyapatite membranes: a time-course study in rabbit. Biomaterials, 18: 629–633.

Gloria, A., Causa, F., Russo, T., Battista, E., Della Moglie, R., Zeppetelli, S., De Santis, R., Netti, P. A., Ambrosio, L. (2012). Three-dimensional poly(ε -caprolactone) bioactive scaffolds with controlled structural and surface properties. Bio-macromolecules, 29: 1-63.

Gomes, M. E., Godinho, J. S., Tchalamov, D., Cunha, A. M., Reis, R. L. (2002). Alternative tissue engineering scaffolds based on starch: processing methodologies, morphology, degradation and mechanical properties. Material Science Engineering Council, 20, 19–26.

Gong, Y., Ma, Z., Gao, C., Wang, W., Shen, J. (2012). Especially Elaborated Thermally Induced Phase Separation to Fabricate Poly (L-lactic acid) Scaffolds with Ultra Large Pores and Good Interconnectivity. Journal of Applied Polymer Science, 101: 3336–3342.

Guarino, V., Causa, F., Salerno, A., Ambrosio, L., Netti, P. A. (2008). Design and manufacture of microporous polymeric materials with hierarchal complex structure for biomedical application. Material Science Technology, 24, 1111–1117.

Guarnieri, D., Capua, A., Ventre, M., Borzacchiello, A., Pedone, C., Marasco, D., Ruvo, M., Netti, P. A. (2010). Covalently immobilized RGD gradient on PEG hydrogel scaffold influences cell migration parameters. Acta Biomater, 6, 2532–2539.

Gulrez, C., Cui, F. Z., Zhu, X. D. (2011). Three-dimensional nano-HAp/collagen matrix loading with osteogenic cells in organ culture. Journal of Biomedical Material Research, 44:407–415.

Hench, L. L. (1998). Bioceramics, Journal of American Biomaterial Society, 81, 1705–1728.

Hench, L. L., Polak, J. M. (2002). Third-generation biomedical materials. Science, 295, 1014–1017.

Hern-a-ndez, R. M., Orive, G., Murua, A., Pedraz, J. L. (2010). Microcapsules and microcarriers for *in situ* cell delivery. Advance Drug Delivery Rev, 62, 711–730.

Hersel, U., Dahmen, C., Kessler, H. (2003). RGD modified polymers: biomaterials for stimulated cell adhesion and beyond. Biomaterials, 24, 4385–4415.

Hildebrand, H. F., Blanchemain, N., Mayer, G., Chai, F., Lefebvre, M., Boschin, F. (2006). Surface coatings for biological activation and functionalization of medical devices. Surface Coat Technology, 200, 6318–6324.

Hing, K. A. (2004). Bone repair in the twenty–first century: biology, chemistry or engineering? Philosophical Transactions of the Royal Society of London. Series A: Mathematical, Physical and Engineering Sciences 362(1825): 2821-2850.

Hong, S., Yu, H., Kim, H. (2009). Tissue engineering polymeric microcarriers with macroporous morphology and bone-bioactive surface. Macro-molecules Bioscience, 9, 639–645.

Hou, Q., De Bank, P. A., Shakesheff, K. M. (2004). Injectable scaffolds for tissue regeneration. Journal of Material Chemistry, 14, 1915–1923.

Hu, Y., Winn, S. R., Krajbich, I., Hollinger, J. O. (2003). Porous polymer scaffolds surface-modified with arginine-glycine-aspartic acid enhance bone cell attachment and differentiation *in vitro*. Journal of Biomedical Material Research, 64A, 583–590.

Huang, S., Fu, X. (2010). Naturally derived materials-based cell and drug delivery systems in skin regeneration. Journal of Biomedical Material Research, 142, 149–159.

Huang, S., Gao, S., Cheng, L., Yu, H. (2011). Remineralization potential of nano-hydroxyapatite on initial enamel lesions: An in vitro study, Caries Research, 45: 460-8.

Huang, S., Gao, S., Cheng, L., Yu, H. (2010). Combined effects of nano-hydroxyapatite and Galla chinensis on remineralisation of initial enamel lesion *in vitro*. Journal of Dentistry, 38: 811-9.

Hutmacher, D.W. (2000). Scaffolds in tissue engineering bone and cartilage. Biomaterials, 21(24): 2529-2543.

Hutmacher, D.W. (2011). Scaffold design and fabrication technologies for engineering tissues state of the art and future perspectives, Journal of Biomaterials, 12: 107-124.

Islam, R., Knowles, J. C., Kim, H. E. (2014). Hydroxyapatite/poly (ε-caprolactone) composite coatings on hydroxyapatite porous bone scaffold for drug delivery. Biomaterials, 25: 1279–1287.

Jansen, J., Boerakker, M. J., Heuts, J., Feijen, J., Grijpma, D. W. (2010). Rapid photocrosslinking of fumaric acid monoethyl ester-functionalized poly(trimethylene carbonate) oligomers for drug delivery applications. Journal of Controlled Release, 147, 54–61.

Jayakumar, R., Prabaharan, M., Nair, S. V., Tamura, H. (2010). Novel chitin and chitosan Nano fibers in biomedical applications. Biotechnology Advances, 28: 142-150.

Jeffrey, C., Wang, M. (2006). Bone grafts: no longer just a chip off the Ol'Hip, UCLA Department of Orthopaedic Surgery.

Jeon, O., Song, S. J., Kang, S., Putnam, A. J., Kim, B. (2007). Enhancement of ectopic bone formation by bone morphogenetic protein-2 released from a heparin-conjugated poly(L-lactic-co-glycolic acid) scaffold. Biomaterials, 28, 2763–2771.

Jiang, T., Khan, Y., Nair, L. S., Abdel-Fattah W. I., Laurencin, C. T. (2009). Functionalization of chitosan/poly(lactic acid-glycolic acid) sintered microsphere scaffolds via surface heparinization for bone tissue engineering. Journal of Biomedical Material Research, 93A, 1193–1208.

Kannan, R. Y., Salacinski, H. J., Sales, K., Butler, P., Seifalian, A. M. (1976). The roles of tissue engineering and vascularization in the development of micro- Dunn GA, Heath JP. A new hypothesis of contact guidance in tissue cells. Experimental Cell Research, 101(1): 1-14.

Karageorgiou, V., Kaplan, D. (2005). Porosity of 3D biomaterial scaffolds and osteogenesis. Biomaterials, 26: 5474-5491.

Karande, T. S., Ong, J. L., Agrawal, C. M. (2004). Diffusion in musculoskeletal tissue engineering scaffolds: Design issues related to porosity, permeability, architecture, and nutrient mixing. Annals of Biomedical Engineering, 32(12): 1728-1743.

Karangeorgiou, V., Kaplan, D. (2005). Porosity of 3D biomaterial scaffolds and osteogenesis. Biomaterials, 26, 5474–5491.

Kean, T., Thanou, M. (2010). Biodegradation, bio distribution and toxicity of chitosan. Advanced Drug Delivery Reviews, 62: 3-11.

Khan, M. N., Islam, J. M., Khan, M. A. (2012). Fabrication and characterization of gelatin-based biocompatible porous composite scaffold for bone tissue engineering. Journal of Biomedical Materials Research, 100: 3020-3028.

Khetani, S. R., Bhatia, S. N. (2006). Engineering tissues for *in vitro* applications, Current Opinion of Biotechnology, 17, 524–531.

Khor, J. C. (1997). Phosphate based glasses for biomedical applications. Journal of Material Chemistry, 13: 2395–2401.

Kim, H. K., Shim, W. S., Kim, S. E., Lee, K., Kang, E., Kim, J., Kim, K., Kwon, I. C., Lee, D. S. (2009). Injectable *in situ*–Forming pH/thermo-sensitive hydrogel for bone tissue engineering. Tissue Engineering, 15, 923–933.

Kim, I. Y., Seo, S. J., Moon, H. S., Yoo, M. K., Park, I. Y., Kim, B. C., Cho, C. S. (2008). Chitosan and its derivatives for tissue engineering applications. Biotechnology Advances, 26: 1-21.

Kim, T. K., Yoon, J. J., Lee, D. S., Park, T. G. (2006). Gas foamed open porous biodegradable polymeric microspheres, Biomaterials, 27, 152–159.

Klokkevold, P. R. (2019). Soft Tissue Management for Implants in the Aesthetic Zone, Implants in the Aesthetic Zone. Springer, 95-119.

Kloxin, A. M., Kasko, A. M., Salinas, C. N., Anseth, K. S. (2009). Photodegradable hydrogels for dynamic tuning of physical and chemical properties. Science, 324, 59–63.

Kong, L., Ma, J. (2002). Preparation of PMN–PT ceramics via a high-energy ball milling process. Journal of Alloys and Compounds, 336(1-2): 242-246.

Kretlow, J. D., Mikos, A. G. (2008). From material to tissue: Biomaterial development, scaffold fabrication, and tissue engineering. AIChE Journal, 54(12): 3048-3067.

Kweh, S.W., Khor, K. A., Cheang, P. (1999). The effect of processing parameters on the characteristics of plasma sprayed hydroxyapatite (HA) coatings. Journal of Materials Process Technology, 89: 373.

Langer, R., Vacanti, J. P. (1993). Tissue engineering. Science, 260, 1920–1926.

LaVan, D. A., McGuire, T., Langer, R. (2003). Small-scale systems for *in vivo* drug delivery. Nature Biotechnolgy, 21, 1184–1191.

LaVan, D. A., McGuire, T., Langer, R. (2003). Small-scale systems for *in vivo* drug delivery. Nature Biotechnology, 21, 1184–1191.

Lee, C. R., Grodzonsky, A. J., Spector, M. (2001). The effects of cross-linking of collagen-glycosaminoglycan scaffolds on compressive stiffness, chondrocyte- mediated contraction, proliferation and biosynthesis. Biomaterials, 22, 3145–3154.

Lee, K., Kim, R. H., Yang, D., Park, S. H. (2008). Advances in 3D nano/microfabrication using two-photon initiated polymerization. Progress in Polymer Science, 33, 631–681.

Levenberg, S., Rouwkema, J., Macdonald, M., Garfein, E., Kohane, D. S., Darland, D. C., Marini, R., Van Blitterswijk, C., Mulligan, R. C., D'Amore, P., Langer, R. (2005). Engineering vascularized skeletal muscle tissue. Nature Biotechnology, 23, 879–884.

Li, J. P., De Wijn, J. R., Van Blitterswijk, C. A., De Groot, K. (2005). Porous Ti6Al4V scaffolds directly fabricated by 3D fibre deposition technique: Effect of nozzle diameter. Journal of Materials Science: Materials in Medicine, 16, 1159–1163.

Li, L., Pan, H., Tao, J., Xu, X., Mao, C., Gu, X. (2008). Repair of enamel by using hydroxyapatite nano particles as the building blocks. Journal of Materials Chemistry, 18: 4079-84.

Li, N., Lutolf, M.P., Napoli, A., Hubbell, J. A. (2010). Poly(ethyleneglycol) block copolymers. Reviews in Molecular Biotechnology, 90: 3–15.

Liu, C., Wang, W., Shen, W., Chen, T., Hu, L., Chen, Z. (1997). Evaluation of the biocompatibility of a nonceramic hydroxyapatite. Journal of Endodontics, 23: 490-3.

Liu, C., Xia, Z., Czernuszka, J. T. (2007). Design and Development of Three-Dimensional Scaffolds for Tissue Engineering. Chemical Engineering Research and Design, 85(7): 1051-1064.

Liu, X., Ma, P. X. (2004). Polymeric scaffolds for bone tissue engineering Annals of biomedical engineering. Biomaterials, 32(3): 477-486.

Lo, C., Wang, H., Dembo, M., Wang, Y. (2000). Cell movement is guided by the rigidity of the substrate. Biophysical Journal, 79, 144–152.

Luo, J., Amsalem, Y., Cohen, S. (2011). Cells, scaffolds, and molecules for myocardial tissue engineering. Pharmacology & Therapeutics, 105: 151–63.

Lutolf, M. P., Hubbell, J. A. (2005). Synthetic biomaterials as instructive extracellular microenvironment for morphogenesis in tissue engineering. Nature Biotechnolgy, 23, 47–55.

Ma, P. X. (2006). Scaffolds for tissue fabrication. Materials Today, 7: 30–40.

Mane, Y. C., Ma, L., Zhou, J., Mao, Z. W., Gao, C. Y. (2005). Collagen/chitosan-silicone membrane bilayer scaffold as a dermal equivalent. Polymers for Advanced Technologies, 16: 789–794.

Marre, S., Jensen, K. F. (2010). Synthesis of micro and nanostructures in microfluidic systems. Chemical Society Reviews, 39, 1183–1202.

Mart-i-nez, E., Engel, E., Planell, J., Samitier, J. (2009). Effects of artificial microand nano-structured surfaces on cell behavior. Annals of Anatomy, 191, 126–135.

Martin, I., Wendt, D., Heberer, M. (2004). The role of bioreactors in tissue engineering. Trends Biotech, 22, 80–86.

Martínez-Ortiz M. A., Hernández-Fuentes, A. D., Pimentel-González, D. J. (2015). Extraction and characterization of collagen from rabbit skin: partial characterization. Journal of Food, Volume 13, 2015 - Issue 2.

Maruyama, C., Ray, R. B. (2005). Biodegradable polymeric scaffolds for musculoskeletal tissue engineering. Journal of Biomedical Materials Research Part B, 55:141–150.

Mata, A., Kim, E. J., Boehm, C. A., Fleischman, A. J., Muschler, G. F., Roy, S.(2009). A three-dimensional scaffold with precise micro-architecture and surface micro-textures, Biomaterials, 30, 4610–4617.

Mathieu, L. M., Mueller, T. L., Bourban, P., Pioletti, D. P., Muller, R., Manson, J. E. (2006). Architecture and properties of anisotropic polymer composite scaffolds for bone tissue engineering. Biomaterials, 27, 905–916.

Mauney, J. R., Sjostorm, S., Blumberg, J., Horan, R., O'Leary, J. P., Vunjak-Novakovic, G., Volloch, V., Kaplan, D. L. (2004). Mechanical stimulation promotes osteogenic differentiation of human bone marrow stromal cells on 3-D partially demineralized bone scaffolds *in vitro*. Calcified Tissue International, 74, 458–468.

Meffert, R. M., Thomas, J. R., Hamilton, K. M., Brownstein, C. N. (1985). Hydroxylapatite as an alloplastic graft in the treatment of human periodontal osseous defects. Twelve month reentry results. Journal of Periodontology, 56: 540-7.

Meijer, G. J., Bruijn, J. D. (2007). Cell-based bone tissue engineering. PLoS medicine 4(2): e9.

Mekala, N. K., Baadhe, R. R., Parcha, S.R. (2012). Review on engineering biomaterials in tissue engineering application, Recent Research in Science and Technology, Vol. 4:5–11.

Melchels, F. P. W., Feijen, J., Grijpma, D. W. (2010). A review on stereolithography and its applications in biomedical engineering. Biomaterials, 31, 6121–6130.

Mikos, A. G., Thorsen, A. J., Czerwonka, L. A., Bao, Y., Langer, L., Winslow, D. N., Vacanti, J. P. (1994). Preparation and characterization of poly(l-lactic acid) foams. Polymer, 35, 1068–1077.

Minetti, E., Berardini, M. (2019). A New Tooth Processing Apparatus Allowing to Obtain Dentin Grafts for Bone Augmentation: The Tooth Transformer. The Open Dentistry Journal, 13: 7.

Mironov, V., Trusk, T., Kasyanov, V., Little, S., Swaja, R., Markwald, R. (2009). Biofabrication: a 21st century manufacturing paradigm. Biofabrication, 1, 022001.

Mitragotri, S., Lahann, J. (2009). Physical approaches to biomaterial design. Nature Materials, 8(1): 1523.

Mitsiades, C., Sourla, A., Doillon, C., Lembessis, P., Koutsilieris, M. (2000). Three dimensional type I collagen co-culture systems for the study of cell-cell interactions and treatment response in bone metastases. Journal of Musculoskeletal and Neuronal Interactions, 1, 153–155.

Moroni, L., De, Wijn J. R., Van, Blitterswijk C. A. (2008). Integrating novel technologies to fabricate smart scaffolds. Journal of Biomaterials, Science-Polymer Edition, 19(5): 543-572.

Muhammad, I. S., Xiaoxue, X., Li, L. (2002). A review on biodegradable polymeric materials for bone tissue engineering applications. Journal of Materials Science, 44(21): 5713–5724.

Munting, E., Verhelpen, M., Li, F., Vincent, A. (1990). Contribution of hydroxyapatite coatings to implant fixations, Handbook of Bioactive Ceramics. Vol. 2. Boca Raton, FLA, USA: CRC Press. International Journal of Biomaterials, 143-8.

Murata, M., Akazawa, T. (2011). Human dentin as novel biomaterial for bone regeneration, Biomaterials-Physics and Chemistry, InTech.

Muzzarelli, A. (2011). Chitosan composites with inorganics, morphogenetic proteins and stem cells, for bone regeneration. Carbohydrate Polymers, 83:1433–1445.

Narbat, M. K., Orang, F., Hashtjin, M. S., Goudarzi, A. (2006). Fabrication of Porous Hydroxyapatite-Gelatin Composite Scaffolds for Bone Tissue Engineering. Iranian Biomedical Journal, vol. 10(4):215-223.

Nie, S. C., Heath, D. J., Coombes, A., Bock, N., Textor, M., Downes, S. (2012). Biodegradable polymer/hydroxyapatite composites: surface analysis and initial attachment of human osteoblasts. Journal of Biomedical Materials Research Part B, 55: 475–486.

Nilles, J. L., Coletti, J. R. (1973). Biomechanical evaluation of bone-porous material interfaces. Journal of Biomedical Materials Research Part B, 7, 231–251.

Nilsen-Nygaard, J., Strand, S. (2015). Chitosan: Gels and interfacial properties. Polymers 7(3): 552-579.

Norotte, C., Marga, F. S., Niklason, L. E., Forgacs, G. (2009). Scaffold-free vascular tissue engineering using bioprinting. Biomaterials, 30, 5910–5917.

O'Brien, F. J. (2011). Biomaterials and scaffolds for tissue engineering. Materials Today, vol. 14(3):88–95.

Oliveira, M., Mansur, H. S. (2007). Synthetic tooth enamel: SEM characterization of a fluoride hydroxyapatite coating for dentistry applications. Materials Research, 10: 115-8.

Ooi, C., Hamdi, M., Ramesh, S. (2007). Properties of hydroxyapatite produced by annealing of bovine bone. Ceramics international, vol. 33:1171–1177.

Orsi, S., De-Capua, A., Guarnieri, D., Marasco, D., Netti, P. A. (2010). Cell recruitment and transfection in gene activated collagen matrix. Biomaterials, 31, 570–576.

Ozgur, N. E., Cuneyt, T. A. (1999). Manufacture of macroporous calcium hydroxyapatite and tri-calcium phosphate bioceramics. Journal of European Ceramic Society, 19: 2569.

Papenburg, B. J., Vogelaar, L., Bolhuis-Versteeg, L. A. M., Lammertink, R. G. H., Stamatialis, D., Wessling, M. (2007). One-step fabrication of porous micropatterned scaffolds to control cell behavior. Biomaterials, 28(11): 1998-2009.

Parkinson, I. H., Fazzalari, N. L. (2013). Characterisation of trabecular bone structure, Skeletal Aging and Osteoporosis. Springer, 31-51.

Pathi, S. P., Kowalczewski, C., Tadipatri, R., Fischbach, C. (2010). A novel 3-D mineralized tumor model to study breast cancer bone metastasis. Plos One, 5, e8849.

Piecuch, J. F. (1986). Augmentation of the atrophic edentulous ridge with porous replamineform hydroxyapatite (Interpore-200). Dental Clinics of North America, 30: 291-305.

Poncin-Epaillard, F., Shavdina, O., Debarnot, D. (2013). Elaboration and surface modification of structured poly (L-lactic acid) thin film on various substrates. Materials Science and Engineering C: Materials for Biological Applications, 33: 2526-2533.

Poth, E. J., Johnson, J. K., Childers, J. H. (1955). The use of plastic fabrics as arterial prostheses. Annals of Surgery, 142, 624–632.

Powell, G., Boyce, J., K. (2004). Structure and interactions in covalently and ionically crosslinked chitosan hydrogels for biomedical applications. European Journal of Pharmaceutics and Biopharmaceutics, 57: 19–34.

Prakasam, M., Locs, J., Salma-Ancane, K., Loca, D., Largeteau, A., Cimdina, B. L. (2015). Fabrication, Properties and Applications of Dense Hydroxyapatite: A Review. Journal of Functional Biomaterials, vol. 6(4):1099-1140.

Rahman, N., Purpura, K. A., Wylie, R. G., Zandstra, P. W., Shoichet, M. S. (2010). The use of vascular endothelial growth factor functionalized agarose to guide pluripotent stem cell aggregates toward blood progenitor cells. Biomaterials, 31, 8262–8270.

Ramli, R. A., Adnan, R., Bakar, M. A., Masudi, S. M. (2011).Synthesis and characterization of pure nanoporous hydroxyapatite. Journal of Physical Science, 22: 25-37.

Ratner, B. D., Bryant, S. J. (2004). Biomaterials: Where we have been and where we are going. Annual Review of Biomedical Engineering, 6, 41–75.

Rezwan, K., Chen, Q. Z., Blaker, J. J., Boccaccini, A. R. (2005). Biodegradable and bioactive porous polymer/inorganic composite scaffolds for bone tissue engineering. Biomaterials, 27, 3413–3431.

Rigo, E. C., Boschi, A. O., Yoshimoto, M., Allegrini, J. S., Kong, J. B., Corbani, M. J. (2004). Evaluation *in vitro* and *in vivo* of biomimetic hydroxyapatite coated on titanium dental implants. Materials Science Engineering, C 24-647.

Rivera-Muñoz, E. M. (2011). Hydroxyapatite-based materials: synthesis and characterization, Biomedical Engineering-Frontiers and Challenges, IntechOpen.

Sabree, I., Gough, J. (2015). Mechanical properties of porous ceramic scaffolds: influence of internal dimensions. Ceramics International 41(7): 8425-8432.

Sachlos, E., Czernuszka, J., (2003). Making tissue engineering scaffolds work. Review: the application of solid freeform fabrication technology to the production of tissue engineering scaffolds. European Cells & Materials, 5(29): 39-40.

Salerno, A., Di-Maio, E., Iannace, S., Netti, P. (2009). Engineering of foamed structures for biomedical application. Journal of Cellular Plastics, 45, 103–117.

Salerno, A., Guarnieri, D., Iannone, M., Zeppetelli, S., Netti, P. A. (2010). Effect of micro- and macroporosity of bone tissue three-dimensional-poly(ε -Caprolactone) scaffold on human mesenchymal stem cells invasion, proliferation, and differentiation *in vitro*. Tissue Engireering, 16, 2661–2663.

Salerno, A., Levato, R., Mateos-Timoneda, M., Engel, E., Netti, P. A., Planell, J. (2012). Modular polylactic acid microparticle-based scaffolds prepared via microfluidic emulsion/solvent displacement process: Fabrication, characterization and *in vitro* mesenchymal stem cells interaction study. Journal of Biomedical Materials Research Part A, 101A, 720–732.

Salerno, A., Oliviero, M., Di Maio, E., Iannace, S., Netti, P. (2009). Design of porous polymeric scaffolds by gas foaming of heterogeneous blends. Journal of Materials Science: Materials in Medicine, 20, 2043–2051.

Salgado, A. J., Coutinho, O. P., Reis, R. L. (2002). Bone tissue engineering: state of the art and future trends. Macromolecular Bioscience, Volume-4, Issue, Pages 743-765.

Salvatone, H., Kasuga. T., Nogami, M., Ueda, M. (2014). Preparation of bone like apatite composite for tissue engineering scaffold. Science and Technology of Advanced Materials, 6: 48–53.

Sands, R. W., Mooney, D. J. (2007). Polymers to direct cell fate by controlling the microenvironment. Current Opinion in Biotechnology, 18, 448–453.

Saondi, M., Ungaro, F., Quaglia, F., Netti, P. (2008). Controlled drug delivery in tissue engineering. Advanced Drug Delivery Reviews, 60, 229–242.

Sanz-Martín, Rojo, I. E. (2019). Structural and histological differences between connective tissue grafts harvested from the lateral palatal mucosa or from the tuberosity area. Clinical oral investigations, 23(2): 957-964.

Savarino, L., Baldini, N., Greco, M., Capitani, O., Pinna, S., Valentini, S., Lombardo, B., Esposito, M. T., Pastore, L., Ambrosio, L., Battista, S., Causa, F., Zeppetelli, S., Guarino, V. and Netti, P. (2007). The performance of poly- ε -caprolactone scaffolds in a rabbit femur model with and without autologous stromal cells andBMP4. Biomaterials, 28, 3101–3109.

Scherer, L. A., Shiver, S. (2002). The vacuum assisted closure device: a method of securing skin grafts and improving graft survival. Archives of Surgery, 137(8): 930-934.

Sharma, R. I., Snedeker, J. G. (2010). Biochemical and biomechanical gradients for directed bone marrow stromal cell differentiation toward tendon and bone, Biomaterials, 31, 7695–7704.

Shea, L. D., Smiley, E., Bonadio, J., Mooney, D. J. (1999). DNA delivery from polymer matrices for tissue engineering. Nature Biotech, 17, 551–554.

Shi, X., Ren, L., Tian, M., Yu, J., Huang, W., Du, C., Wang, D., Wang, Y. (2010). *In vivo* and *in vitro* osteogenesis of stem cells induced by controlled release of drugs from microspherical scaffolds. Journal of Materials Chemistry, 20, 9140–9148.

Si, J. K., Tang, K. (2015). Orthokeratology for myopia control: a meta-analysis. Optometry and Vision Science, 92(3): 252-257.

Simon, J. L., Michna, S., Lewis, J. A., Rekow, E. D., Thompson, V. P., Samy, J. E., Yampolsky, A., Parsons, J. R., Ricci, J. L. (2007). *In vivo* bone response to 3D periodic hydroxyapatite scaffolds assembled by direct ink writing. Journal of Biomedical Materials Research, 83A, 747–758.

Sionkowska, A., and Kozłowska, J. (2013). Properties and modification of porous 3-D collagen/hydroxyapatite composites. International Journal of Biological Macromolecules, 52: 250-259.

Slowing, I. I., Trewyn, B. G., Giri, S., Lin, V. S. (2007). Mesoporous silica nanoparticles for drug delivery and biosensing applications. Advanced Functional Materials, 17, 1225–1236.

Sommar, P., Pettersson, S., Ness, C., Johnson, H., Kratz, G., Junker, J. P. E. (2010). Engineering three-dimensional cartilage- and bonelike tissues using human dermal fibroblasts and macroporous gelatine microcarriers. Journal of Plastic, Reconstructive & Aesthetic Surgery, 63, 1036–1046.

Staiger, M. P., Pietak, A. M., Huadmai, J., Dias, G. (2006). Magnesium and its alloys as orthopedic biomaterials: A review, Biomaterials, 27, 1728–1734.

Steele, D. G., Bramblett, C. A. (1988). The anatomy and biology of the human skeleton, Texas A&M University Press.

Streubel, A., Siepmann, J., Bodmeier, R. (2006). Drug delivery to the upper small intestine window using gastroretentive technologies. Current Opinion in Pharmacology, 6, 501–508.

Sultana, N., Wang, M. (2008). Fabrication of HA/PHBV composite scaffolds through the emulsion freezing/freeze-drying process and characterisation of the scaffolds. Journal of Materials Science: Materials in Medicine, 19(7): 2555.

Sung, H. Meredith, C., Johnson, C., Galis, Z. S. (2004). The effect of scaffold degradation rate on three-dimensional cell growth and angiogenesis. Biomaterials, 25, 5735–5742.

Swain, S. K., D. Sarkar (2014). Fabrication, bioactivity, in vitro cytotoxicity and cell viability of cryo-treated nanohydroxyapatite–gelatin–polyvinyl alcohol macroporous scaffold. Journal of Asian Ceramic Societies, 2(3): 241-247.

Tayalia, P., Mendonca, C. R., Baldacchini, T., Mooney, D. J., Mazur, E. (2008). 3D cell-migration studies using two-photon engineered polymer scaffolds. Advanced Materials, 20, 4494–4498.

Telis, H. W., Knowles, J. C., Kim., H E. (2006). Hydroxyapatite/poly(e-caprolactone) composite coatings on hydroxyapatite porous bone scaffold for drug delivery. Biomaterials, 25:1279–1287.

Teng, S., Shi, J., Peng, B., Chen, L. (2006). The effect of alginate addition on the structure and morphology of hydroxyapatite/gelatin nanocomposites. Composites Science and Technology, vol. 66:1532–1538.

Trandafir, I., Hoogewijs, G., Altieri, F. (2007). Neuroglobin and cytoglobin as potential enzyme or substrate. Gene, 398 (2007) 103–113.

Ungaro, F., Biondi, M., D'angelo, I., Indolfi, L., Quaglia, F., Netti, P. A., La Rotonda, M. I. (2006). Microsphere-integrated collagen scaffolds for tissue engineering: Effect of microsphere formulation and scaffold properties on protein release kinetics. Journal of the Controlled Release, 113, 128–136.

Urciuolo, F., Imparato, G., Palmiero, C., Trilli, A., Netti, P. A. (2010). Effect of Process Conditions on the Growth of Three-Dimensional Dermal-Equivalent Tissue Obtained by Microtissue Precursor Assembly. Tissue Engineering, 17, 155–164.

Vacanti, J. P., Shin, Y. M., Ogilvie, J., Svy, A., Maemura, T., Ishii, O., Kaazempur-Mofrad, M. R., Borenstein, J. T., King, K. R., Wang, C., Weinberg, E. (2010). Fabrication of vascularized tissue using microfabricated two-dimensional molds, US patent, 2010/0267136 A1.

VandeVord, P. J., Matthew, H. W., DeSilva, S. P. (2002). Evaluation of the biocompatibility of a chitosan scaffold in mice. Journal of Biomedical Materials Research, 59(3): 585–590.

VandeVord, J., Matthew, T., DeSilva, P., Mayton, L., Wu, B., Wooley, H. (2002). Evaluation of the biocompatibility of a chitosan scaffold in mice. Journal of Biomedical Materials Research, 59:585–590.

Verma, C., Sinha, B. (2000). Formation of calcium phosphate/collagen composites, 3th edition.

Vos, T., Barber, R. M, (2015). Global, regional, and national incidence, prevalence, and years lived with disability for 301 acute and chronic diseases and injuries in 188 countries, 1990–2013: a systematic analysis for the Global Burden of Disease Study 2013." The Lancet 386(9995): 743-800.

Wahl, D. A., Czernuszka, J. T. (2006). Collagen-Hydroxyapatite Composites for Hard Tissue Repair. European Cells and Materials, Vol. 11:43-56, ISSN 1473-2262.

Watanabe, K., Nakamura, H., Toyama, Y. (2007). Establishment of three-dimensional culture of neural stem/progenitor cells in collagen Type-1 Gel. Restorative Neurology and Neuroscience. 25:545-558.

Webster, T. J. (2007). Nanotechnology for the regeneration of hard and soft tissues, World Scientific.

Wolfinbarger, J. L., Lange, P. (2019). Decellularized soft-tissue grafts, Google Patents.

Xu, J., McCarthy, S. P., Gross, R. A., Kaplan, D. L. (1996). Chitosan film acylation and effects on biodegradability. Macromolecules, 29: 3436-3440.

KHULNA UNIVERSITY
Central Library
KHULNA

Yan, J., Miao, Y., Tan, H., Zhou, T., Ling, Z., Chen, Y., Xing, X., Hu, X. (2016). Injectable alginate/hydroxyapatite gel scaffold combined with gelatin microspheres for drug delivery and bone tissue engineering, Materials science & engineering. C, Materials for biological applications, vol. 63:274-84.

Yi, H., Wu, L. Q., Bentley, W. E., Ghodssi, R., Rubloff, G. W., Culver, J. N., Payne, G. F. (2005). Biofabrication with Chitosan. Bio macromolecules, 6: 2881–2894.

Yunfeng, L., Fudong, Z., Huiyong, Z. (2009). Review on techniques of design and manufacturing for bone tissue engineering scaffold, Biomedical Engineering and Informatics. 2nd International Conference, vol. 17-19.

Zanetti, A. S., Sabliov, C., Gimble, J. M., Hayes, D. J. (2013). Human adipose-derived stem cells and three dimensional scaffold constructs: a review of the biomaterials and models currently used for bone regeneration, Journal of Biomedical Materials Research Part B Applied Biomaterials, 101: 187-199.

Zeeman, L., Gao, C. Y., Mao, Z. W., Zhou, J., Shen, J. C., Hu, X. Q., Hang, C. M. (1999) Collagen/chitosan porous scaffolds with improved biostability for skin tissue engineering. Biomaterials, 24: 4833–4841.

Zheng, W., Wang, Z., Song, L., Zhao, Q., Zhang, J., Li, D., Wang, S., Han, J., Zheng, X., Yang, Z. and Kong, D. (2012). Endothelialization and patency of RGD functionalized vascular grafts in a rabbit carotid artery model. Biomaterials, 33, 2880–2891.

Zhou, J., Xu, C., Wu, G., Cao, X., Zhang, L., Zhai, Z., Zheng, Z., Chen, X., Wang, Y. (2011). *In vitro* generation of osteochondral differentiation of human marrow mesenchymal stem cells in novel collagen-hydroxyapatite layered scaffolds. Acta Biomateralials, 7: 3999-4006.

Appendix - I

List of Abbreviations (Symbol)

%	:	Percentage
°C	:	Degree Centigrade
g/cm^3	:	Gram per centimeter cube
=	:	Equal
~	:	Proportional
G	:	Gram
cm^{-1}	:	Per centimeter
mol/L	:	Mole per milliliter
H	:	Hour
U/ml	:	Unit per milliliter
&	:	And
et.al	:	And others
Etc	:	Etcetera
Fig	:	Figure
Mol	:	Molar
Ml	:	Milliliter
Mg	:	Milligram
(+)Ve	:	Positive
(-)Ve	:	Negative
µm	:	Micrometer
kGy	:	Kilogray
V	:	Volume

List of Abbreviations (General Terms)

HA	:	Hydroxyapatite
M:P	:	Mineral:polymer
L:S	:	Liquid:solid
W/V	:	Weight/volume
SD	:	Standard deviation
NS	:	Normal Saline

OD	:	Optical density
GTA	:	Gluteraldehyde
HEMA	:	Hydroxyethyl methacrylate
P:P	:	Polymer:polymer
DW	:	Distilled water
DIW	:	Deionized water
HBA	:	Human Bone Allograft
BTE	:	Bone tissue engineering
TE	:	Tissue engineering
PBS	:	Phosphate buffered saline
FTIR	:	Fourier transform infrared spectroscopy
ESC	:	Embryonic stem cell
ASC	:	Adult stem cell
Ang	:	Angiopoietin
BMP	:	Bone morphogenetic protein
EGF	:	Epidermal growth factor
EPO	:	Erythropoietin
FGF	:	Fibroblast growth factor
G-CSF	:	Granulocyte-colony stimulating factor
GM-CSF	:	Granulocyte-macrophage colony-stimulating factor
HGF	:	Hepatocyte growth factor
IGF	:	Insulin-like growth factor
GDF	:	Growth and differentiation factor
NGF	:	Nerve growth factor
PDGF	:	Platelet-derived growth factor
TGF	:	Transforming growth factor
TGF	:	Thrombopoietin
VEGF	:	Vascular endothelial growth factor
GAG	:	Glycosaminoglycan
ECM	:	Extracellular matrix
PLLA	:	Poly(L-lactic acid)
PGA	:	Phosphoglyceric acid
PA	:	Peptide ampholites
RP	:	Rapid prototyping
CAD	:	Computer added design
FDM	:	Fused deposition modeling
SLS	:	Selective laser sintering
PLGA	:	Poly lactic-*co*-glycolic acid

Appendix-II

APPARATUS

The equipments used in this study were as follows:

a. **Hot air oven:** (For sterilization of glassware) **(Salves Lab, SWISS)**
b. **Autoclave:** (For sterilization of glassware) **(HYSC, Model: AC-100, Korea)**
c. **Magnetic Stirrer associated with heat up to 400°c:** (For mixing different composite) **(Phoenix Instrument, RSM-0.2HD)**
d. **Sonicator :**(For proper mixing of Hydroxyapatite) **(Power Sonic-420)**
e. **Water Bath:** (for proper mixing gelatin)
f. **pH meter :(pH-98107, HANNA,USA)**
g. **Freeze**: (For freezing composite) **(Lab Cold, Model: RLHE0845, UK)**
h. **Freeze Dryer:** (For drying scaffold) **(Alpha1-4LD, CHRIST)**
i. **Weighing balance: (EP 420A, SWISS)**
j. **Furnace machine** (for sintering bone) (Lenton Thermal Designs Ltd., South Korea)
k. **Ball-mill machine.**
l. **Distilled water machine: (CHINA)**

Glassware and Other Accessories:

a). Beakers (250ml, 500ml)
b). Conical flasks (100ml, 250ml, 500ml)
c). Measuring cylinder (50ml, 500ml, and 1000ml).
d). Pipettes (10ml).
e). Pipette Holder.
f). Petri dishes.
g). Scissors.
h). Forceps.
I). Sterile cotton.
j) Inoculation needle.
k). Sterile aluminum foil.
l). Filter Paper.
m).Glass rod
n). Spatula.
o). Tissue paper.
p). Glass pipette.

Materials:

- **Chitosan** (Pharmaceutical-grade Sodium Alginate procured from Sigma-Aldrich (St. Louis, MO, USA).
- **Hydroxyapatite** powder (produce in lab.)
- **Collagen** powder (produce in lab.)

Chemicals:

- A 25% solution of Gluteraldehyde (Merck Inc. 2927, Germany),
- $CaCl_2$
- HEMA (2-hydroxyethylmethacrylate)
- KH_2PO_4 (BDH Chemicals Inc. 10203, Canada)
- $Na_2HPO_4.2H_2O$ (Merck Inc. 106573, Germany)
- KCl (Merck Inc.4936, Germany) and
- NaCl (Merck Inc. 106400, Germany) for PBS (phosphate buffer saline) preparation.

Cross linker:

- HEMA (2-Hydroxyethyl Methacrylate, sigma USA)
- Glutaraldehyde (Sigma, USA)
- $CaCl_2$

Solvents:

- Deionized water
- Ethanol
- Xylene